

**SEMI-AUTOMATIC LAND USE AND LAND COVER
MAP UPDATING USING OBJECT-BASED CHANGE
DETECTION IN LAO PDR**



**A Thesis Submitted in Partial Fulfillment of the Requirements for the
Degree of Master of Science in Geoinformatics
Suranaree University of Technology
Academic Year 2017**

การปรับปรุงแผนที่การใช้ประโยชน์ที่ดินและสิ่งปกคลุมดินแบบกึ่ง-
อัตโนมัติโดยการตรวจสอบการเปลี่ยนแปลงเชิงวัตถุในสาธารณรัฐ
ประชาธิปไตยประชาชนลาว



วิทยานิพนธ์นี้เป็นส่วนหนึ่งของการศึกษาตามหลักสูตรปริญญาวิทยาศาสตรมหาบัณฑิต
สาขาวิชาภูมิสารสนเทศ
มหาวิทยาลัยเทคโนโลยีสุรนารี
ปีการศึกษา 2560

**SEMI-AUTOMATIC LAND USE AND LAND COVER MAP
UPDATING USING OBJECT-BASED CHANGE DETECTION IN
LAO PDR**

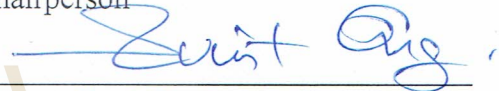
Suranaree University of Technology has approved this thesis submitted in partial fulfillment of the requirements for a Master's Degree.

Thesis Examining Committee



(Assoc. Prof. Dr. Songkot Dasananda)

Chairperson



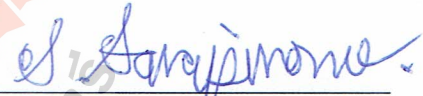
(Assoc. Prof. Dr. Suwit Ongsomwang)

Member (Thesis Advisor)



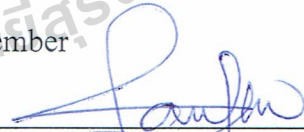
(Assoc. Prof. Dr. Sura Pattanakiat)

Member



(Asst. Prof. Dr. Sunya Sarapirome)

Member



(Dr. Pantip Piyatadsananon)

Member



(Asst. Prof. Dr. Worawat Meewasana)



(Prof. Dr. Santi Maensiri)

Vice Rector for Academic Affairs
and Internationalization

Dean of Institute of Science

สิทธิณรงค์ สิทธิเดช : การปรับปรุงแผนที่การใช้ประโยชน์ที่ดินและสิ่งปกคลุมดินแบบ
กึ่ง-อัตโนมัติโดยการตรวจสอบการเปลี่ยนแปลงเชิงวัตถุในสาธารณรัฐประชาธิปไตย
ประชาชนลาว (SEMI-AUTOMATIC LAND USE AND LAND COVER MAP
UPDATING USING OBJECT-BASED CHANGE DETECTION IN LAO PDR)
อาจารย์ที่ปรึกษา : รองศาสตราจารย์ ดร.สุวิทย์ อ่องสมหวัง, 191 หน้า.

ผลจากการพัฒนาเศรษฐกิจและสังคมในทศวรรษที่ผ่านมาส่งผลให้การใช้ประโยชน์ที่ดิน
และสิ่งปกคลุมของประเทศสาธารณรัฐประชาธิปไตยประชาชนลาวมีการเปลี่ยนแปลงอย่างรวดเร็ว
ในขณะเดียวกัน การทำแผนที่การใช้ประโยชน์ที่ดินแบบดั้งเดิมของกรมแผนที่แห่งชาติจำเป็นต้อง
ใช้เวลาในการรวบรวมและปรับปรุงแผนที่การใช้ประโยชน์ที่ดินให้เป็นปัจจุบัน ดังนั้น ขั้นตอน
วิธีการตรวจสอบการเปลี่ยนแปลงเชิงวัตถุจึงถูกนำมาใช้ในการแก้ปัญหาดังกล่าวข้างต้น
วัตถุประสงค์หลักของการศึกษาคือ (1) เพื่อพัฒนาชุดกฎข้อบังคับสำหรับใช้จำแนกการใช้
ประโยชน์ที่ดินและสิ่งปกคลุม โดยอาศัยการวิเคราะห์ SEparability and THresholds (SEaTH)
ภายใต้การวิเคราะห์ข้อมูลภาพเชิงวัตถุตามระบบการจำแนกการใช้ประโยชน์ที่ดินของประเทศ
สาธารณรัฐประชาธิปไตยประชาชนลาว และ (2) เพื่อประยุกต์ขั้นตอนวิธีแบบ Class-object change
detection กับชุดกฎข้อบังคับเพื่อปรับปรุงแผนที่การใช้ประโยชน์ที่ดินและสิ่งปกคลุมในปี พ.ศ.
2560 ในการศึกษาครั้งนี้ กรอบงานของวิธีการวิจัยซึ่งประกอบด้วย การรวบรวมและจัดเตรียมข้อมูล
การพัฒนาชุดกฎข้อบังคับสำหรับการตรวจสอบการเปลี่ยนแปลงและการปรับปรุงแผนที่การใช้
ประโยชน์ที่ดินและสิ่งปกคลุม และการประเมินความถูกต้อง ได้ถูกนำมาใช้ทดสอบในพื้นที่
ต้นแบบ 4 แห่งของพื้นที่เมือง นาข้าว ป่าที่มีผลผลิตต่ำ และป่าเบญจพรรณในนครหลวงเวียงจันทน์
ของสาธารณรัฐประชาธิปไตยประชาชนลาว

ผลการศึกษาในพื้นที่ต้นแบบพื้นที่เมือง พบว่า ในระหว่างปี พ.ศ. 2555 ถึง 2560 พื้นที่เมือง
เพิ่มขึ้น 2.12 ตร. กม. ในทางตรงกันข้าม พื้นที่นาข้าวในคาบเวลาเดียวกันลดลงอย่างรวดเร็ว 12.99
ตร. กม. พื้นที่นาข้าวในปี พ.ศ. 2555 เปลี่ยนเป็นพื้นที่ทุ่งหญ้า พื้นที่เปิดโล่ง แหล่งน้ำและเมืองในปี
พ.ศ. 2560 ความถูกต้องโดยรวมและสัมประสิทธิ์แคปปาของแผนที่การเปลี่ยนแปลงการใช้
ประโยชน์ที่ดินและสิ่งปกคลุมมีค่าเท่ากับร้อยละ 93.75 และ 90.45 ตามลำดับ ในขณะที่ ผล
การศึกษาในพื้นที่ต้นแบบพื้นที่นาข้าว พบว่า ในระหว่างปี พ.ศ. 2555 ถึง 2560 พื้นที่นาข้าวลดลง
8.40 ตร. กม. ในทางตรงกันข้าม พื้นที่ทุ่งหญ้าและเมืองในคาบเวลาเดียวกันเพิ่มขึ้น 9.35 และ 8.5
ตร. กม. ตามลำดับ ความถูกต้องโดยรวมและสัมประสิทธิ์แคปปาของแผนที่การเปลี่ยนแปลงการใช้
ประโยชน์ที่ดินและสิ่งปกคลุมมีค่าเท่ากับร้อยละ 95.14 และ 92.36 ตามลำดับ ในขณะเดียวกัน

ผลการศึกษาในพื้นที่ต้นแบบพื้นที่ป่าที่มีผลผลิตต่ำ พบว่า ในระหว่างปี พ.ศ. 2555 ถึง 2560 พื้นที่ป่าที่มีผลผลิตต่ำลดลง 8.22 ตร. กม. ในทางตรงกันข้าม พื้นที่ทุ่งหญ้าและพื้นที่เปิดโล่งในคาบเวลาเดียวกันเพิ่มขึ้น 6.53 และ 0.96 ตร. กม. ตามลำดับ ความถูกต้องโดยรวมและสัมประสิทธิ์แคปปาของแผนที่ใช้การเปลี่ยนแปลงการใช้ประโยชน์ที่ดินและสิ่งปกคลุมเท่ากับร้อยละ 97.92 และ 95.98 ตามลำดับ ในขณะที่ ผลการศึกษาในพื้นที่ต้นแบบป่าเบญจพรรณ พบว่า ในระหว่างปี พ.ศ. 2555 ถึง 2560 พื้นที่ป่าเบญจพรรณลดลง 5.81 ตร. กม. ในทางตรงกันข้าม พื้นที่ทุ่งหญ้า เมืองและพื้นที่เปิดโล่งในคาบเวลาเดียวกันเพิ่มขึ้น 26.54 8.36 และ 5.13 ตร. กม. ตามลำดับ ความถูกต้องโดยรวมและสัมประสิทธิ์แคปปาของแผนที่ใช้การเปลี่ยนแปลงการใช้ประโยชน์ที่ดินและสิ่งปกคลุมเท่ากับร้อยละ 93.06 และ 85.14 ตามลำดับ

จากผลการศึกษาสามารถสรุปได้ว่า ขั้นตอนวิธีแบบ Class-object change detection กับการวิเคราะห์ SEparability and THresholds (SEaTH) สามารถนำมาใช้พัฒนาชุดกฎข้อบังคับสำหรับการตรวจสอบการเปลี่ยนแปลงและการปรับปรุงแผนที่ใช้ประโยชน์ที่ดินและสิ่งปกคลุมได้อย่างมีประสิทธิภาพในพื้นที่ต้นแบบทั้งหมด 4 แห่ง



สาขาวิชาภูมิสารสนเทศ
ปีการศึกษา 2560

ลายมือชื่อนักศึกษา _____

ลายมือชื่ออาจารย์ที่ปรึกษา _____

SITHNALONG SITTHIDETH : SEMI-AUTOMATIC LAND USE AND
LAND COVER MAP UPDATING USING OBJECT-BASED CHANGE
DETECTION IN LAO PDR. THESIS ADVISOR : ASSOC. PROF. SUWIT
ONGSOMWANG, Dr. rer. Nat. 191 PP.

SEMI-AUTOMATIC LAND USE AND LAND COVER MAP UPDATING/
OBJECT-BASED CHANGE DETECTION// VIENTIANE/ LAO PDR

Land use and land cover (LULC) of Laos PDR had been rapidly change due to social and economic development in recent decade. Meanwhile, the traditional land use mapping by National Geographic Department (NGD) consumed a lot of time to comply and update the recent land use map. To solve the mentioned problem, object-based change detection (OBCD) was here applied for LULC map updating in this study. Main research objectives were (1) to develop rule set for LULC classification using SEparability and THresholds (SEaTH) analysis under object-based image analysis according to land use classification system of Lao PDR and (2) to apply the class-object change detection algorithm with developed rule set to update LULC map in 2017. Herein, the research methodology framework, which consisted of data collection and preparation, development of rule set for LULC change detection and map updating and accuracy assessment, were examined in four prototype areas of urban, paddy field, unstock forest and mixed deciduous forest areas in Vientiane Capital of Lao PDR.

As results of urban prototype area, it was found that urban area between 2012 and 2017 was increased 2.12 sq. km. On contrary, paddy field in this period was

dramatic decreased 12.99 sq. km. Paddy field in 2012 was changed to be grass land, bare land, water body and urban in 2017. The overall accuracy and Kappa hat coefficient of LULC change map was 93.75% and 90.45%, respectively. In the meantime, results of paddy field prototype area showed that paddy field area between 2012 and 2017 was decreased 8.40 sq. km. On contrary, grass land and urban in this period was increased 9.35 and 8.56 sq. km., respectively. The overall accuracy and Kappa hat coefficient of LULC change map was 95.14% and 92.36%, respectively. Meanwhile, results of unstock prototype area revealed that unstock forest area between 2012 and 2017 was decreased 8.22 sq. km. On contrary, grass land and bare land in this period was increased 6.53 and 0.96 sq. km., respectively. The overall accuracy and Kappa hat coefficient of LULC change map was 97.92% and 95.98%, respectively. For the meantime, results of mixed deciduous forest prototype area discovered that mixed deciduous forest area between 2012 and 2017 was decreased about 5.81 sq. km. On contrary, grass land, urban, bare land in this period was increased about 26.54 sq. km. 8.36 sq. km. and 5.13 sq. km., respectively. The overall accuracy and Kappa hat coefficient of LULC change map was 93.06% and 85.14%, respectively.

In conclusion, it can be here concluded that OBCD algorithm with SEaTH analysis was efficiently applied to develop rule set for LULC change detection and map updating in all four prototype areas.

School of Geoinformatics

Academic Year 2017

Student's Signature _____

Advisor's Signature _____

ACKNOWLEDGEMENTS

I would like to express my sincere appreciation to my thesis advisor, Assoc. Prof. Dr. Suwit Ongsomwang for his constant guidance and encouragement, without which this work would not have been possible. For his unwavering support, I am truly grateful.

I am also grateful to all lecturers in the school of remote sensing, especially Assoc. Prof. Dr. Songkot Dasananda, Asst. Prof. Dr. Sunya Sarapirome, and Assoc. Prof. Dr. Sura Pattanakiat for serving as committee members and providing suggestions. Additionally, I am thankful to Dr. Pantip Piyatadsananon who provided me valuable comments and suggestions. I am also grateful to Suranaree University of Technology for providing scholarship.

Finally, I would like to thank you my family for their encouragement and more support me.

Sithnalong Sithideth

CONTENTS

	Page
ABSTRACT IN THAI.....	I
ABSTRACT IN ENGLISH	III
ACKNOWLEDGEMENTS.....	V
CONTENTS.....	VI
LIST OF TABLES.....	X
LIST OF FIGURES	XVI
LIST OF ABBREVIATIONS.....	XXII
CHAPTER	
I INTRODUCTION.....	1
1.1 Background and significance of the study	1
1.2 Research objectives	7
1.3 Scope of the study.....	8
1.4 Limitation of the study.....	8
1.5 Study area.....	9
1.6 Benefits of the study.....	11
1.7 Outline of the thesis.....	12
II BASIC CONCEPTS AND LITERATURE REVIEWS.....	14
2.1 Land use classification system and mapping of Lao PDR.....	14
2.2 Object-Based Image Analysis (OBIA)	21

CONTENTS (Continued)

	Page
2.2.1 Multiscale (multiresolution) image Segmentation.....	22
2.2.2 Feature extraction.....	25
2.2.3 Semantic modeling and classification.....	30
2.3 Object-based change detection (OBCD).....	31
2.3.1 Image-object change detection.....	32
2.3.2 Class-object change detection.....	36
2.3.3 Multi-temporal-object change detection.....	41
2.3.4 Hybrid change detection.....	44
2.4 Literature review.....	46
III RESEARCH METHODOLOGY.....	53
3.1 Data collection and preparation.....	53
3.1.1 GIS data.....	53
3.1.2 Remote Sensing data.....	55
3.2 Development of rule set for LULC change detection and updating.....	62
3.2.1 Image segmentation.....	62
3.2.2 Feature extraction by SEaTH analysis.....	62
3.2.3 Semantic modelling and classification and LULC map updating.....	63
3.3 Accuracy assessment.....	64
IV PREPROCESSING OF REMOTE SENSING AND GIS DATA.....	66
4.1 Interpretation of LULC data in 2012.....	66

CONTENTS (Continued)

	Page
4.2 Pan-sharpening process	72
4.3 Optimum pan-sharpening method identification.....	72
4.4 Additional band generation	77
V LULC UPDATING IN URBAN AREA	80
5.1 Development of rule set for land use/land cover classification	80
5.1.1 Image segmentation by Multiresolution segmentation	80
5.1.2 Feature extraction by SEaTH analysis	83
5.1.3 Semantic modelling and classification	91
5.2 Land use and land cover in 2017 updating.....	101
5.3 Accuracy assessment.....	103
VI LULC UPDATING IN PADDY FIELD	105
6.1 Development of rule set for land use/land cover classification	105
6.1.1 Image segmentation by Multiresolution segmentation	105
6.1.2 Feature extraction by SEaTH analysis	108
6.1.3 Semantic modelling and classification	115
6.2 Land use and land cover in 2017 updating.....	124
6.3 Accuracy assessment.....	126
VII LULC UPDATING IN UNSTOCK FOREST	128
7.1 Development of rule set for land use/land cover classification	128
7.1.1 Image segmentation by Multiresolution segmentation	128

CONTENTS (Continued)

	Page
7.1.2 Feature extraction by SEaTH analysis	131
7.1.3 Semantic modeling and classification	139
7.2 Land use and land cover in 2017 updating.....	145
7.3 Accuracy assessment.....	147
VIII LULC UPDATING IN MIXED DECIDUOUS FOREST	149
8.1 Development of rule set for land use/land cover classification	149
8.1.1 Image segmentation by Multiresolution segmentation	149
8.1.2 Feature extraction by SEaTH analysis	152
8.1.3 Semantic modelling and classification	160
8.2 Land use and land cover in 2017 updating.....	167
8.3 Accuracy assessment.....	169
IX CONCLUSION AND RECOMMENDATION	170
9.1 Conclusion	170
9.1.1 LULC updating in urban area.....	170
9.1.2 LULC updating in paddy field	172
9.1.3 LULC updating in unstock forest.....	172
9.1.4 LULC updating in mixed deciduous forest	173
9.2 Recommendation.....	176
REFERENCES	177
CURRICULUM VITAE.....	191

LIST OF TABLES

Table		Page
1.1	Land use statistics of Laos under Forest Resources Assessment Report (2015).....	4
1.2	Independent power producer (IPP) Hydropower Project.....	6
1.3	The major land use types of Vientiane Capital	11
2.1	Land use classification system of Lao PDR	15
2.2	Definition of land use class at Level I	16
2.3	Definition of land use class at Level II	17
2.4	Summary of literature reviews for OBCD.....	49
3.1	Sensors and number band of Landsat 8	57
3.2	Characteristics of selected pan-sharpening algorithm	61
3.3	The error matrix	65
4.1	Area and percentage of LULC classes in urban prototype area.....	71
4.2	Area and percentage of LULC classes in paddy field area.....	71
4.3	Area and percentage of LULC classes in unstock forest area	71
4.4	Area and percentage of LULC classes in mixed deciduous forest area.....	72
4.5	Comparison of the image quality from different pan-sharpening methods for Landsat 8 data of 2012 based on Q-average value..	77
5.1	Configuration of multiresolution segmentation at Level 2 and Level 1 with thematic layer.....	83

LIST OF TABLES (Continued)

Table		Page
5.2	Pairwise of mean and variance between urban and bare land for threshold value calculation	88
5.3	Pairwise of mean and variance between urban and grass land (2) for threshold value calculation	88
5.4	Pairwise of mean and variance between urban and grass land (1) for threshold value calculation	88
5.5	Pairwise of mean and variance between urban and deep water body for threshold value calculation	89
5.6	Pairwise of mean and variance between urban and shallow water body for threshold value calculation.....	89
5.7	Semantic model for bare land change between 2012 and 2017 in urban area.....	93
5.8	Semantic model for grass land change (1) between 2012 and 2017 in urban area.....	94
5.9	Semantic model for grass land change (2) between 2012 and 2017 in urban	95
5.10	Semantic model for urban change between 2012 and 2017 in urban area.....	96
5.11	Semantic model for deep water body change between 2012 and 2017 in urban area.....	98

LIST OF TABLES (Continued)

Table	Page
5.12 Semantic model for shallow water body change between 2012 and 2017 in urban	100
5.13 Comparison of area and percent of LULC in 2012 and 2017 in urban area.....	103
5.14 Change matrix of LULC classes between 2012 and 2017.....	103
5.15 Error matrix and accuracy assessment of LULC change between 2012 and 2017.....	104
6.1 Configuration of multiresolution segmentation at Level 2 and Level 1 with thematic layer.....	109
6.2 Pairwise of mean and variance between water body and urban for threshold value calculation	113
6.3 Pairwise of mean and variance between bare land and water body for threshold value calculation	113
6.4 Pairwise of mean and variance between grass land and urban for threshold value calculation	114
6.5 Pairwise of mean and variance between urban and water body for threshold value calculation	114
6.6 Semantic model for bare land change between 2012 and 2017 in paddy field area.....	117

LIST OF TABLES (Continued)

Table		Page
6.7	Semantic model for grass land change between 2012 and 2017 in paddy field area.....	119
6.8	Semantic model for urban change between 2012 and 2017 in paddy field area.....	120
6.9	Semantic model for water change between 2012 and 2017 in paddy field area.....	122
6.10	Comparison of area and percent of LULC in 2012 and 2017 in paddy field area.....	126
6.11	Change matrix of LULC classes between 2012 and 2017.....	126
6.12	Error matrix and accuracy assessment of LULC change between 2012 and 2017.....	128
7.1	Configuration of multiresolution segmentation at Level 2 and Level 1 with thematic layer.....	132
7.2	Pairwise of mean and variance between water body and urban for threshold value calculation	136
7.3	Pairwise of mean and variance between bare land and water body for threshold value calculation	136
7.4	Pairwise of mean and variance between grass land and urban for threshold value calculation	137

LIST OF TABLES (Continued)

Table	Page
7.5 Pairwise of mean and variance between urban and water body for threshold value calculation	137
7.6 Semantic model for bare land change between 2012 and 2017 in unstock forest area	140
7.7 Semantic model for grass land change between 2012 and 2017 in unstock forest area	141
7.8 Semantic model for urban change between 2012 and 2017 in unstock forest area.....	142
7.9 Semantic model for water body change between 2012 and 2017 in unstock forest area	143
7.10 Comparison of area and percentage of LULC in 2012 and 2017 in unstock forest area	147
7.11 Change matrix of LULC classes between 2012 and 2017 in unstock forest area.....	147
7.12 Error matrix and accuracy assessment of LULC change between 2012 and 2017.....	149
8.1 Configuration of multiresolution segmentation at Level 2 and Level 1 with thematic layer.....	153
8.2 Pairwise of mean and variance between water body and urban for threshold value calculation	157

LIST OF TABLES (Continued)

Table	Page
8.3	Pairwise of mean and variance between bare land and water body for threshold value calculation 157
8.4	Pairwise of mean and variance between grass land and urban for threshold value calculation 158
8.5	Pairwise of mean and variance between urban and water body for threshold value calculation 158
8.6	Semantic model for bare land change between 2012 and 2017 in mixed deciduous forest area..... 161
8.7	Semantic model for grass land change between 2012 and 2017 in mixed deciduous forest area..... 162
8.8	Semantic model for urban change between 2012 and 2017 in mixed deciduous forest area..... 164
8.9	Semantic model for water body change between 2012 and 2017 in mixed deciduous forest area..... 165
8.10	Comparison of area and percentage of LULC in 2012 and 2017 in mixed deciduous forest area..... 169
8.11	Change matrix of LULC classes between 2012 and 2017 in mixed deciduous forest area..... 169
8.12	Error matrix and accuracy assessment of LULC change between 2012 and 2017..... 171

LIST OF FIGURES

Figure	Page
1.1 Administrative boundary of Lao PDR and its neighboring country	3
1.2 Key existing and proposed dams in Laos	7
1.3 Study site.....	9
1.4 Distribution of four prototype areas in Vientiane	10
1.5 The land use types in 2012 of study site.....	10
1.6 Structure of the thesis.....	13
2.1 Schematic workflow of land use mapping	20
2.2 Workflow of object-based image analysis in eCognition software	21
2.3 Multiresolution concept flow diagram.....	24
2.4 Multiresolution segmentation of Landsat-8 data acquired date: 07 May 2016, with scale of 10, Color=0.9, Shape=0.1, Compactness and Smoothness = 0.5	24
2.5 Examples of probability distributions.....	27
2.6 Threshold identification	29
2.7 Classification model of Research Centre Juelich (FZJ).....	30

LIST OF FIGURES (Continued)

Figure	Page
2.8	Change dataset: (a) original SPOT image, (b and c) change dataset in original scale, (d to h) multi-scale change dataset 35
2.9	Second image object level and automated classification. (A) SPOT 5 supermode R 2.5 m image. (B) Multi-resolution segmentation. (C) Building extraction (buildings in red) 41
2.10	Workflow of multi-temporal object change detection with medium spatial resolution. 44
3.1	Schematic workflow of research methodology..... 54
3.2	Spatial subset of Google earth images with band combination of 1, 2, and 3 as RGB for four representative land use class (a) Urban, (b) Paddy field, (c) Unstock forest and (d) Mixed deciduous forest 56
3.3	Spatial and spectral subset of Landsat 8 acquired on 19 February 2017 (a) Multispectral band composite [Band 5, 4, 3: NIR, R, G], (b) PAN image 58
4.1	Prototype area of urban class 67
4.2	Prototype area of paddy field class 68
4.3	Prototype area of unstock forest class..... 69
4.4	Prototype area of mixed deciduous forest class..... 70

LIST OF FIGURES (Continued)

Figure	Page
4.5	False color composite of original Landsat 8 image in 2012 and the pan-sharpened images, band 5, 4, 3 (RGB): (a) original image, (b) WT, (c) HPF, (d) MIHST, (e) EF, and (f) GS..... 73
4.6	Structure of Model Builder model for Universal Image Quality Index calculation. 76
4.7	Normalized Different Vegetation Index (NDVI) image..... 78
4.8	Modified Normalized Different Water Index (MNDWI) image. 78
4.9	Normalized Different Built-Up Index (NDBI) image.. 79
5.1	Image object of optimum pan-sharpened Landsat 8 data of 2012 by Multiresolution segmentation at level 2..... 81
5.2	Image object of optimum pan-sharpened Landsat 8 data of 2017 by Multiresolution segmentation at level 1..... 82
5.3	Class-related feature properties: Existence of..... 84
5.4	Class hierarchy structure of Super-object at Level 2 84
5.5	Class description of Super-object at Level 2 85
5.6	Structure of Mean diff to super-object parameter for changed object identification. 86
5.7	Training areas of changed objects in 2017 for SEaTH analysis 87
5.8	Rule set of urban change under class description. 90

LIST OF FIGURES (Continued)

Figure	Page
5.9	Membership function and assigned value of mean diff to-super object of layer 1. 91
5.10	Class hierarchy of LULC2012 and Object Change 91
5.11	LULC change between 2012 and 2017 in urban area..... 101
5.12	Final LULC map in 2017 in urban area. 102
6.1	Image object of optimum pan-sharpened Landsat 8 data of 2012 by Multiresolution segmentation at level 2..... 107
6.2	Image object of optimum pan-sharpened Landsat 8 data of 2017 by Multiresolution segmentation at level 1..... 108
6.3	Class-related feature properties: Existence of..... 110
6.4	Class hierarchy structure of Super-object at Level 2..... 110
6.5	Class description of Super-object at Level 2 111
6.6	Structure of Mean diff to super-object parameter for changed object identification. 112
6.7	Training areas of changed objects in 2017 for SEaTH analysis 112
6.8	Rule set of urban change under class description. 115
6.9	Membership function and assigned value of mean diff to-super object of layer 1. 115
6.10	Class hierarchy of LULC2012 and Object Change 116

LIST OF FIGURES (Continued)

Figure	Page
6.11 LULC change between 2012 and 2017 in paddy field area.....	124
6.12 Final LULC map in 2017 in paddy field area.....	125
7.1 Image object of optimum pan-sharpened Landsat 8 data of 2012 by Multiresolution segmentation at level 2.....	130
7.2 Image object of optimum pan-sharpened Landsat 8 data of 2017 by Multiresolution segmentation at level 1.....	131
7.3 Class-related feature properties: Existence of.....	133
7.4 Class hierarchy structure of Super-object at Level 2.....	133
7.5 Class description of Super-object at Level 2.....	134
7.6 Structure of Mean diff to super-object parameter for changed object identification.....	135
7.7 Training areas of changed objects in 2017 for SEaTH analysis.....	135
7.8 Rule set of urban change under class description.....	138
7.9 Membership function and assigned value of mean diff to-super object of layer 1.....	139
7.10 Class hierarchy of LULC2012 and Object Change.....	139
7.11 LULC change between 2012 and 2017 in unstock forest area.....	145
7.12 Final LULC map in 2017 in unstock forest area.....	146
8.1 Image object of optimum pan-sharpened Landsat 8 data of 2012 by Multiresolution segmentation at level 2.....	151

LIST OF FIGURES (Continued)

Figure	Page
8.2	Image object of optimum pan-sharpened Landsat 8 data of 2017 by Multiresolution segmentation at level 1 152
8.3	Class-related feature properties: Existence of..... 154
8.4	Class hierarchy structure of Super-object at Level 2..... 154
8.5	Class description of Super-object at Level 2 155
8.6	Structure of Mean diff to super-object parameter for changed object identification 156
8.7	Training areas of changed objects in 2017 for SEaTH analysis 156
8.8	Rule set of urban change under class description 159
8.9	Membership function and assigned value of mean diff to-super object of layer 1 160
8.10	Class hierarchy of LULC2012 and Object Change 160
8.11	LULC change between 2012 and 2017 in mixed deciduous forest area..... 167
8.12	Final LULC map in 2017 in mixed deciduous forest area..... 168
9.1	Workflow of practical procedure using class-object change detection and SEaTH analysis for LULC map updating. 176

LIST OF ABBREVIATIONS

COD	=	Commercial Operation Date
CVA	=	Change Vector Analysis
DSM	=	Digital Surface Model
DTM	=	Digital Terrain Model
EF	=	Ehlers Fusion
FAO	=	Food Agriculture Organization
FRA	=	Forest Resources Assessment
GIS	=	Geographic Information System
GOL	=	Government of Lao PDR
GS	=	Gram-Schmidt pan-sharpening
HPF	=	High Pass Filtering
IPP	=	Independent Power Producer
Lao PDR	=	Lao People's Democratic Republic
LULC	=	Land Use and Land Cover
MIHS	=	Modified IHS transformation
MIHST	=	Modified Intensity Hue Saturation Transform
MLC	=	Maximum Likelihood Classification
MNDWI	=	Modified Normalized Difference Water Index
NDBI	=	Normalized Difference Built-up Index
NDVI	=	Normalized Difference Vegetation Index

LIST OF ABBREVIATIONS (Continued)

NGD	=	National Geographic Department
NIR	=	Near Infrared
OBCD	=	Object-Based Change Detection
OBIA	=	Object-Based Image Analysis
OIF	=	Optimum Index Factor
OL	=	Other Land
OLI	=	Operational Land Imager
OWL	=	Other Wooded Land
PA	=	Producer Accuracy
PBIA	=	Pixel-Based Image Analysis
PCA	=	Principle Component Analysis
SEaTH	=	SEparability and Thresholds
SWIR	=	Short-Wavelength Infrared
TIRS	=	Thermal Infrared Sensor
UA	=	User Accuracy
UIQI	=	Universal Image Quality Index
USGS	=	United States Geological Survey
VHR	=	Very High Resolution
WT	=	Wavelet Fusion

CHAPTER I

INTRODUCTION

1.1 Background and significance of the study

Laos, officially the Lao People's Democratic Republic, is a landlocked state in Southeast Asia, situated at a latitude of 14 to 23 degrees North and longitude 100 to 108 degrees East. Lao PDR shares a 505 km. border with China to the north, 435 km. of border with Cambodia to the south, 2,069 km. of border with Vietnam to the east, 1,835 km. of border with Thailand to the west, and a 236 km. border with Myanmar to the northwest (Figure 1.1). The total area is 236,800 sq. km., three quarters of land are mountains and plateau (Asia Pacific Parliamentary Forum, Vientiane Capital, Lao PDR, 2009).

In thousands of years ago, people began converting forests to other land use and land cover (LULC) using fire, primitive tools and grazing to facilitate hunting and agriculture. Today, humankind has greater technological capacity than ever before to bring about rapid LULC change on a very large scale. National policies and consequent land management decisions can significantly affect patterns of LULC change. For example, the expansion of agricultural land may be promoted in response to a need to increase food production or agricultural export revenues, and increase forest area may be promoted as a way of improving livelihoods, protecting biodiversity and delivering environmental services (State of the World's forests. FAO, 2016).

Land cover change in Southeast Asia is illustrious on logging and slash and burn practice. In Laos, there are many factors affecting the changes of LULC in past four to five decades. The civil war during 1963 to 1975 had claimed forest destruction from bombing, the collectivization system needed expansion of agricultural during the early socialist era (1975-1985), market liberalization and trade (1985-1990) also increased the expansion of cash-crop garden and the post-socialist era (1990-present) to stabilize slash and burn cultivation and normalization of trade still need more land cash crop-plantation as well as infrastructure development (Fujita, 2006).

Based on Forest Resources Assessment (FRA) statistics of Laos in 2014, it was found that urban areas had been continuously increased from 20,092.18 ha in 1992 to 29,487.27 ha in 2002, 54,539.45 ha in 2010 meanwhile other land cover classes were fluctuated as shown in Table 1.1.

Lao PDR is starting to urbanize rapidly, with the highest rates of urban spatial expansion and urban population increase in East Asia. Urban population was more double increased between 2000 and 2010. Vientiane capital is very small by East Asia standards, but it doubled in size and population during this period. Urban population densities in Lao PDR were among the lowest in the region (World Bank, 2015).

In addition, Vongdeuane (2005) had reported the status and change of forest. In 1982 forest cover was 11,636,900 ha or about 49%, in 1992 it was 11,168,000 ha or 47% and in 2002 it was 9,824,700 ha or 41.5%. This shows a rapid decrease from 1992 to 2002 by 1,343,300 ha or about 5.5%, while from 1982 to 1992 it was only 468,900 ha or about 2%. The area of dry dipterocarp forest increased from 1,235,100 ha in 1982 to 1,317,200 ha in 2002 generated mostly by unsustainable harvesting or commercial logging.



Source: United Nation (2004).

Figure 1.1 Administrative boundary of Lao PDR and its neighboring country.

Table 1.1 LULC statistics of Laos under Forest Resources Assessment Report (2015).

National LULC Class	Area in ha		
	1992	2002	2010
Forest			
Dry dipterocarp	1,483,252.00	1,343,346.00	1,205,022.00
Dry evergreen	2,635,870.00	1,330,111.00	1,367,399.00
Mixed deciduous	7,790,934.00	7,523,422.00	10,181,170.00
Gallery forest	N/A	33,008.00	N/A
Coniferous	12,664.00	21,910.00	86,501.00
Mixed coniferous /broadleaved	N/A	153,162.00	28,990.00
Plantation	1,263.00	54	69,010.00
Bamboo	858,459.00	403,846.00	255,862.00
Temporarily unstock forest	4,638,676.00	5,493,343.00	4,621,608.00
Total	17,421,118.00	16,302,202.00	17,815,562.00
Other wooded Land (OWL)			
Rest temporarily unstock forest	3,092,450.42	3,662,228.50	3,081,072.13
Savannah / open woodlands	35,448.48	168,391.07	176,531.80
Heath, scrub forest	217,403.31	165,849.37	30,718.71
Total	3,345,302.21	3,996,468.94	3,288,322.64
Other land (OL)			
Upland rice	469,320.68	709,823.10	618,009.18
Paddy field	947,840.80	1,117,493.33	999,571.94
Agriculture plantation	88,462.14	189,227.95	44,382.16
Other agriculture land	27,785.77	36,646.39	165,041.50
Barren lands/ rock	222,919.05	184,422.37	195,330.86
Grass land	891,908.31	589,811.49	162,702.46
Urban areas	20,092.18	29,487.27	54,539.45
Other land	10,516.20	4,736.34	28,989.86
Swamps	48,196.38	58,739.23	9,731.78
Total	2,727,041.49	2,920,387.46	2,278,299.19
Water body	186,538.64	460,940.32	297,815.65

Source: Somchay (2015).

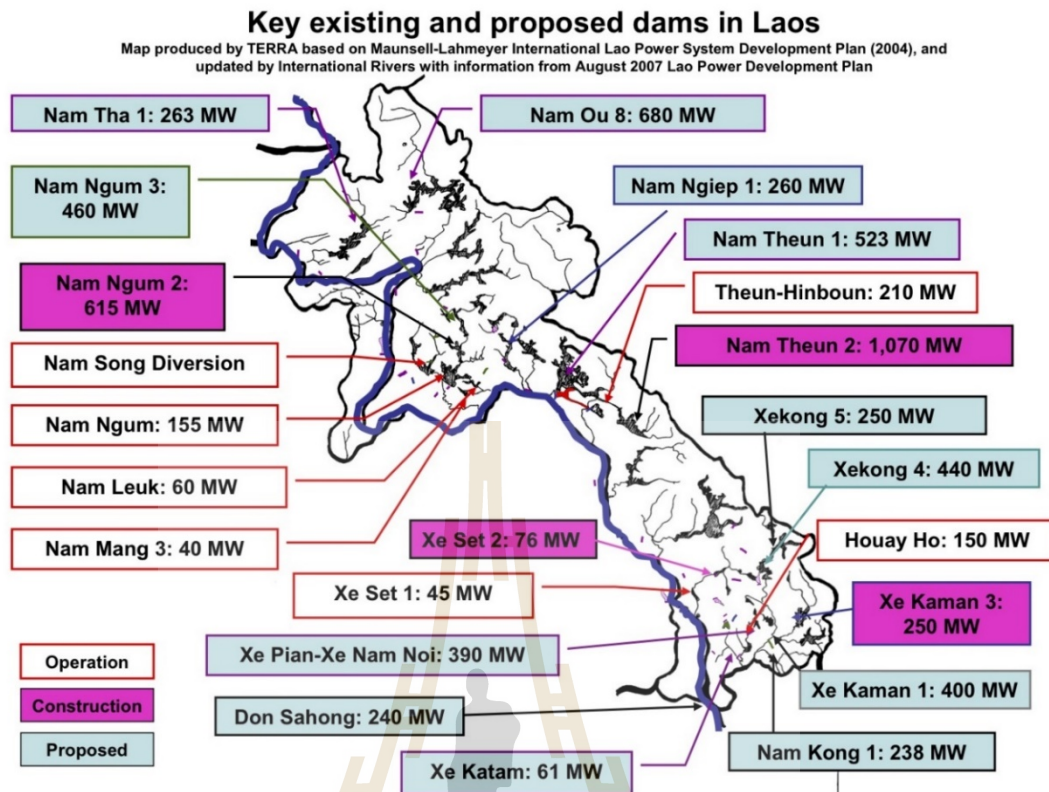
Meanwhile, the development of hydropower facilities, with planned and managed environmental impacts, is seen as an ideal opportunity for Lao PDR to enhance its economic prosperity and improve the lives of its people. Lao PDR possesses a large, almost untapped, hydropower potential beyond its own needs and has a central location in a regional market of the Greater Mekong Sub-region characterized by expanding electricity demand. Exports of electricity have been an important foreign exchange earner since 1971. However, the Government of Lao PDR (GOL) is relying on an expansion of this activity to boost revenues to further its social objectives (Pholsena and Phonekeo, 2004). Lao PDR had proposed 20 concession agreements of independent power producer (IPP) hydropower project (Ministry of Energy and Mines, 2016) as summary in Table 1.2. Distribution of key existing and proposed dams in Laos is displayed in Figure 1.2. Based on the LULC change influence factors, there are positive and negative changes. The tentative hydropower dams will convert the land currently use for grazing, forestry and agriculture into the reservoir.

According to the previous mentioned statement, LULC of Laos had been rapidly change due to social and economic development in recent decade. The land use data is a basic GIS dataset required by various users such as land and resources manager, city planner or decision maker (Jensen, 2005). Meanwhile, the traditional land use mapping by National Geographic Department (NGD) consumes a lot of time to comply and update the recent land use map. Therefore, object-based change detection (OBCD) is here applied for land use map updating based on the existing land use map in 2012 of NGD. The expected result will be benefit to existing government organizations of Lao PDR that are responsible for land use mapping.

Table 1.2 Independent power producer (IPP) Hydropower Project.

No.	Name of Projects	Location	Installed Capacity	COD	Planned Market
1	Nam Ngiep 2	Xiangkhouang	180 MW	2015	Laos
2	Hongsa	Xayaboury	1878 MW	2015	Thailand/Laos
3	Nam Ou 2	Luangphabang Phongsaly	120 MW	2015	
4	Nam Ou 5	Phongsaly	240 MW	2015	Laos
5	Nam Ou 6	Phongsaly	180 MW	2015	
6	Nam Kong 2	Attapue	66 MW	2015	Laos
7	Xekaman 1	Attapue	322 MW	2016	Vietnam/Laos
8	Nam Sim	Houaphanh	8 MW	2016	Laos
9	Nam Mang 1	Bolikhamsay	64 MW	2016	Laos
10	Nam Beng	Oudomxay	34 MW	2016	Laos
11	Nam Sane 3A	Xiengkhuang	69 MW	2016	Laos
12	Nam Sane 3B	Xiengkhuang	45 MW	2016	Laos
13	Nam Lik 1	Vientiane	61 MW	2017	Laos
14	Nam Phay		86 MW	2018	Laos
15	Nam Tha 1	Louangnamtha & Borkeo	168 MW	2018	Laos
16	Xayabouly (Mekong)	Xayabouly-Luangphabang	1285 MW	2019	Thailand/Laos
17	Sepian-Xenamnoy	Attapeu and Champasak	410MW	2019	Thailand/Laos
18	Nam Ngiep 1	Bolikhamsay	290MW	2019	Thailand/Laos
19	Nam Pha	Luangnamtha	130 MW	2019	Laos
20	Nam Phak	Champasak	45 MW	2020	Laos
21	Don Sahong	Champasak	240 MW	N/A	Laos
22	Nam Ou 1, 3, 4 & 7	Luangphabang Phongsaly	732 MW	N/A	Laos

Source: Ministry of Energy and Mines (2016).



Source: International River (2007).

Figure 1.2 Key existing and proposed dams in Laos.

1.2 Research objective

The ultimate goal of the research is to apply OBCD algorithm to update the existing land use map. The specific research objectives are as follow:

1. To develop rule set for land use classification using Separability and Thresholds analysis in four prototype areas (urban, paddy field, unstock forest and mixed deciduous forest) under object-based image analysis (OBIA) according to land use classification system of Lao PDR;
2. To apply the class-object change detection algorithm with developed rule set to update land use map in 2017.

1.3 Scope of the study

1. Landsat 8 data (multispectral and panchromatic bands) acquiring in 2017 are used to develop semantic model and classification with SEaTH analysis for LULC extraction.

2. The existing land use map in 2012 of NGD is firstly visually verified and updated based on Landsat 8 data in 2012. The corrected LULC data is then used as base map to extract four prototype areas for LULC updating in 2017.

3. An optimum pan-sharpening technique, which include (1) Ehlers fusion (EF), (2) Gram-Schmidt pan-sharpening (GS), (3) High pass filtering (HPF) (4) Modified IHS transformation (MIHS), and (5) Wavelet fusion (WT), is identified for Landsat 8 (LDCM) data in 2017 based on average of Universal Image Quality index (Q-average).

4. The rule set for LULC classification is developed based on SEaTH analysis using MS Excel spreadsheet software to calculate the J separability and threshold identification.

5. The change objects are classified by rule set to extract change of LULC class under class-object change detection algorithm.

6. The updating LULC map in 2017 is assessed accuracy with overall accuracy and Kappa hat coefficient based on Google Earth image in 2017.

1.4 Limitation of the study

Although the research proposal has been set up with specific aims, there are some unavoidable limitations. Because of the time limit, so that four prototype areas in Vientiane Capital is chosen as the study areas that covers main land use classes.

1.5 Study area

Vientiane Capital of Laos, which consists of 9 districts include Sangthong, Naxaythong, Xaithani, Pakngum, Sikhottabong, Chanthabouly, Xaisettha, Sisattanak, and Hatxayfong (Figure 1.3) and covers area of 3,920 sq. km., is chosen as study site. Distribution of four prototype areas for urban, paddy field, unstock forest and mixed deciduous forest in the study site is displayed in Figure 1.4.

According to the land use data of Department of Forest Resource Management in 2012, top three main land use types in the study area are unstock forest (28.95%), paddy field (24.83%), and mixed deciduous forest (22.79%) as display in Figure 1.5 and summary in Table 1.3.

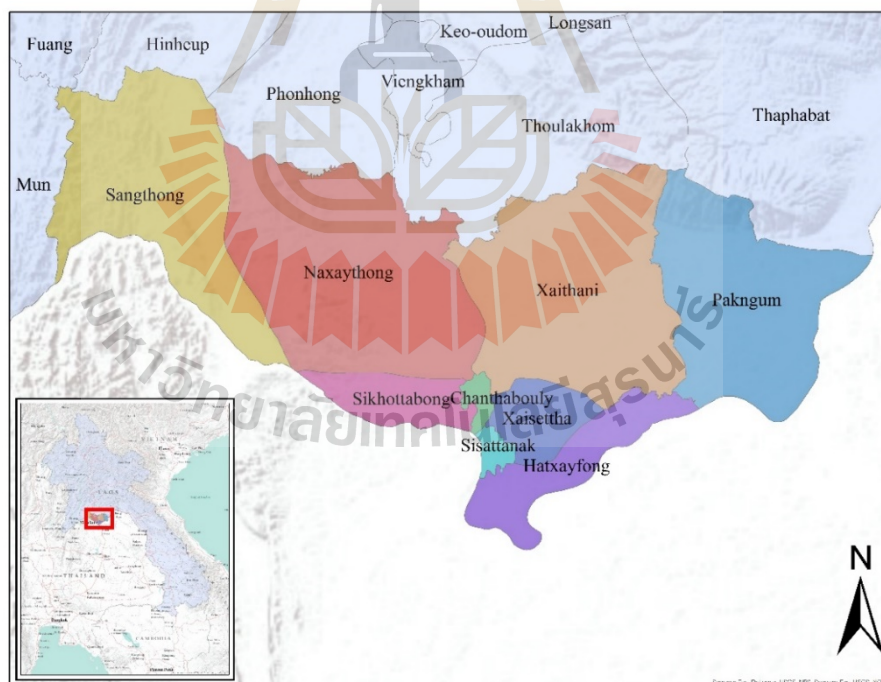


Figure 1.3 Study site.

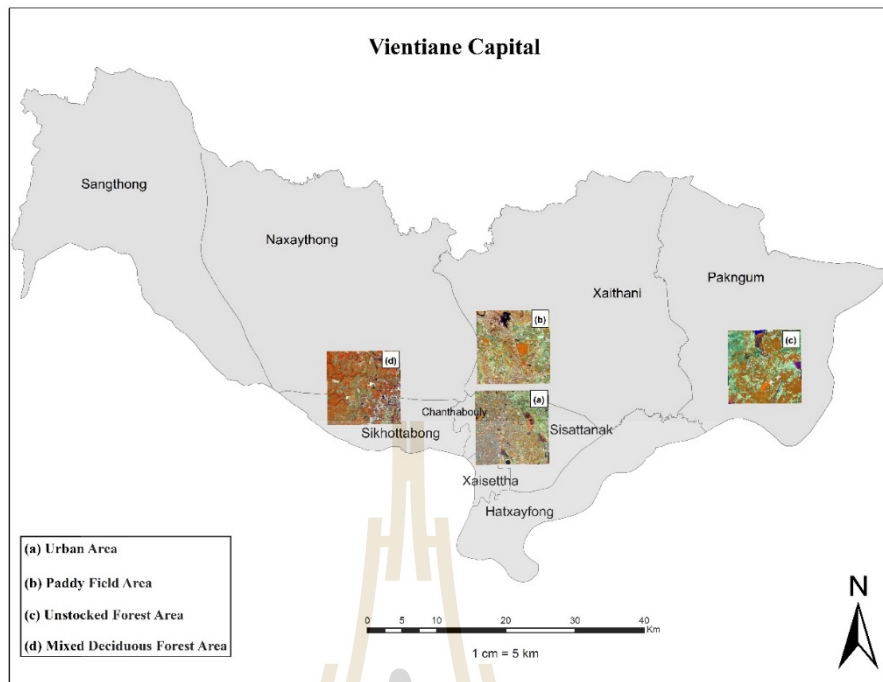


Figure 1.4 Distribution of four prototype areas in Vientiane.

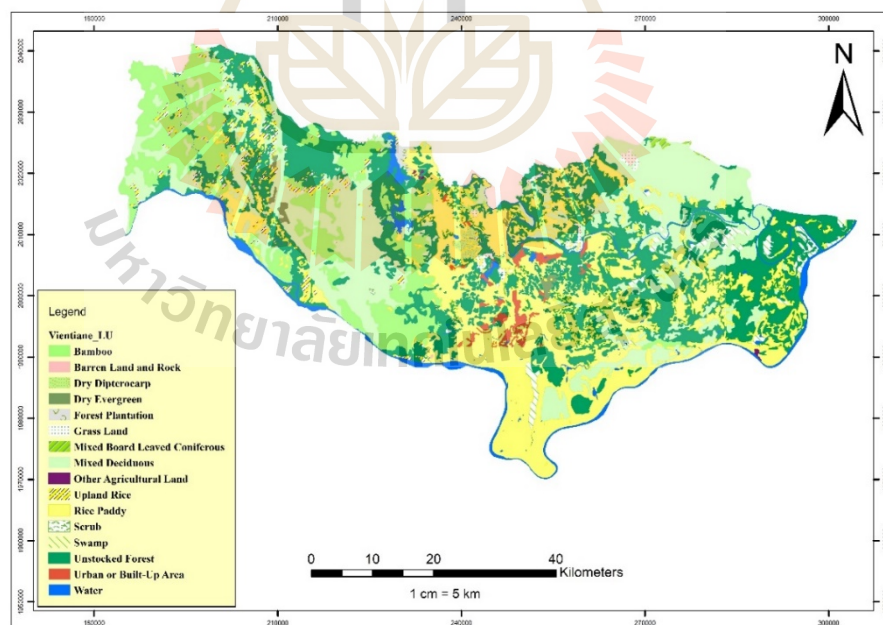


Figure 1.5 The land use types in 2012 of study site (DFRM, 2012).

Table 1.3 The major land use types of Vientiane Capital (DFRM, 2012).

No	Land Use Type	Area in sq. km.	%
1	Bamboo	492.44	13.53
2	Barren Land and Rock	0.27	0.01
3	Dry Dipterocarp	12.25	0.34
4	Dry Evergreen	15.08	0.41
5	Forest Plantation	6.66	0.18
6	Grass Land	22.50	0.62
7	Mixed Broad Leaved Coniferous	4.80	0.13
8	Mixed Deciduous	829.34	22.79
9	Other Agricultural Land	2.31	0.06
10	Upland Rice	75.28	2.07
11	Paddy Field	903.68	24.83
12	Scrub	0.81	0.02
13	Swamp	52.74	1.45
14	Unstock Forest	1053.49	28.95
15	Urban or Built-Up Area	42.98	1.18
16	Water body	124.97	3.43
	Total	3,639.61	100.00

1.6 Benefits of the study

The benefits of the study are as follows:

- (1) An optimum method of pan-sharpening image for land use classification,
- (2) The semantic model and classification with rule-based classifier for land use classification from Landsat data under OBIA,
- (3) The change objects with land use class and change matrix,
- (4) The updated land use map in 2017.

1.7 Outline of the thesis

Chapter I “Introduction” contains background problem and significance of the study, research objectives, scope of the study, limitation of the study, study area, benefits of the study and outline of the thesis. Chapter II “Basic concepts and literature reviews” contains land use classification system and mapping of Lao PDR, object-based image analysis (OBIA), object-based change detection (OBCD) and literature review. Chapter III “Research methodology” contains data collection and preparation, development of rule set for land use classification in 2017, semantic modelling and classification and object-based change detection and accuracy assessment. Chapter IV “Preprocessing of remote sensing and GIS data” contains preprocessing of GIS and remote sensing data for OBCD, development of rule set for land use/land cover classification. Chapter V “LULC updating in urban area” contains development of rule set for land use/land cover classification, land use and land cover in 2017 updating and accuracy assessment. Chapter VI “LULC updating in paddy field area” contains development of rule set for land use/land cover classification, land use and land cover in 2017 updating and accuracy assessment. Chapter VII “LULC updating in unstock forest area” contains development of rule set for land use/land cover classification, land use and land cover in 2017 updating and accuracy assessment. Chapter VIII “LULC updating in mixed deciduous forest area” contains development of rule set for land use/land cover classification, land use and land cover in 2017 updating and accuracy assessment and chapter IX “Conclusion and recommendation” contains conclusion and recommendation.

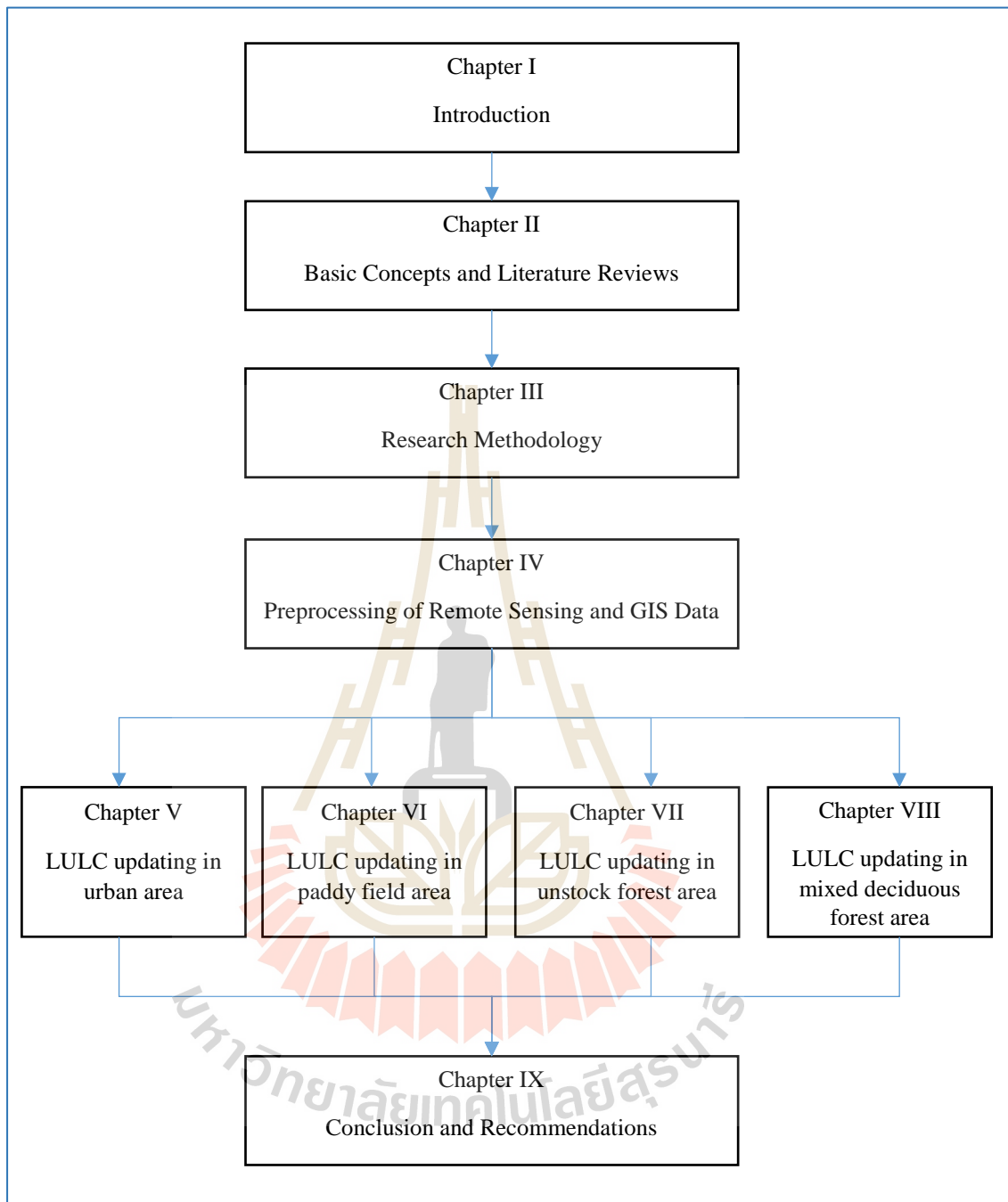


Figure 1.6 Structure of the thesis.

CHAPTER II

BASIC CONCEPTS AND LITERATURE REVIEWS

The related concept and theories to the thesis includes land use classification system and mapping of Lao PDR, object-based image analysis (OBIA), object-based change detection (OBCD) and its literature review are here briefly summarized.

2.1 Land use classification system and mapping of Lao PDR

National land use classification of Lao PDR is classified into two levels (level I and II). At level I, 4 main classes include forest land, other wooded land, other land and water. Detail of land use classification system at level I and II is presented in Table 2.1 while definition of each category of both levels is separately described in Tables 2.2 and 2.3.

Meanwhile, workflow of land use mapping which was described by Mr. Soukanh Bounthabandid, Forest officer, Forest Inventory and Planning Division is schematic displayed in Figure 2.1. Major step can be summarized as follows:

Remote sensing data (satellite image and aerial photographs) are normally used to extract land use by visual interpretation and digital image analysis. For digital image processing, it is frequently performed by authorized office such as Forest Inventory and Planning Division using ERDAS Imagine software.

Table 2.1 Land use classification system of Lao PDR.

Level I	Level II	Code
Forest land	Dry dipterocarp forest	15
	Upper dry evergreen forest	11
	Lower dry evergreen forest	12
	Mixed deciduous forest	13
	Gallery forest	16
	Coniferous forest	17
	Mixed coniferous /broadleaved	18
	Plantation	19
	Bamboo	21
Other wooded land (OWL)	Rest temporarily unstock forest	22
	Savannah / open woodlands	31
	Heath/scrub forest.	32
Other land (OL)	Rai (Upland rice)	24
	Paddy field	41
	Agriculture plantation	42
	Other agriculture	43
	Land, barren lands/ rock	51
	Grassland	52
	Urban areas	54
	Other land	55
	Swamps.	53
Water		61

Source: Somchay (2015).

Table 2.2 Definition of land use class at Level I (Somchay, 2015).

Land use class	Definition
Forest land	Land spanning more than 0.5 hectares with trees higher than 5 meters and a canopy cover of more than 10 % or trees able to reach these thresholds in situ. It does not include land that is predominantly under agricultural or urban land use.
Other wooded land	Land not classified as “Forest” spanning more than 0.5 hectares with trees higher than 5 meters and a canopy cover of 5-10 % or trees able to reach these thresholds; or with a combined cover of shrubs bushes and trees above 10 %. It does not include land that is predominantly under agricultural or urban land use.
Other land	All land that is not classified as “Forest” or “Other wooded land”.
Water:	The land use class Water includes rivers, water reservoirs (i.e. ponds and dams for irrigation and hydro power) and lakes. Water reservoirs and lakes should have an area of 0.5 ha and rivers should be at least 10m wide to be classified as Water. In other cases it should be joined to adjacent land use class.
Dry dipterocarp forest	The dry dipterocarp forest occurs in open stands. The tree diameter is comparably small and the height of the stand varies from 8 to 25 m. The crowns do not spread out widely. This type of forest is normally found in places with shallow soil, where the hard pan emerges above the ground, and on laterite soil. On the most poor and shallow soils the trees are crooked and do not exceed 10 m in height: If the crown cover is less than 20 % and the stand is undisturbed the vegetation type should be classified as Savannah.
Upper dry evergreen and Lower dry evergreen:	The evergreen forest type is a multi-stories forest consisting of more than 80% trees of evergreen species. Most of the trees have long and cylindrical boles, many of them with a big buttress. Usually, the height of the trees of the upper storey type is more than 30 m. Another typical characteristic of this forest type are climbers and lichen on the tree stems. Bamboo is usually not found except when the canopy has been opened. Evergreen forest located at an altitude above 200 m is classified as Lower Evergreen Forest.

Table 2.3 Definition of land use class at Level II (Somchay, 2015).

Land use class	Definition
Gallery forest	Gallery forest is not characterized by tree species composition but it could be either deciduous or evergreen. Clues used for identification of this forest type are the occurrence of some other land use types in its vicinity such as stream and villages. In areas where streams are likely to overflow seriously, the forest is often left along the low bank of the streams (both persistent and intermittent ones) forming a long band of forest with the streambed on one side and, for example paddy fields on the other. The width of the Gallery Forest will not be more than 100 m.
Coniferous forest	Coniferous forest is usually single storey and open but the young growth may sometimes form a dense second storey. This forest type occurs in higher elevations with a cool climate. The characteristic species of this type are pines (<i>Pinus kesiya</i> or <i>Pinus merkusii</i>) but other coniferous trees such as <i>Cunninghamia</i> may also be predominate.
Mixed coniferous and Broadleaved	Mixed coniferous forest is a transition type between the coniferous and the broadleaved forest types. The coniferous trees could be mixed with either deciduous or evergreen trees. It is also found in higher elevations.
Bamboo	If an area is covered with bamboo and the over storey has a crown cover less than 5% it should be classified as bamboo. Abandoned field (“Rai”) is often recovered by bamboo. Some species of bamboo may last for many years. Bamboo brakes may vary in height from 2 m to 25 m depending on their species. If the bamboo represents less than 80% of the total vegetation cover of the under storey I the vegetation type should not be classified as bamboo.
Unstock forest	If an area is covered with bamboo and the over storey has a crown cover less than 5% it should be classified as bamboo. Abandoned filed (“Rai”) is often recovered by bamboo. Some species of bamboo may last for many years. Bamboo brakes may vary in height from 2 m to 25 m depending on their species. If the bamboo represents less than 80% of the total vegetation cover of the under storey I the vegetation type should not be classified as bamboo.

Table 2.3 (Continued).

Land use class	Definition
Other agriculture land	Agricultural land being used for other agricultural purposes than agricultural crop cultivation, i.e. grazing of cattle, should be classified as Other Agricultural Land, unless the tree cover exceeds 20%. In that case it should be classified as some type of Current Forest depending on the tree species composition.
Upper mixed deciduous and Lower mixed deciduous	Mixed deciduous forest type the deciduous tree species represent more than 50% of the stand. The forest stories are not as dense as evergreen type. Most often bamboo occurs in this type of forest. Mixed deciduous forest located at an altitude above 200 m is classified as Upper Mixed deciduous forest. Mixed deciduous forest locates at an altitude of 200 m and below is classified as lower mixed deciduous forest.
Wood plantation	Forest plantation, the planted trees could still be identified (i.e. by even height, even spacing or by species typical for plantations) although they may be mixed up with other non-cultivated plants. All sustainable plantations including young ones with a crown density less than 20% should be classified as forest plantations. Rubber plantations are also classified as forest plantations. Coffee, tea and shade providing trees for coffee and tea as well as fruit trees are not classified as forest plantations.
Upland rice (Rai)	Upland rice is an area where the forest has been cut and burnt for temporary cultivation of rice and other crops. The area should be classified as Upland rice from the time of clear cut until one year after it has been abandoned. Areas being prepared for clear cut but not yet clear cut and areas that have been abandoned for more than 1 year should not be classified as Upland rice.
Savannah/open wood land:	The Savannah is an area where the soil conditions are unsuitable for tree growth as well as agriculture production. The tree cover in the Savannah should be at least 1% but not more than 20%. The trees are drought resistant and mostly short with graminaceous and herbaceous plants forming an understory. Savannah should not be mixed up with those grass covered areas that sometimes occur after shifting cultivation. Normally, the Savannah does not occur on steep slopes but in plain areas.

Table 2.3 (Continued).

Land use class	Definition
Heath, scrub forest	This is an area covered with scrub and stunted trees. The soil is shallow and rocky.
Agriculture plantation	Areas of agricultural land being used for production of other crops than rice, i.e. various kinds of vegetables, for fruit tree cultivation etc. Plantations with cash crops, such as coffee, tea, cocoa and cotton are also referred to this land use class.
Swamps	Swamps are areas where the soil is saturated with water. The soil may basically be fertile but the lack of oxygen limits its agriculture or forest-production capacity. The Swamp could have a high ecological or environmental value and the flora and fauna may be rich. The typical tree species found in the Swamps are trees which can grow in water, i.e. <i>Adina cordifolia</i> , <i>Rhus succedanea</i> and <i>Barringtonia acutangula</i> .
Barren land, Rock	Unfertile or seriously degraded land on shallow soil and rocky areas on which neither trees nor grasses can grow.
Grassland	Unfertile or degraded land on which no trees or shrubs grow. It might be an area that is too dry for tree growth that has been covered by grasses. It could also be an area that has originally been covered by trees which has been heavily disturbed by cutting and fire and gradually depleted. One reason for the absence of trees could be that of big areas have been deforested that the seed supply from surrounding forest has ceased. Areas being burnt over and over again (every year) for production of fodder I for hunting purposes etc. could also be classified as Grassland. That type of Grassland could be found on higher elevations in the Northern part of Laos. Grassland could also occur on deep sand with high moisture content.
Urban area	Urban Areas include all areas being used for permanent settlements such as villages, towns, public gardens etc. It also includes roads having a width of more than 5 m and areas under electric high power lines. Any type of land under high power lines, except Paddy Field, should be classified as Urban Areas.
Paddy field	Areas permanently being used for rice cultivation. Old paddy that has been abandoned and not. Been in use for more than one year should not be classified as Paddy Field.

For ground verification and correction of the preliminary land use map, it is performed by Forest Inventory and Planning Division, Ministry of Agriculture and Forestry.

After that, Department of Forest Resources Management under Ministry of Natural Resources and Environment will compile land use data for land use production at Department of National Geography under Ministry of Home Affairs.

The final land use map are produced with specific detail at three scales: land use and forest type map, 1: 50,000, standard topographic map with grid coordinate, 1: 100,000 and provincial land use map, 1: 250,000

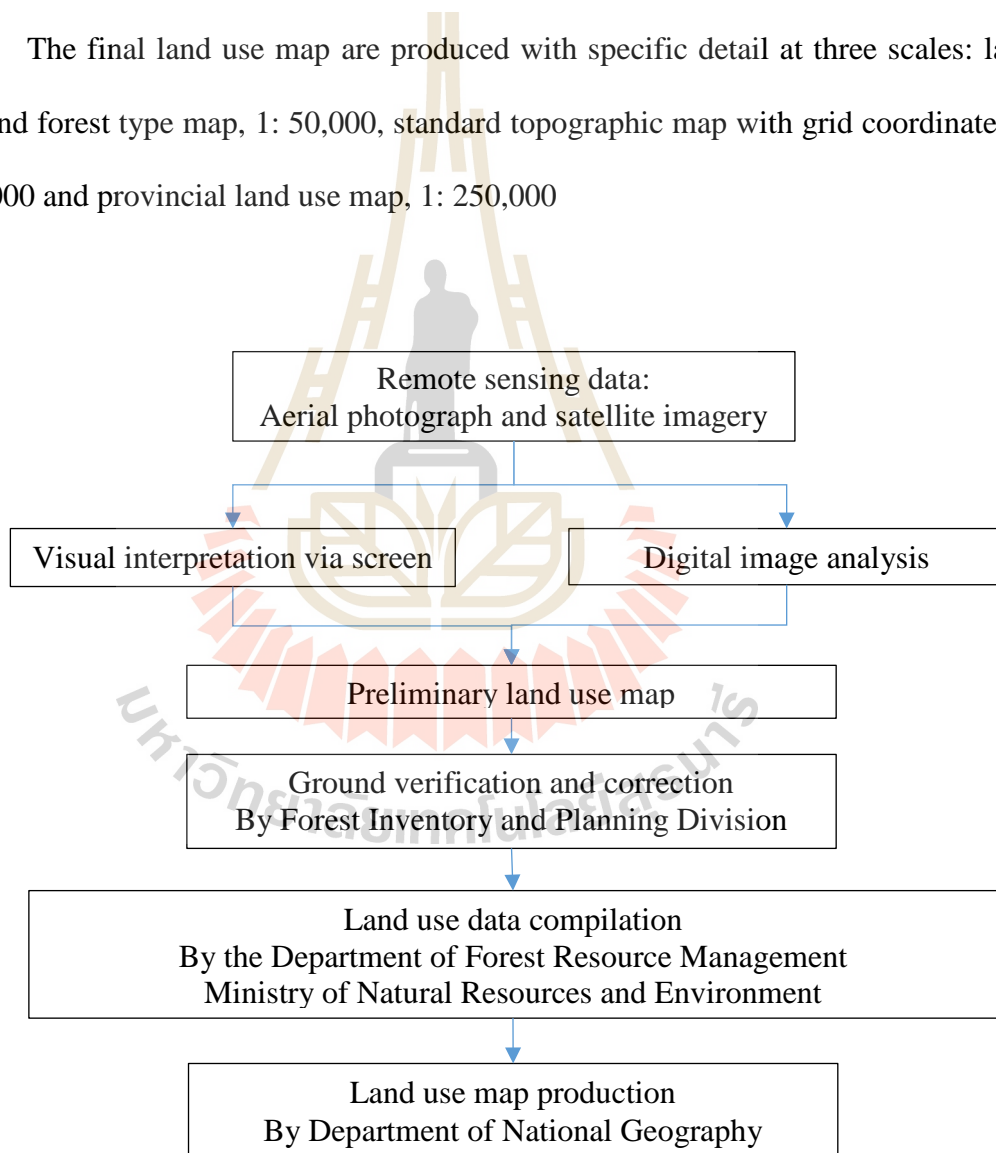
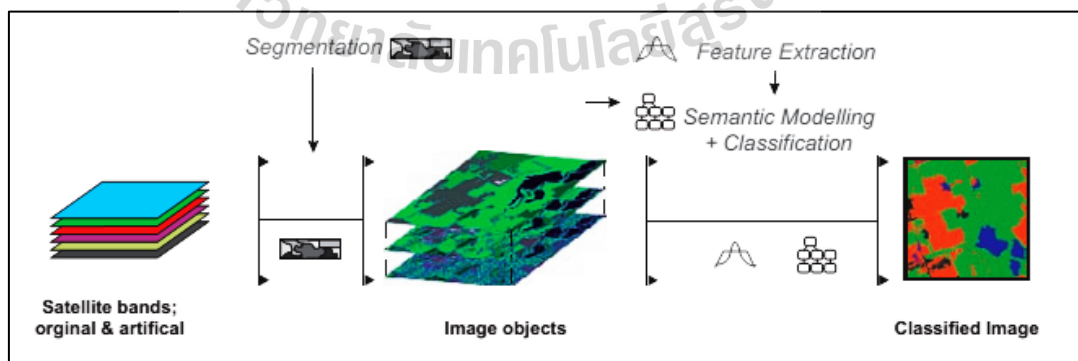


Figure 2.1 Schematic workflow of land use mapping.

2.2 Object-Based Image Analysis (OBIA)

The OBIA are patches or segments by used multi-resolution image segmentation process that used with very high-spatial-resolution imagery. An object can be defined as a grouping of pixels of similar spectral and spatial properties. Thus, applying the object-oriented paradigm to image analysis refers to analyzing the image in object space rather than in pixel space, and objects can be used as the primitives for image classification rather than pixels, which that became an area of increasing research interest in the late 1990s, is a contextual segmentation and classification approach that may offer an effective method for overcoming some of the limitations inherent to traditional pixel-based classification of very high resolution (VHR) images. Particularly, the OBIA can overcome within-class spectral variation inherent to VHR imagery (Yu, Gong, Clinton, Biging and Shirokauer, 2006).

Nussbaum and Menz (2008) suggested an operational workflow for OBIA using eCognition software as shown in Figure 2.2. Herewith major tasks of OBIA are consist of (a) image segmentation, (b) feature extraction and (c) semantic modelling and classification. Detail of each task is separately described in the following sections.



Source: Nussbaum and Menz (2008).

Figure 2.2 Workflow of object-based image analysis in eCognition software.

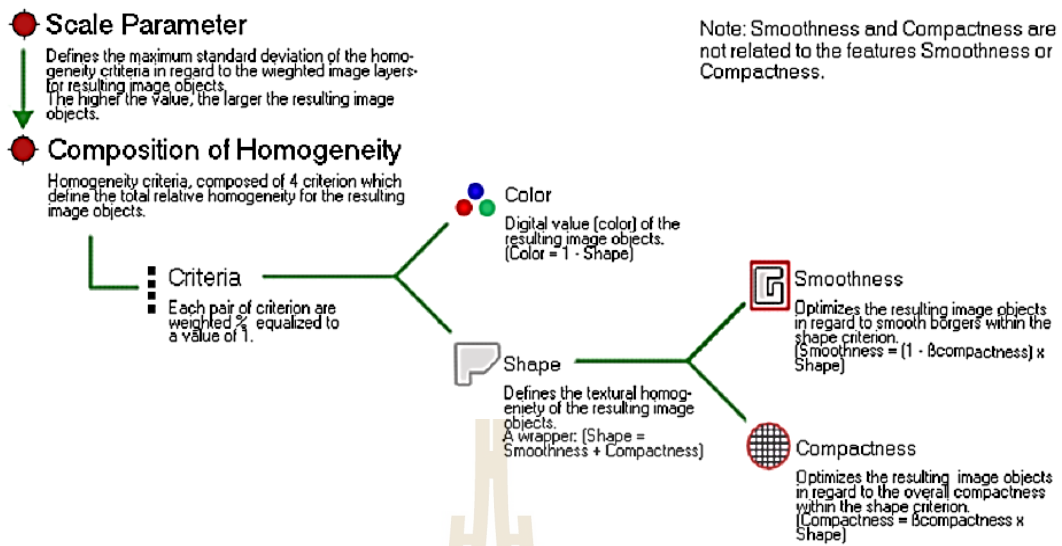
2.2.1 Multiscale (multiresolution) image segmentation

To success segment an image, it is imperative to take into account the scale at which the objects of interest occur in conjunction with the spatial resolution of the image. In most cases, it is not possible to specify the exact scale level beforehand as there is no universally “ideal” scale for all features. This is especially true in urban areas where ground objects occur at a unique scale of their own. The appearance and characteristics of even the same type of objects vary with the scale of their rendition on satellite imagery. Segmentation of such objects must take place at multiscales. Scale is a unit less parameter related to image resolution. Thus, multiscale segmentation is synonymous with multiresolution segmentation. Analysis at multiresolution is necessitated by the fact that not all ground features occur at the same physical scale. The best segmentation result is achievable by segmenting an image at different scales (Burnett and Blaschke, 2003).

In multiresolution segmentation the input image is first segmented at a small scale by uniting the most similar objects, followed by a set of multiscale objects with their topological relationship fully obtained (Sun, Chen and Li, 2006). During multiresolution segmentation, the image is converted into object primitives that share a certain spectral behavior, shape, and context. These preliminary object features are then segmented at a higher level.

Multiresolution segmentation is a bottom-up region-merge starting with singular seed pixels, each of which is regarded as a potential region. In subsequent steps, these small regions are merged to form fewer big ones. A pair of neighboring image objects is evaluated to see if they meet the merging criteria. Whether adjoining objects should be merged is governed by the principle of

homogeneity or lack of it (i.e., heterogeneity). Specifically, a merge should result in minimal growth in the selected heterogeneity criteria. Commonly used amalgamation criteria include area, perimeter, compactness, texture, and shape, all of which are derived from the segmented regions. Determination of their specific values is critical to achievement of segmentation results suitable for a particular type of application. Objects grow in size through successive iterations in which small objects are incrementally merged to form larger ones. This pairwise clustering is accompanied by an even and simultaneous growth of segments over a scene, and the calculation of the above indices for the newly formed objects. Such indices are applied to determining whether they should be amalgamated to form a large object after evaluation against a number of object properties. Expert knowledge may be involved in forming objects at different scales. As the merging process continues, the merged object becomes increasingly heterogeneous. Hence, the heterogeneity criterion must be updated following every merge. It is imposed as a constraint on the merging process. The break-off criterion or the stop criterion is based on the relationship between these two objects and the comparison with the squared scale parameter. The merging process is terminated if all pixels have been assigned to regions or when the threshold derived from the user-defined parameters is reached (Baatz and Schäpe, 2000). Summary of multiresolution concept by eCognition Developer software are presented in Figure 2.3 while an example of multiresolution image segmentation over Suranaree University of Technology campus is displayed in Figure 2.4.



Source: Trimble Germany GmbH (2011).

Figure 2.3 Multiresolution concept flow diagram.

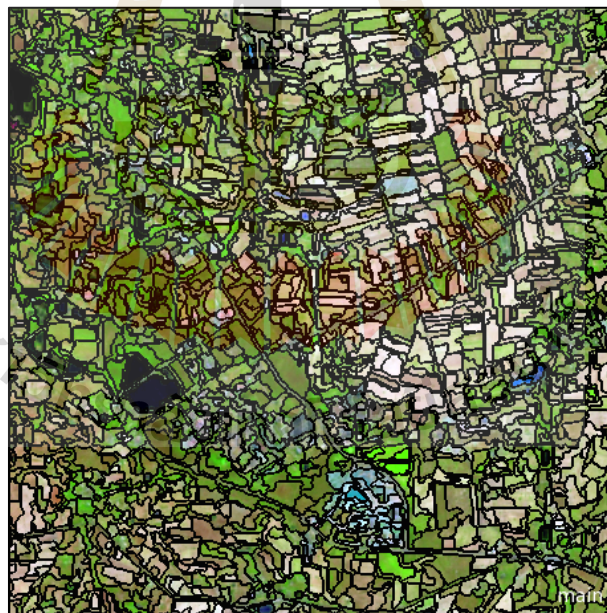


Figure 2.4 Multiresolution segmentation of Landsat-8 data acquired date: 07 May 2016, with scale of 10, Color=0.9, Shape=0.1, Compactness and Smoothness = 0.5.

2.2.2 Feature extraction

The OBIA is a promising methodology as it is close to human perception. A typical object-based classification system starts with segmenting the image into smaller homogeneous regions (or image objects). These objects correspond to approximations of real-world objects. Every object is characterized by several features defined based on layer values, texture, shape and context of the object. This is where the possibility to automate the classification process becomes difficult. With a few input samples for every class and using the enormous object feature-space to our advantage, it is possible to automatically generate a rule base. However, the essential issue is to manage the huge information given by the color, shape, texture and context of the object. A good feature extraction is a basic prerequisite for successful work in OBIA. So, SEaTH (**SE**parability and **TH**resholds) analysis which was introduced by Nussbaum and Menz (2008) for feature extraction are here summarized.

(1) SEaTH analysis

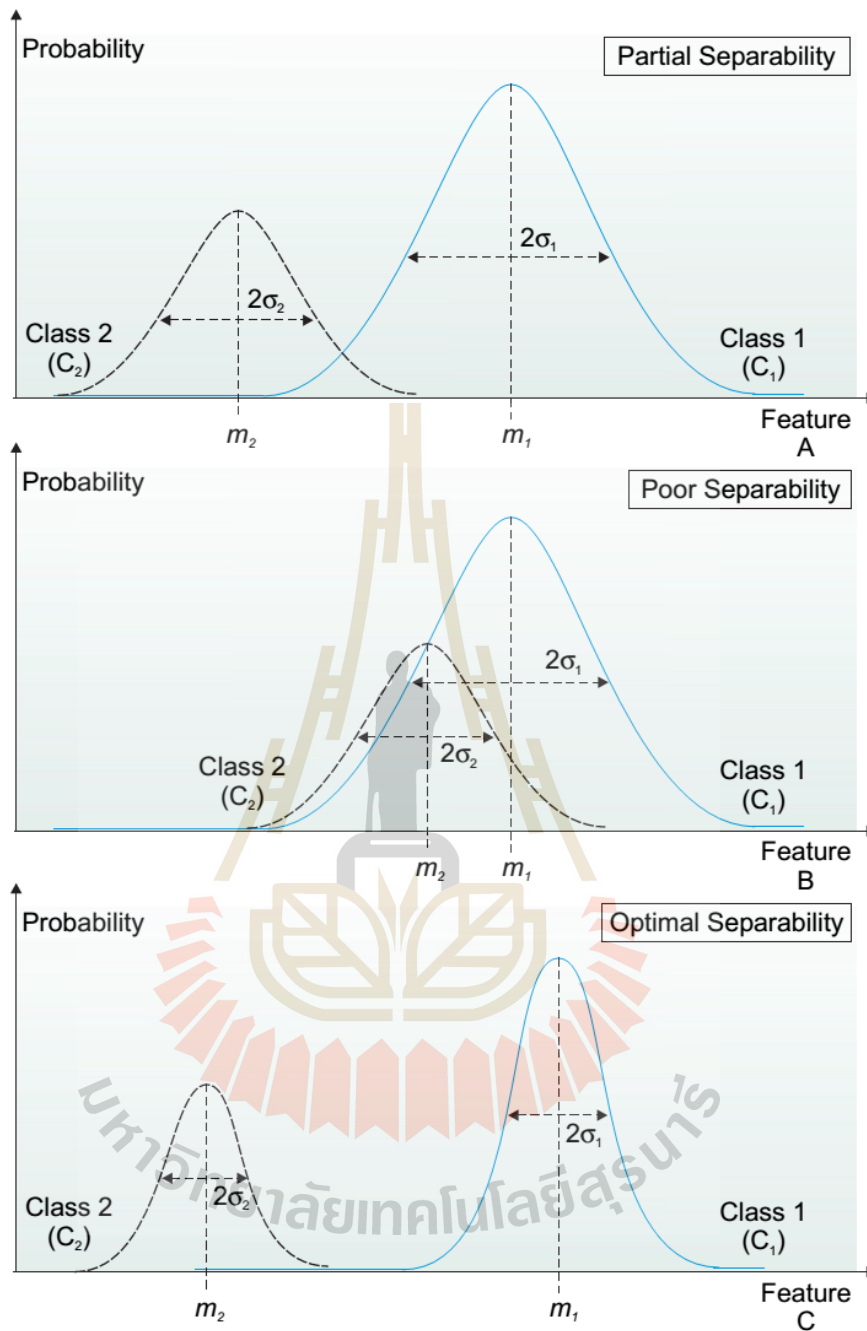
The feature extraction tool of SEaTH analysis identifies separability and thresholds characteristic features with a statistical approach based on training objects. These training objects represent a small subset out of the total amount of image objects and should be representative objects for each object class. The statistical measure for determining the representative features for each object class is the pairwise separability of the object classes among each other. Subsequently, SEaTH analysis calculates the threshold values which allow the maximum separability in the chosen features.

On the basis of representative training data for each object class, the probability distribution for each class can be estimated and used to calculate the separability between two object classes. Under the assumption of normal probability distributions, the Bhattacharyya distance (B) is used as a suitable separability measure. Bhattacharyya distance is justified as a measure of separability from the Bayesian decision rule for misclassification probability as:

$$B = \frac{1}{8} (m_1 - m_2)^2 \frac{2}{\sigma_1^2 + \sigma_2^2} + \frac{1}{2} \ln \left[\frac{\sigma_1^2 + \sigma_2^2}{2\sigma_1\sigma_2} \right] \quad (2.1)$$

Where, m_i and σ_i^2 , $i = 1, 2$, are the mean and the variance, respectively, for the two feature distributions. If the means coincide, the first term vanishes, whereas the second term vanishes if the two feature distributions have equal variances

Figure 2.5 shows the probability distribution exemplified for two object classes (C_1 and C_2) and three notional feature (A, B and C). In feature A both object classes show a *partial separability*, this means that there is an area where the probability distributions of the object classes (C_1 and C_2) overlap in their feature characteristic. Given feature B this overlap is so large that its use for classification would result in a huge object misclassification rate. This feature therefore provides *poor separability* relative to object classes C_1 and C_2 . The ideal case is represented by feature C. Here the object classes have no overlap in the feature characteristic it is therefore well-suited for classification: the feature has *complete separability*.



Source: Nussbaum and Menz (2008).

Figure 2.5 Examples of probability distributions.

A more useful measure for separation in classification contexts is the Jeffries–Matusita distance (J) which has, unlike Bhattacharyya distance, a finite dynamic range. This allows a better comparison of the feature analysis results to identify that feature which has the best separability. The Jeffries–Matusita distance measures the separability of two classes on a scale [0–2] in terms of Bhattacharyya distance (B) as:

$$J = 2(1 - e^{-B}) \quad (2.2)$$

Complete separability of the two classes with respect to the analyzed feature is indicated by $J = 2$. On the basis of the training objects used, there will be no misclassifications if this feature is used for classification. The lower J is, the worse is the separability and the higher the number of misclassified objects. SEaTH analysis calculates the separability for any number of given object classes and object class combinations.

Besides determining the features separating optimally the object classes among each other, it is essential to know also the decision threshold for the maximum separability. The knowledge of the optimum threshold is necessary for the assembly of a ruled-based classification model.

The optimum threshold is calculated by SEaTH analysis using a Gaussian probability mixture model of the form:

$$p(x) = p(x|C_1)p(C_1) + p(x|C_2)p(C_2) \quad (2.3)$$

is fit to the frequency distribution of a feature for two object classes C_1 and C_2 where $p(x|C_1)$ is a normal distribution with mean, m_{C_1} and variance, $\sigma^2_{C_1}$ and similarly for $p(x|C_2)$. The decision threshold, which minimizes the error probability is obtained by solving.

$$p(x|C_1)p(C_1) = p(x|C_2)p(C_2) \quad (2.4)$$

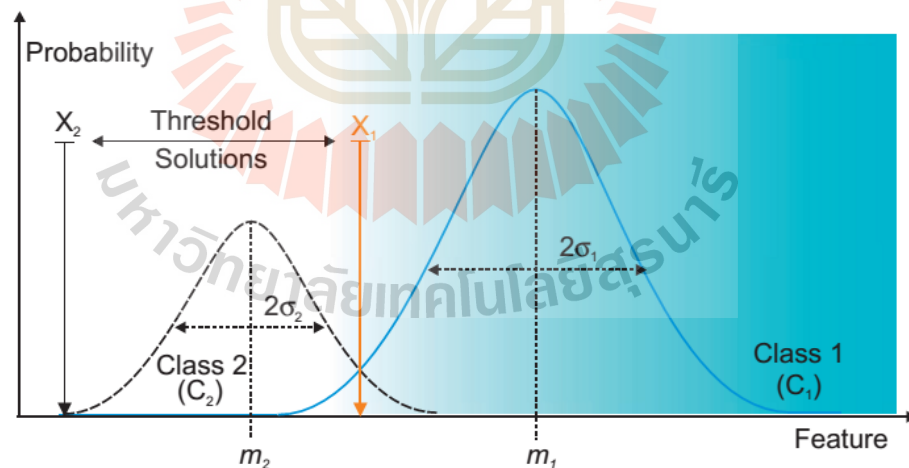
for x . Taking logarithms,

$$\frac{1}{2\sigma_{C_2}^2}(x - m_{C_2})^2 - \frac{1}{2\sigma_{C_1}^2}(x - m_{C_1})^2 = \log \left[\frac{\sigma_{C_1}}{\sigma_{C_2}} * \frac{p(C_2)}{p(C_1)} \right] = A \quad (2.5)$$

$$x_{1(2)} = \frac{1}{\sigma_{C_1}^2 - \sigma_{C_2}^2} \left[m_{C_2}\sigma_{C_1}^2 - m_{C_1}\sigma_{C_2}^2 \pm \sigma_{C_1}\sigma_{C_2}\sqrt{(m_{C_1} - m_{C_2})^2 + 2A(\sigma_{C_1}^2 - \sigma_{C_2}^2)} \right] \quad (2.6)$$

Where m_i , σ_i^2 and σ_i are the mean, variance, and standard deviation respectively, for the two classes, C_1 and C_2 .

The relevant solution of the two can be determined by requiring that it lies between the two means m_1 , m_2 of the probability distributions. Thus, for the example in Figure 2.6, x_1 is the correct choice. Since the distributions are only partially separated, there will be some misclassifications when using this feature for classification of unknown object classes.



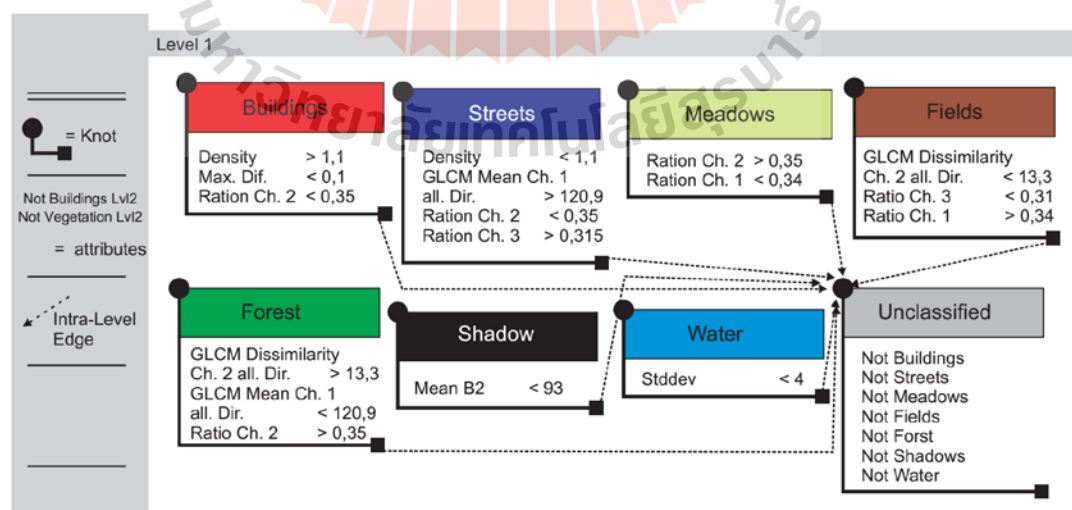
Source: Nussbaum and Menz (2008).

Figure 2.6 Threshold identification.

2.2.3 Semantic modeling and classification

Under OBIA, an object can be described by characteristic features such as its spectral signature, shape, size, texture and neighborhood relations to other objects. These representative features enable a later classification into object classes. For semantic modelling, these typical features of the object classes must first be determined by feature extraction as aforementioned and combined in a semantic model as rule-based dataset. Figure 2.7 shows the classification model developed from the SEaTH analysis for land cover extraction.

After that, the semantic classification is performed, dividing the image objects into object classes. The semantic classification determines whether or not an object belongs to a certain object class on the basis of its significance. A rating function determines a level of confidence by comparing the individual features of the object to be classified with the attributes. This confidence level provides information about whether the object belongs a class, so that the rating various approaches (Nussbaum and Menz, 2008).



Source: Nussbaum and Menz (2008).

Figure 2.7 Classification model of Research Centre Juelich (FZJ).

In Figure 2.7 the individual object classes are shown with the associated classification rules. The dotted arrows represent an internal linkage, which is termed the “intralevel edge” in semantic modelling. The class unclassified is thus simply composed of all image objects that do not belong to any other object class.

2.3 Object-based change detection (OBCD)

Change detection is the process of identifying and quantifying temporal differences in the state of an object or phenomenon (Singh, 1989). When using remotely sensed imagery from two acquisition times, each image pixel or object from the first time can be compared with the corresponding pixel or object from the second time in order to derive the degree of change between the two times. (Niemeyer, 2003).

It is not easy to determine the most appropriate method of detecting changes in a particular area under study because of the varying nature of the physical characteristics of the features of interest, problems with image registration, cloud/haze detection, sensor anisotropy or hysteresis, advantages and disadvantages of change detection methods themselves and lack of knowledge about approach (Macleod and Congalton, 1998; Nielsen, Conradsen and Simpson, 1998). In general, to select a suitable method of detecting change is very significant because there is no single method that is can be efficiently applied to all study areas. Selection of an appropriate change-detection technique, in practice, often depends on the nature of the change detection problem under investigation, which considers a critical step in change detection studies, the requirement of information, application, the data sets availability and quality, time and cost constraints of the data sets, analysis skill and experience, and registration of multiple image data sets (Macleod and Congalton,

1998; Johnson and Kasischke, 1998; Nielsen, Conradsen and Simpson, 1998; Cracknell, 1998; Dai and Khorram, 1998). Regardless of the technique used, the success of change detection from imagery can be affected by many factors: the quality of image registration between multi-temporal images, the atmospheric conditions, acquisition times, illumination, viewing angles, soil moisture, noise, shadow present in the images (Singh, 1989), vegetation phenological variability or differences (Lu, Mausel, Brondizio and Moran, 2002; Rogan, Franklin and Roberts, 2002) and sensor calibration (Lillesand and Keifer, 1994). In addition to the landscape and topography characteristics of the study areas, analyst's skill and experience, selection of the change detection technique, besides, the different steps during the implementation of change detection procedure that can produce problems and errors and affect the success of change detection, for example, image pre-processing (Lu, Mausel, Brondizio and Moran, 2004; Jensen, 2005)

The state of the art, object-based change detection (OBCD) algorithms are classified into four categories (Chen, Hay, Carvalho and Wulder, 2012): Image-object, Class-object, Multi-temporal-object and Hybrid change detections.

2.3.1 Image-object change detection

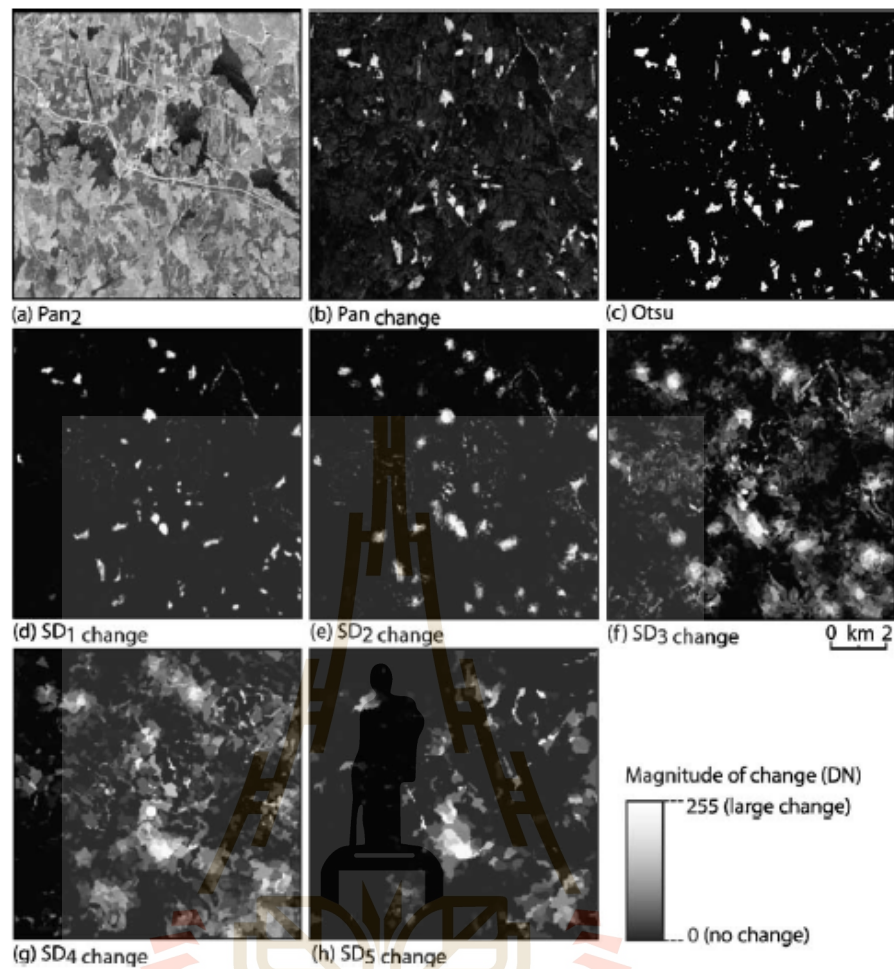
Similar to pixel-based change detection, OBCD can be performed by directly comparing image-objects defined by a threshold. Typically, multi-temporal images are segmented separately with change analysis based on an object's spectral information (e.g. averaged band values) or other features extracted from the original objects (e.g. image-texture and geometry). The OBCD algorithms that emphasize direct image-object comparisons are grouped as image-object change detection (Chen, Hay, Carvalho and Wulder, 2012).

Miller, Pikaz and Averbuch (2005) presented an OBCD algorithm to detect the change of significant blobs (i.e. objects) between a pair of grey-level images. Two main steps were used. First, objects were extracted by using a connectivity analysis. Second, each object from the base image was searched for a corresponding object in another image. To detect whether two corresponding objects were really different (i.e. changed), a matching method was used to capture the relationship between two object boundary pixels. By applying this object-based concept, the authors argued that the proposed algorithm worked for noisy input images and that no pre-defined windows were required, as processing was directly undertaken on the extracted objects. Lefebvre, Corpetti and Hubert-Moy (2008) further evaluated the use of geometry (i.e. size, shape and location) and content (i.e. wavelet transform-derived texture) information in OBCD. Their qualitative results indicated that both object contour and texture features were effective to detect changes in very high-resolution airborne images at the sub-meter level and further recommended the application of their algorithm to spaceborne images.

The major advantage of image-object change detection is the straightforward comparison of objects. The algorithms are also easy to implement. Typically, all objects are directly extracted through image segmentation, and steps, such as image differencing, are similar to those in pixel-based change detection or simple GIS intersection operations. However, as objects are of different sizes and shapes, a critical procedure is the search for spatially 'corresponding' objects in multi-temporal images. Errors in locating these objects will potentially lead to incorrect change detection results. This might explain why the direct comparison approach is suitable for detecting specific objects of interest, such as artificial landscape features

(Miller, Pikaz and Averbuch, 2005; Gong, Sui, Sun, Ma and Liu, 2008). Another challenge with image-object change detection is the requirement to select an appropriate change threshold. Since the threshold value is often intuitively defined by researchers, a bias may be introduced.

The aforementioned studies have been conducted at one certain scale. To delineate image-objects and identify their change through scales, (Hall and Hay, 2003) developed an OBCD framework by first segmenting panchromatic SPOT scenes from two dates and then directly applying an image differencing method to detect object changes at different up-scaled resolutions (Figure 2.8). The final step involves identifying areas of change in derived datasets. The change detection strategy used here is image differencing. Image differencing is a straightforward and commonly used method in remote sensing with the purpose to access the degree of change between two dates on a pixel by pixel basis (Dale, Chandica and Evans, 1996). A general problem with image differencing is that the maximum difference (in 8-bit data) ranges between -255 to +255, thus the result of the subtraction operation requires scaling to a suitable range (i.e. 0-255). Consequently, no change (i.e. zero value) is replaced with 127. Value greater than 127 indicate change in one temporal direction, and values below 127 represent change in the opposite direction. Due to its ease in processing and visualization, the author have used the absolute (Abs) difference between dates: $Abs [Pan1 - Pan2]$.



Source: Hall and Hay, 2003.

Figure 2.8 Change dataset: (a) original SPOT image, (b and c) change dataset in original scale, (d to h) multi-scale change dataset.

2.3.2 Class-object change detection

A direct comparison of image-objects cannot readily indicate the “from-to” change of landscape classes (i.e. from clear-cut to vegetation), which requires additional classification information. The class-object change detection represents a group of OBCD algorithms that detect landscape changes by comparing the independently classified objects from multi-temporal images. Since each object belongs to a specific class, the object comparison step in OBCD has no need to consider features such as object spectral and texture values (Chen, Hay, Castilla, St-Onge and Powers, 2011). The update of existing maps or GIS layers is an immediate application for using class-object change detection.

Walter (2004) evaluated the importance of using different input channels (i.e. spectral and vegetation indices and texture) in an object-based classification, which led to different results when updating GIS layers. Chen et al. (2012) suggested that the assessment of additional object characteristics derived from laser data, texture measures and multi-temporal data would improve both classification and change detection performance. They note that in the aforementioned studies, GIS polygons (or the existing maps) were considered as the base layer, with the change classes updated from a comparison with single-date imagery. However, this is not the case in many other studies, which require creating objects from multi-temporal remote-sensing images.

Laliberte et al. (2004) conducted an object-based classification on 11 aerial photos and 1 QuickBird image spanning 67 years. As the authors were only interested in the change of vegetation area, the total change values were calculated without considering their change in spatial distribution. In related studies, the results

only involved a change map by directly overlaying two-date classified images or several change metrics, such as total area, mean nearest neighbor distance and mean elevation (Willhauck, Schneider, De Kok and Ammer, 2000; Owojori and Xie, 2005; Mouflis, Gitasa, Iliadoua and Mitria, 2008). Although multi-temporal data were processed in these studies, the change detection procedure emphasized the use of object statistics. To better understand how an individual object changes over time (such as spatial distribution, total area, perimeter, shape, complexity, etc.), additional efforts are required to compare each pair of the correspondingly classified objects. However, as discussed by Blaschke (2005), it is difficult to distinguish whether the object difference is due to real change or geometric inconsistency (e.g. caused by a misregistration error or a segmentation-induced difference). This leads to the development of a GIS conceptual framework, where a series of rules were defined by taking into account object size, shape and location (Blaschke 2005). Similar ideas were also applied in many other independent studies (Hazel, 2001; Li and Narayanan, 2003; Gamanya, De Maeyer and De Dapper, 2009; Grenzdörffer, 2005; De Chant and Kelly, 2009), with specific rules adapted to particular conditions. For example, since forest gap dynamics are important to monitor tree diseases, De Chant and Kelly (2009) converted raster polygons, classified as gaps, to vector layers and performed object intersection functions with GIS software. Changes were tracked by analyzing object metrics including perimeter, area, shape and Euclidean nearest neighbor. To detect military object changes, Hazel (2001) compared corresponding objects derived from two dates by calculating association confidence, which includes the spatial distance between the object centroids, the degree of spatial overlap, a distance between spatial and spectral feature vectors and differences in assigned classification

and classification confidence. Similarly, Li and Narayanan (2003) quantified lake change using a shape similarity measure.

In addition to geometric information, it is still valuable to use spectral and/or texture measures to compare the classified objects. In the studies conducted by He, Li, Zhang, Pan and Chen (2005) and An, Zhang and Xiao (2007), an object-based classification was simply used to detect possible' changed objects (e.g. non-urban to urban). Further verification of whether the change was real involved the calculation of object similarity using spectral and texture characteristics.

Change detection based on classified objects is a common type of OBCD approach, which can produce straightforward results (e.g. a change matrix) indicating the “from-to” landscape change. However, specific rules have to be defined to compare objects when GIS processing is involved. One interesting idea, referred to as object-fate (Schöpfer, Lang and Albrecht, 2008) is to define buffers of possibility or states of change around each object. Similar to pixel-based change detection, the performance of OBCD is also strongly influenced by the initial classification procedure. Details of pixel-based classification accuracy assessment have been discussed by Foody (2002) and Fuller, Smith and Devereux (2003). As for the object paradigm, classification accuracy is also related to the selection of appropriate image segmentation techniques, of which many exist (Pal and Pal, 1993). Practitioners must also note that error propagation in both segmentation and classification will affect the OBCD performance.

A detailed example of class-object change detection came from Durieux, Lagabrielle and Nelson (2008). They applied an object-based classification approach (using fuzzy membership functions) to extract urban sprawl building over 6

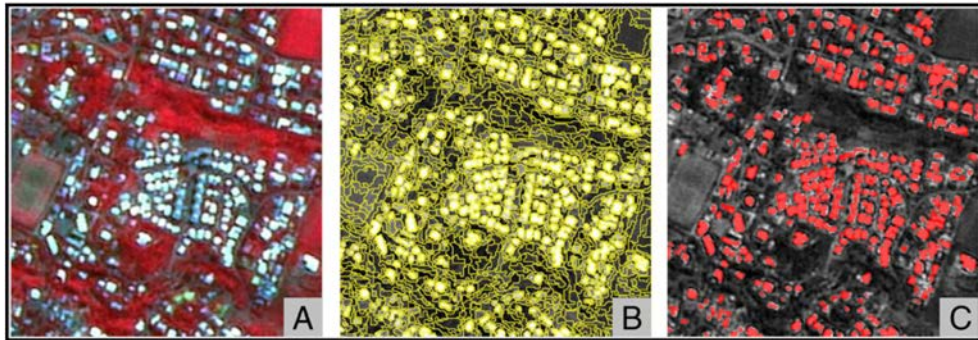
years from a 2.5 m SPOT mosaic covering an entire island of 2,512 sq. km. The processing chain of the building extraction was composed of the six following steps: (1) object-based cloud screening, (2) object-based multi-temporal image compositing, (3) tiling with overlap, (4) object-based image analysis for building extraction, (5) object-based image editing and (6) object-based stitching. Herein, the most important step was OBIA for building extraction.

In their study, building extraction from SPOT 5 images was done in three steps: creating a hierarchical network of image objects using the multi-resolution segmentation, classifying the derived objects by their physical properties and describing the semantic relationships of the network's objects in terms of neighborhood relationships or being a sub- or super-object. Image objects resulting from the coarse segmentation used for cloud screening were used as the first level of the hierarchical network. A second level was created with a much finer multi-resolution segmentation to reach building objects' scale (with a medium object size of 330 m²). A class hierarchy defining the class descriptions is built on this two level hierarchical network. Class descriptors are a combination of fuzzy membership functions used to describe intervals of feature characteristics wherein the objects do belong to a certain class or not by a certain degree of membership. A class is described by combining one or more class descriptors by means of fuzzy-logic operators and/or by means of inheritance.

On the first level, large bright objects such as sugarcane mulch and coral sand beach were identified based on fuzzy rule-sets using the following spectral features of the image objects: mean in the green channel, mean in the red channel, ratio in the green channel, and standard deviation in the red channel. Those features

were chosen according to an expert visualization of the different features of the objects obtained from the segmentation. Features that helped in identifying visually the large bright objects from the other objects were retained. The expert visualization defined also the boundaries of the fuzzy membership functions for each feature. A layer mean value and standard deviation were calculated from the layer values of all pixels forming an image object, while the ratio of the green layer is the green layer mean value of an image object divided by the sum of all spectral layer mean values. A minimum area threshold of 3,000 m² also described large bright objects.

On the second level, a first building class was described by fuzzy membership functions of the mean in the green channel, and the mean in the red channel. A second class was created to complete missing buildings not identified by the first class description. This class was defined with a membership function of the feature 'mean difference to neighbor of the green layer'. For each neighboring object, the green layer mean difference was computed and weighted with regard to the length of the border between the objects (if they were direct neighbors) or the area covered by the neighbor objects (if the neighborhood was defined within a certain perimeter (in pixels) around the image object in question). Both building classes' descriptions are also defined with a maximum object area and look at the super-object classification from level 1. If an object from level 2 has a super-object classified as a "large bright object", then it is not considered as a building in level 1. Finally, the two buildings classes were merged into one class (Durieux, Lagabrielle and Nelson, 2008). Figure 2.9 shows the second image object level and the classification result before manual editing.



Source: Durieux, Lagabrielle, and Nelson (2008).

Figure 2.9 Second image object level and automated classification. (A) SPOT 5 supermode R 2.5 m image. (B) Multi-resolution segmentation. (C) Building extraction (buildings in red).

2.3.3 Multi-temporal-object change detection

Images acquired from different dates rarely capture the landscape surface in the same way due to many factors including illumination conditions, view angles and meteorological conditions (Wulder, Ortlepp, White and Coops, 2008). Thus, segmentation-generated image-objects from different dates often vary geometrically, even though they represent the same geographic feature(s). Instead of separately segmenting multi-temporal images, the concept of multi-temporal-*object change detection* takes advantage of all multi-temporal states of the scene. Specifically, temporally sequential images are combined and segmented together, producing spatially corresponding change objects.

The pioneering work of Desclée, Bogaert and Defourny (2006) presented an explicit algorithm to implement a multi-temporal-object change detection approach. The authors segmented an entire multi-date image-set together followed by a calculation of its spectral features (i.e. mean and standard deviation) from each date for all image-objects. Finally, discrimination between changed and

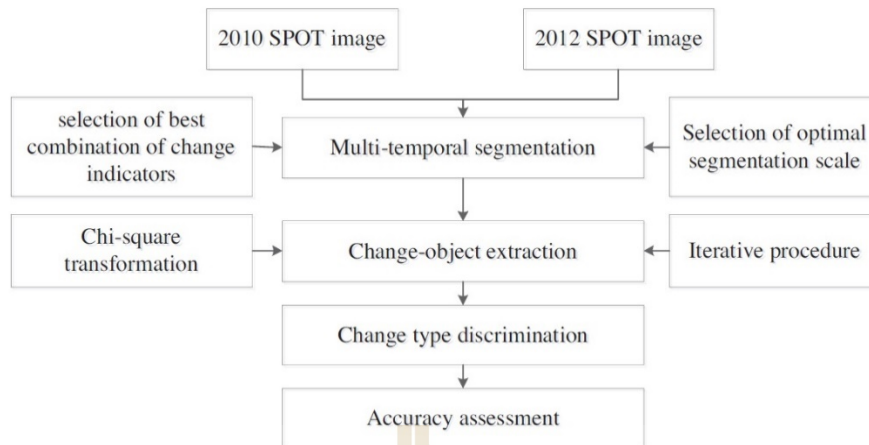
unchanged objects was performed using a statistical analysis based on the chi-square test. Using this approach, the authors reported high detection accuracy (>90%) and overall kappa (>0.80).

Following a similar approach, additional studies developed OBCD algorithms with an emphasis on developing new ways to characterize object-level change. Bontemps, Bogaert, Titeux and Defourny (2008) integrated the Mahalanobis distance calculation and a threshold method to identify change objects. Conchedda, Durieux and Mayaux (2008) used a nearest-neighbor supervised classification approach and reference data to quantify changes. Similarly, Stow, Hamada, Coulter and Anguelova (2008) compared a nearest-neighbor classifier and fuzzy membership functions to monitor shrub change with the results demonstrating superior performance using the nearest-neighbor classifier. Other studies evaluated several unsupervised solutions with the ISODATA classification algorithm (Duveiller, Defourny, Desclée and Mayaux, 2008) and change vector analysis (CVA) (Park and Chi, 2008).

In addition to comparing different classifiers, (Im, Jensen and Tullis, 2008) evaluated the performance of adding object correlation images and neighborhood correlation images within the classification feature space. Their results revealed that the incorporation of these new features produced more accurate change feature classes (kappa > 0.85). Rather than conducting a combined segmentation of multi-temporal images, (Li, Yeh, Qian, Ai and Qi, 2009) described an incremental segmentation procedure designed for radar imagery, where they started by (1) segmenting the first-date image, (2) treating the result as a thematic layer, then (3) segmenting the derived layer together with the second-date image. Their intent was

that the previous segmentation would constrain each subsequent segmentation so as to avoid inconsistent results when using unique segmentations (e.g. objects with varied boundaries). A single segmentation step using all multi-temporal images facilitates OBCD by creating image-objects consistent in size, shape and location coordinate over time. However, it is unclear whether this form of change detection is influenced by segmenting before- and after-change images together, as the same geographic location may have different objects. Similarly, the effect of mixed-object spectral information (from different atmospheric, meteorological, illumination and viewing angles) on change results remains to be explored.

Figure 2.10 displays an example of multi-temporal object change detection flowchart with medium spatial resolution by Yang, Liu and Gao (2015). It was composed of four stages: multi-temporal segmentation, changed objects extraction, change type discrimination and accuracy assessment. In the multi-temporal segmentation, they first selected the best combination of change indicators by the Optimum Index Factor (OIF). Then, the optimal segmentation parameters was selected using comparison index. In the changed objects extraction stage, they applied chi-square transformation to select a threshold to differentiate changed object from the unchanged ones, meanwhile they optimized the changed object class using an iterative procedure (Desclée, Bogaert and Defourny, 2006). In the change type discrimination, they discriminated the “from-to” change type for each changed object based on an unsupervised classifier, the ISODATA algorithm. In the last stage, a polygon-based accuracy assessment method was applied. This method was used for the accuracy assessment of both the changed/unchanged objects detection result and the change type discrimination.



Source: Yang, Liu and Gao (2015).

Figure 2.10 Workflow of multi-temporal object change detection with medium spatial resolution.

2.3.4 Hybrid change detection

The hybrid change detection algorithm involves the use of both object and pixel paradigms. A widely used hybrid approach comes from the idea that the preliminary change information should be derived from pixels and that object schemes should subsequently be applied to better extract the change results.

A novel hybrid change detection algorithm was proposed by Carvalho, Fonseca, Murtagh and Clevers (2001). The authors showed that wavelet inter-scale correlation computed from pixel-based difference images (e.g. differencing, ratioing, PCA, CVA) were effective to identify all land-cover changes over a study area. Region-growing segmentation was then performed to extract objects solely where changes occurred, avoiding the time-consuming task of segmenting all remotely sensed images. The authors concluded that this approach was insensitive to geometric misregistration and atmospheric discrepancies between the multitemporal images, as well as to differences in the phenological state of vegetation patches. This procedure

aids automation and, since 2003, has been used on an operational basis by the government of Minas Gerais, Brazil, to update vegetation maps. In another study, Al-Khudhairy, Caravaggi and Glada (2005) applied pixel-based PCA and image differencing to high-spatial-resolution imagery. The change images were then analyzed by an object-based classification, which improved upon the pixel-based change detection. In the studies conducted by McDermid et al. (2008) and Linke et al. (2009), multispectral images were transformed into wetness bands, which were effective for detecting forest disturbance (Franklin et al., 2001). This transformation was followed by a pixel-based image differencing using wetness information with an object-based classification applied to the changed areas. Niemeyer, Nussbaum and Canty (2005) used a similar procedure; however, their research emphasized the creation of pixel-based mutually orthogonal difference images, rather than employing the traditional image differencing method. Yu, Hyypä, Kaartinena and Maltamo (2004) applied segmentation to a difference image from a forest canopy height model, generated from small footprint, high sampling density LiDAR. Results showed that individually harvested trees were accurately delineated.

The hybrid algorithms that combined pixel and object-based schemes successfully reduced noisy changes, as well as the small and spurious changes introduced by the inconsistent delineation of objects McDermid et al. (2008). However, as many steps are involved in hybrid change detection, it remains unclear how the final change result are influenced by the different combination of pixel-based and object-based schemes.

2.4 Literature review

Gladstone, Gardiner and Holland (2012) used semi-automatic method for detecting changes to ordnance survey topographic data in rural environments. The input data is 4 bands aerial imagery (R, G, B, NIR) to create orthomosaic at the native multispectral capture resolution (a ratio of 3:1 to the pan resolution, so 45-75 cm GSD). A Digital Surface Model (DSM) at 50-75 cm GSD is generated automatically from the panchromatic imagery. The final input dataset is the topographic data. Being used as the comparison dataset for detecting changes. The image classification is a fully automatic process that requires no training data or calibration. This is achieved using a rule-based classification built using eCognition process tree.

Wang, He and Liu (2012) applied a new classification method for high spatial resolution remote sensing image based on mapping mechanism. This paper proposed a new object-based image classification method based on mapping mechanism for high spatial resolution remote sensing image. IKONOS including the pan band with the resolution of 1.0 meter and four multispectral images with the resolution of 4.0 meters and SPOT-5 satellite data including the pan band with the resolution of 2.5 meters and four multispectral bands with 10.0 meters were applied to make a series of experiments and comparative analysis on the mapping mechanism based classification method. The classification framework used a special mapping strategy to fit in the special data format and content of high spatial resolution remote sensing data. First, the multi spectral image was segmented by multiscale watershed segmentation and at the same time classified by a traditional pixel-based classification method (maximum likelihood); then the pixel-based multi spectral classification result was mapped to the segmentation result by area of dominant principle to get the object

based multi spectral classification result. In order to make good use of the information in the pan image, it was also segmented, and the final classification result was gotten by mapping the object-based multi spectral classification result to pan image segmentation result. Finally improve the classification accuracy.

Dupuy and Herbreteau (2012) studied land cover dynamics in Southeast Asia using object-oriented techniques for change detection. In this study, they investigated land cover changes at landscape level over a twenty-year period in seven sites located in Cambodia, Lao PDR and Thailand. For each site, they acquired high spatial resolution scenes from SPOT 1, 2, 3, 5 satellites at three dates from 1987 to 2008 and the SPOT scene was segmented using the 'multi-resolution segmentation' algorithm (eCognition developer software). The same segmentation parameters were used for all sites. In the first level of segmentation, water bodies and built-up areas were extracted using Boolean or fuzzy membership functions. Other objects were classified into different slope classes. These latter were classified in a second level of segmentation into different wooded and agriculture classes (e.g. rice field, rubber tree or teak plantations, secondary tropical rainforest) classes, based on a supervised nearest neighbor classifier requiring the selection of training samples. Classification accuracy was assessed by field observations and photo interpretation using Google Earth.

Walter (2004) applied object-based classification of remote sensing data for change detection to evaluate the importance of using different input channels (i.e. spectral and vegetation indices and texture) in an object-based classification. Basic input data include aerial photo, resolution of 2 m (four multispectral channels [blue 440-525 nm, green 520-600 nm, red 610-685 nm, near infrared 770-890 nm])

and existing GIS database. In this study, supervised maximum likelihood classification was performed in the first step, the training areas were derived automatically from GIS database. Then, the classified remote sensing data had to be matched with the existing GIS objects in order to find those objects where a change occurred, or which were collected wrongly in the second step,. The results showed that approximately 8.6% of all objects (82 objects from 951) were marked as changes. From 82 objects, 45% were real changes, 31% were potential changes, and 23% were wrongly classified. That means that the amount of interactive checking of the data can be decreased significantly. They can only distinguish between the land-use classes, forest, settlement, green land, and water. This can be refined if more object characteristics are evaluated. Some possible object characteristics are defined in this paper and have to be tested in future work.

Willhauck (2000) studied the comparison of object oriented classification techniques and standard image analysis for the use of change detection between SPOT multispectral satellite images and aerial photos. Two important features were presented. One was the classification of SPOT multispectral data for determination of land cover in Tierra del Fuego. The other was the use of object-oriented classification for change detection using aerial photos combined with SPOT multispectral data. SPOT multispectral in 1995, aerial photos from 1960, a vegetation map, digitized from the aerial photos covering about 50.000 ha of forest, GIS data covering infrastructure, water bodies, ownership and provincial as well as state boundaries

The significant contents of the reviewed literature on OBCD is synthesized in the Table 2.4 shown below.

Table 2.4 Summary of literature reviews for OBCD.

Topic	Year	Objective	Input	Process/Model	Result
(1). C. S. Gladstone, A. Gardiner, D. Holland Semi-Automatic method for detecting changes to ordnance survey topographic data in rural environments.	2012	-To create a semi-automatic for change detection in rural environment.	4 bands aerial imagery (R, G, B, NIR), Digital Surface Model (DSM), Digital Terrain Model (DTM), Topographic dataset.	Rule-based for image classification and identify changes between the imagery and the topographic database using eCognition software.	A trial of the method found 81.7% of the genuine changes, which require a map update, while 25.8% of the change candidates were genuine change. The automatic image classification could be used to filter DSMs to DTMs and whether it could contribute to a new land cover product for the Ordnance Survey.
(2).Guizhou Wang, Guojin He, Jianbo Liu. A new classification method for high spatial resolution remote sensing image based on mapping mechanism.	2012	-To classify high spatial resolution remote sensing image based on mapping mechanism.	IKONOS, SPOT-5 satellite data	Pixel-based classification (MLC) method and object-based segmentation and classification was integrated by mapping mechanism.	The classification result tested with two datasets show that the presented method can make use of the information both in pan and multispectral bands, integrate the pixel-based and object-based classification method, and finally improve the classification accuracy.

Table 2.4 (Continued).

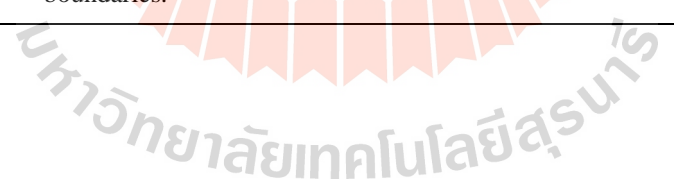
Topic	Year	Objective	Input	Process/Model	Result
(3). S. Dupuy, V. Herbreteau, T. Feyfant et al. Land cover dynamics in Southeast Asia: contribution of object-oriented techniques for change detection.	2012	To investigate land cover changes at landscape level over a twenty-year period.	SPOT1,2,3,5 satellite from 1987 to 2008, DEM.	Pre-processing included accurate spatial registration, radiometric calibration and resampling of the multispectral images to the higher resolution of the panchromatic, Segmented using Multiresolution segmentation algorithm and classification of the most recent scene. For change detection, new objects were delineated on older scenes using the same segmentation algorithm.	According to results, annual deforestation rates ranged from 0.65% to 1.84%, the highest changes rates being observed in Cambodia and Lao PDR.

Table 2.4 (Continued).

Topic	Year	Objective	Input	Process/Model	Result
(4). Volker Walter. Object-based classification of remote sensing data for change detection.	2004	To evaluate the importance of using different input channels (i.e. spectral and vegetation indices and texture) in an object-based classification.	Aerial photo, resolution of 2 m. Four multispectral channels [blue 440-525 nm, green 520-600 nm, red 610-685 nm, near infrared 770-890 nm]. Existing GIS database.	First step, supervised maximum likelihood classification. The training areas are derived automatically from GIS database. Second step, the classified remote sensing data have to be matched with the existing GIS objects in order to find those objects where a change occurred, or which were collected wrongly.	The results show that approximately 8.6% of all objects (82 objects from 951) are marked as changes. From these 82 objects, 45% are real changes, 31% are potential changes, and 23% are wrongly classified. That means that the amount of interactive checking of the data can be decreased significantly. They can only distinguish between the land-use classes, forest, settlement, green land, and water. This can be refined if more object characteristics are evaluated. Some possible object characteristics are defined in this paper and have to be tested in future work.

Table 2.4 (Continued).

Topic	Year	Objective	Input	Process/Model	Result
(5). G. Willhauck Comparison of object oriented classification techniques and standard image analysis for the use of change detection between SPOT multispectral satellite images and aerial photos.	2000	1. To classify land cover using SPOT multispectral data in Tierra del Fuego. 2. To apply object-oriented classification for change detection using aerial photos combined with SPOT data.	SPOT multispectral in 1995, Aerial Photos from 1960, A vegetation map, digitized from the aerial photos covering about 50.000 ha of forest, GIS data covering infrastructure, water bodies, ownership and provincial as well as state boundaries.	Pixel based classification with standard maximum likelihood classifier and object-oriented classification with rule base approach are applied to compare accuracy in the study. Concept to detect changes in the vegetation cover was to compare a vegetation map digitized manually from the aerial photos with the classification results of the satellite images.	The results showed that classification accuracy of the pixel based classification is 93.21% while classification accuracy of the object oriented classification is 96.09 %.



CHAPTER III

RESEARCH METHODOLOGY

The research methodology for semi-automatic land use and land cover map updating using OBCD is presented in Figure 3.1. It consists of three main components: (1) data collection and preparation, (2) development of rule set for LULC change detection and updating and (3) accuracy assessment. Details of each component with major tasks can be separately summarized as following.

3.1 Data collection and preparation

3.1.1 GIS data

Land use map in 2012 of NGD was firstly modified based on Google Earth images using visual interpretation via screen technique by considering seasonality and phenological patterns of land use classes. In this study, there were 4 different prototype areas for representing main land use classes including urban, paddy field, unstock forest and mixed deciduous forest as shown in Figure 3.2.

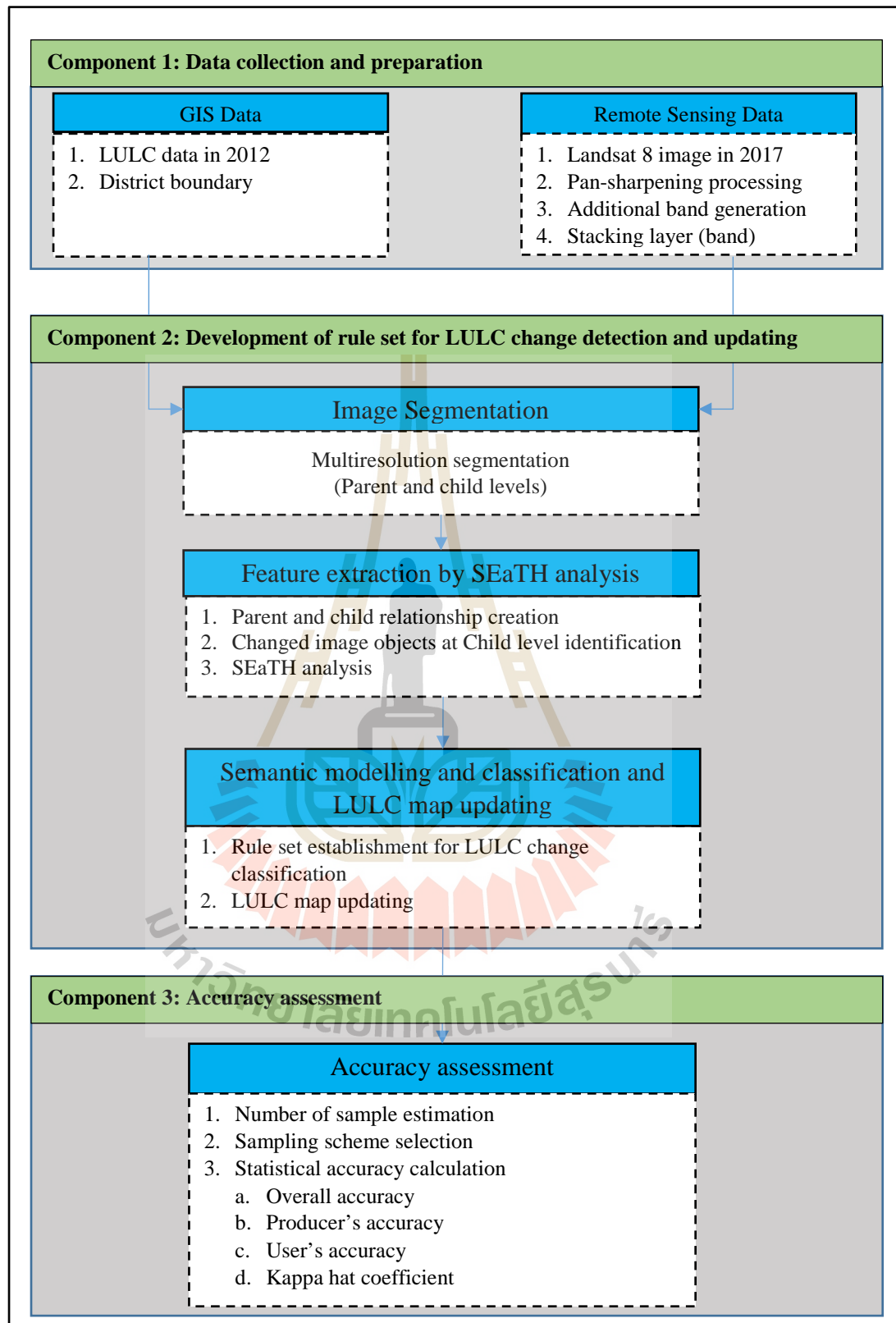


Figure 3.1 Schematic workflow of research methodology.

In practice, Google Earth image dated on 20 February 2012 was firstly downloaded using Google Earth software and imported to ArcGIS for LULC interpretation. Then LULC data are visual interpreted according land use classification system of NGD. Herein, there is no accuracy assessment for the result of visual interpretation map because the appearance of land use classes on the image is easy to delineate with very high spatial resolution image.

3.1.2 Remote Sensing data

In this study, the remotely sensed image was Landsat 8 image, Path 128 and Row 48 for OBCD. It was acquired on 19 February 2017 and downloaded from website: www.earthexplorer.usgs.gov. Landsat 8 measures different ranges of frequencies along the electromagnetic spectrum with 11 bands as shown in Table 3.1 and Figure 3.3.

Major preprocessing of remote sensing data are here implemented including (a) pan-sharpening process, (b) additional band generation and (c) stacking layer.

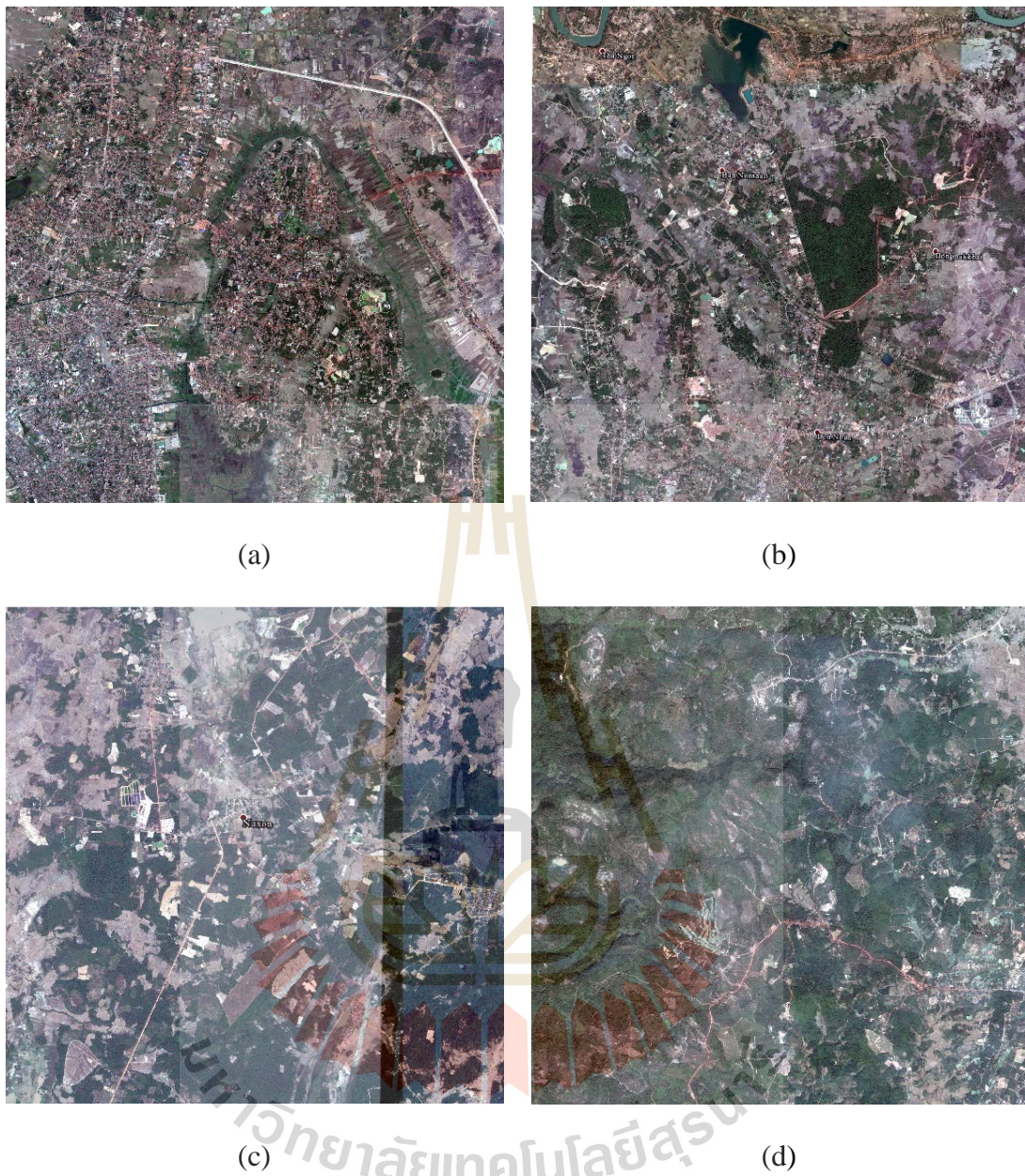
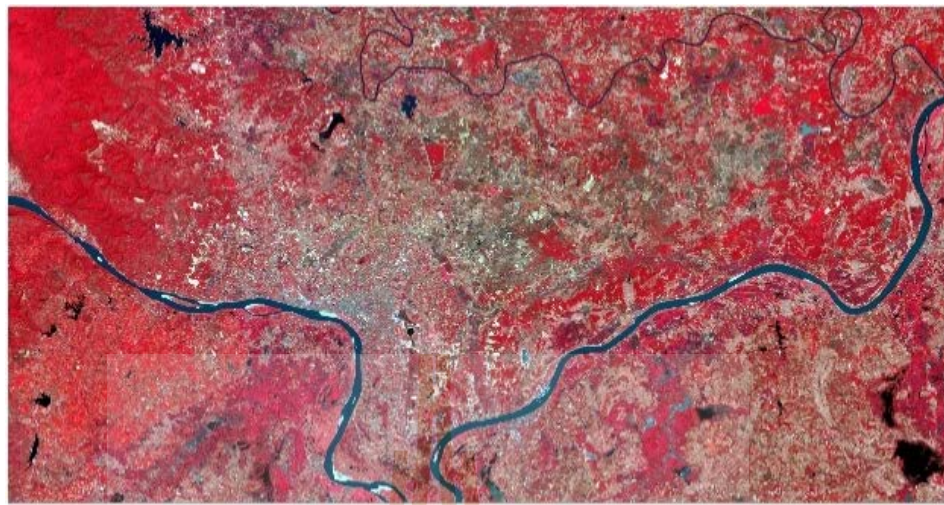


Figure 3.2 Spatial subset of Google earth images with band combination of 1, 2, and 3 as RGB for four representative land use class (a) Urban, (b) Paddy field, (c) Unstock forest and (d) Mixed deciduous forest.

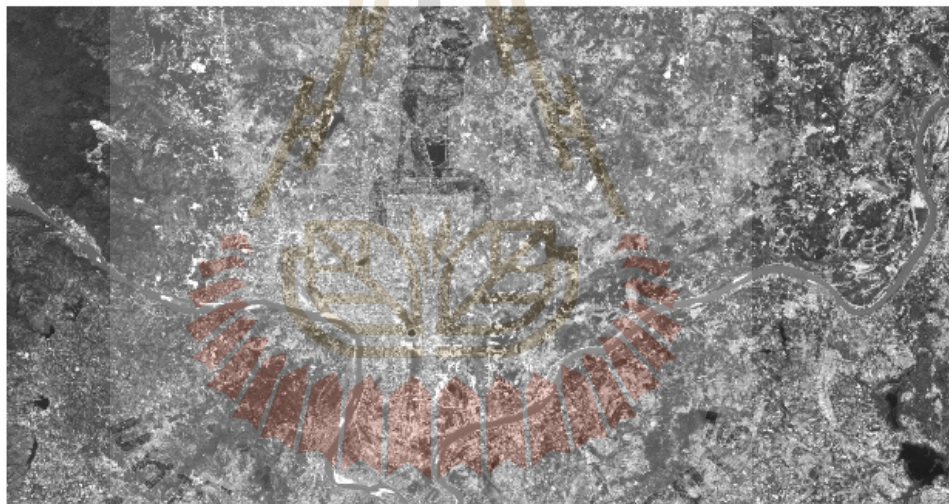
Table 3.1 Sensors and number band of Landsat 8.

Sensor	Bands	Wavelength (μm)	Resolution (m)
Operational Land Imager (OLI)	Band 1 - Coastal aerosol	0.43 - 0.45	30
	Band 2- Blue	0.45 - 0.51	30
	Band 3 - Green	0.53 - 0.59	30
	Band 4 - Red	0.64 - 0.67	30
	Band 5 - Near Infrared (NIR)	0.85 - 0.88	30
	Band 6 - SWIR 1	1.57 - 1.65	30
	Band 7 - SWIR 2	2.11 - 2.29	30
	Band 8 - Panchromatic	0.50 - 0.68	15
	Band 9 - Cirrus	1.36 - 1.38	30
Thermal Infrared Sensor (TIRS)	Band 10 - Thermal Infrared (TIRS) 1	10.60 - 11.19	100 * (30)
	Band 11 - Thermal Infrared (TIRS) 2	11.50 - 12.51	100 * (30)

Source: USGS, [www](http://www.usgs.gov), 2017.



(a)



(b)

Figure 3.3 Spatial and spectral subset of Landsat 8 acquired on 19 February 2017 (a) Multispectral band composite [Band 5, 4, 3: NIR, R, G], (b) PAN image.

(1) Pan-sharpening processing

In this study, Landsat 8 data was firstly processed pan-sharpening using the selected methods including (1) Ehlers fusion (EF), (2) Gram-Schmidt pan-sharpening (GS), (3) High pass filtering (HPF) (4) Modified IHS transformation (MIHS), and (5) Wavelet fusion (WT). Herein, multispectral bands of Landsat-8 included band 2 (Blue), 3 (Green), 4 (Red), 5 (NIR), 6 (SWIR-1), and 7 (SWIR-2) and 8 (PAN) were selected to process pan-sharpening. The characteristic of the selected pan-sharpening methods are summarized in Table 3.2.

Then, the derived results were applied to identify an optimum pan-sharpening image for OBCD using the Universal Image Quality index of Wang and Bovik (2002) as:

$$Q = \frac{\sigma_{xy}}{\sigma_x \sigma_y} * \frac{2\bar{x}\bar{y}}{(\bar{x}^2) + (\bar{y}^2)} * \frac{2\sigma_x \sigma_y}{\sigma_x^2 + \sigma_y^2} \quad (3.1)$$

Herewith x is pixel value of original image and y is test image, where

$$\bar{x} = \frac{1}{N} \sum_{i=1}^N x_i,$$

$$\bar{y} = \frac{1}{N} \sum_{i=1}^N y_i,$$

$$\sigma_x^2 = \frac{1}{N-1} \sum_{i=1}^N (x_i - \bar{x})^2,$$

$$\sigma_y^2 = \frac{1}{N-1} \sum_{i=1}^N (y_i - \bar{y})^2,$$

$$\sigma_{xy} = \frac{1}{N-1} \sum_{i=1}^N (x_i - \bar{x})(y_i - \bar{y})$$

The first factor in the Eq. 3.1 gives the correlation coefficient of x and y. This factor measures the degree of linear agreement and in the ideal case (two images are identical) is thus equal 1 and if there is no correlation then equal 0. The second factor compares the means of the two images. The range of values is between

0 and 1. The third factor finally examines the variance of the two images. In this case, the dynamic range is also [0, 1]. In conformity with the correlation, mean value and variance, these three factors provide a value of 1 and thus Q is also equal to 1 (Wang and Bovik, 2002). Therefore, pan-sharpening method that provides the highest average Q values is considered as an optimum pan-sharpening method and its product is further used to create additional band under ERDAS imagine software for OBCD.

(2) Additional band generation

Additional spectral bands that are included NDVI, MNDWI and NDBI were created using following equations:

$$\text{NDVI} = (\text{NIR} - \text{RED}) / (\text{NIR} + \text{RED}) \quad (3.2)$$

$$\text{MNDWI} = (\text{GREEN} - \text{SWIR}) / (\text{GREEN} + \text{SWIR}) \quad (3.3)$$

$$\text{NDBI} = (\text{SWIR} - \text{NIR}) / (\text{SWIR} + \text{NIR}) \quad (3.4)$$

Where:

GREEN is Brightness of Band 3 of Landsat-8;

RED is Brightness of Band 4 of Landsat-8;

NIR is Brightness of Band 5 of Landsat-8;

SWIR is Brightness of Band 6 of Landsat-8.

(3) Stacking layer

The optimum pan-sharpened image and additional spectral bands were combined together as one dataset for OBCD using ERDAS Imagine software.

Table 3.2 Characteristics of selected pan-sharpening algorithm.

Method	Basic characteristics	Reference
Ehlers fusion (EF)	This method is based on IHS transformation coupled with Fourier domain filtering.	Klonus and Ehlers (2009)
Gram-Schmidt pan-sharpening (GS)	This method is firstly simulated a panchromatic band from lower spatial resolution spectral bands. Then Gram-Schmidt transformation is performed on the simulated panchromatic band and the spectral bands and replaced the high spatial resolution panchromatic band with the first Gram-Schmidt band. Finally, inverse Gram-Schmidt transformation is performed to generate a pan-sharpened image.	Laben and Brower (2000)
High pass filtering (HPF)	This method involves a convolution using high pass filter on PAN image and merging the result with MS image.	Gangkofner et al. (2008)
Modified intensity hue saturation transform (MIHST)	This method was firstly proposed by Siddiqui (2003). It allows combining multispectral image with panchromatic image more than three bands at a time. The method works best when there is significant overlap of wavelengths of combining images (Nikolakopoulos, 2008).	Nikolakopoulos (2008) Siddiqui (2003)
Wavelet transform (WT)	This method is a modification of the work of King and Wang (2001). The process involves separating original image into different image components by wavelet decomposition and substituting their components between MS and PAN image components to produce a pan-sharpened image.	Klonus and Ehlers (2009) King and Wang (2001)

3.2 Development of rule set for LULC change detection and updating

Major tasks for development of rule set for LULC change detection and updating included (1) image segmentation, (2) feature extraction by SEaTH analysis, and (3) semantic modelling and classification and LULC map updating.

3.2.1 Image segmentation

The prepared Landsat data in 2017 and its derivative data was segmented using multiresolution segmentation algorithm with two different levels: pixel level as parent level (Level 2) and image object level as child level (Level 1) under eCognition software.

For multiresolution segmentation at parent level (Level 2), the modified LULC data in 2012 as thematic map was here applied to control boundary of segmented image objects for pixel level. Meanwhile, for multiresolution segmentation at child level (Level 1), the segmented image object at parent level (Level 2) was here further segmented to create a relationship between parent and child image object levels for Class-object change detection.

3.2.2 Feature extraction by SEaTH analysis

Parent–child relationship between image objects at Level 2 and Level 1 was applied to extract changed and unchanged objects between 2012 and 2017. In this study, two main steps are applied for feature extraction by SEaTH analysis.

At the first step, the existence of LULC class from 2012 at Level 2 as parent level was created under class-related feature properties. Herein, the created existence LULC classes in prototype area were applied as super-object (parent) of Level 1 as Child level. This image object property was applied to create super-object

class hierarchy under Level 2. This structure was applied to classify LULC map in 2012 according to class description. It consists of LULC code of each LULC class and Level number (Level 2).

At the second step, mean diff to super-object under to super-object parameter of layers values was applied to identify changed image objects at Child level (Level 1). In practice, mean value of each layer (BLUE, GREEN, RED, NIR, SWIR-1, SWIR-2, MNDWI, NDBI, and NDVI) from 5 training areas were extracted and exported to MS-Excel software for SEaTH analysis. These image properties were applied to calculate J separability value using Eq. 2.1 and 2.2 and to identify an optimum threshold value between pairwise LULC classes using Eq. 2.6. The derived optimum threshold value of changed object were added to class description for rule set of LULC change class. In practice, an optimum threshold value and the membership function (ascending or descending) is assigned for each feature under rule set. Finally, all rule set of object change were applied to create semantic model for classification.

3.2.3 Semantic modelling and classification and LULC map updating

Most outstanding features as rule set from SEaTH analysis were selected to establish semantic model to classify LULC change map between 2012 and 2017. Later, LULC change data was further applied to update LULC map in 2012 for final LULC map in 2017 using Matrix function under ERDAS imagine software.

3.3 Accuracy assessment

The change LULC map between 2012 and 2017 is assessed accuracy with number of sample points. In this study, number of sample points was estimated based on binomial probability distribution theory as suggested by Fitzpatrick-Lins (1981) as:

$$N = \frac{Z^2(p)(q)}{E^2} \quad (3.5)$$

Where P is the expected percent accuracy of the entire map,

q is $100 - p$

E is the allowable error

Z is 2 from the standard normal deviate of 1.96 for the 95% two side confidence level.

Meanwhile, stratified random sampling technique was selected to allocate sample points for accuracy assessment by using Google Earth image in 2017 as reference data.

In practice, error matrix or confuse matrix or coincident matrix was prepared according to classified change LULC class and reference information (Table 3.3). Then, statistical accuracy data was calculated included overall accuracy, producer's accuracy, user's accuracy, and Kappa hat coefficient.

Table 3.3 The error matrix.

		Ground reference data					
		Class	1	2	3	k	Row total
Remote sensing classification	1		$n_{1,1}$	$n_{1,2}$	$n_{1,3}$	$n_{1,k}$	n_{1+}
	2		$n_{2,1}$	$n_{2,2}$	$n_{2,3}$	$n_{2,k}$	n_{2+}
	3		$n_{3,1}$	$n_{3,2}$	$n_{3,3}$	$n_{3,k}$	n_{3+}
	4		$n_{k,1}$	$n_{k,2}$	$n_{k,3}$	$n_{k,k}$	n_{k+}
Column total			n_{+1}	n_{+2}	n_{+3}	n_{+k}	N

The formula for calculation of accuracy values are as follows:

$$\text{Overall accuracy} = \frac{\sum_{i=1}^k n_{ii}}{n} \quad (3.6)$$

$$\text{Producer's accuracy } j = \frac{n_{jj}}{n_{+j}} \quad (3.7)$$

$$\text{User's accuracy } i = \frac{n_{ii}}{n_{+i}} \quad (3.8)$$

$$\text{Khat} = \frac{N \sum_{i=1}^k n_{ii} - \sum_{i=1}^k (n_{i+} \times n_{+i})}{N^2 - \sum_{i=1}^k (n_{i+} \times n_{+i})} \quad (3.9)$$

Where:

k is the number of rows (land-cover classes) in the matrix

n_{ii} is the number of the observation in row i and column i

n_{i+} is the marginal totals for row i

n_{+i} is the marginal totals for column i

N is the total number of observations.

CHAPTER IV

PREPROCESSING OF REMOTE SENSING AND GIS DATA

Results of four major tasks of preprocessing of remote sensing data and GIS for semi-automatic LULC map updating using OBCD including (1) interpretation of LULC data in 2012, (2) pan-sharpening processing, (3) the optimum pan-sharpening method identification and, (4) additional band generation are described and discussed in this chapter.

4.1 Interpretation of LULC data in 2012

Land use map in 2012 of NGD is firstly modified using visual interpretation based on Google Earth images in 2012. Results of 4 different areas that was chosen as a representative of main LULC class: urban, paddy field, unstock forest and mixed deciduous forest are displayed in Figures 4.1 to 4.4. Area and percentage of LULC classes in four prototype areas are presented in Tables 4.1 to 4.4. The boundaries of the modified LU/LC data of each area are further used to control boundary of image objects during image segmentation for OBCD

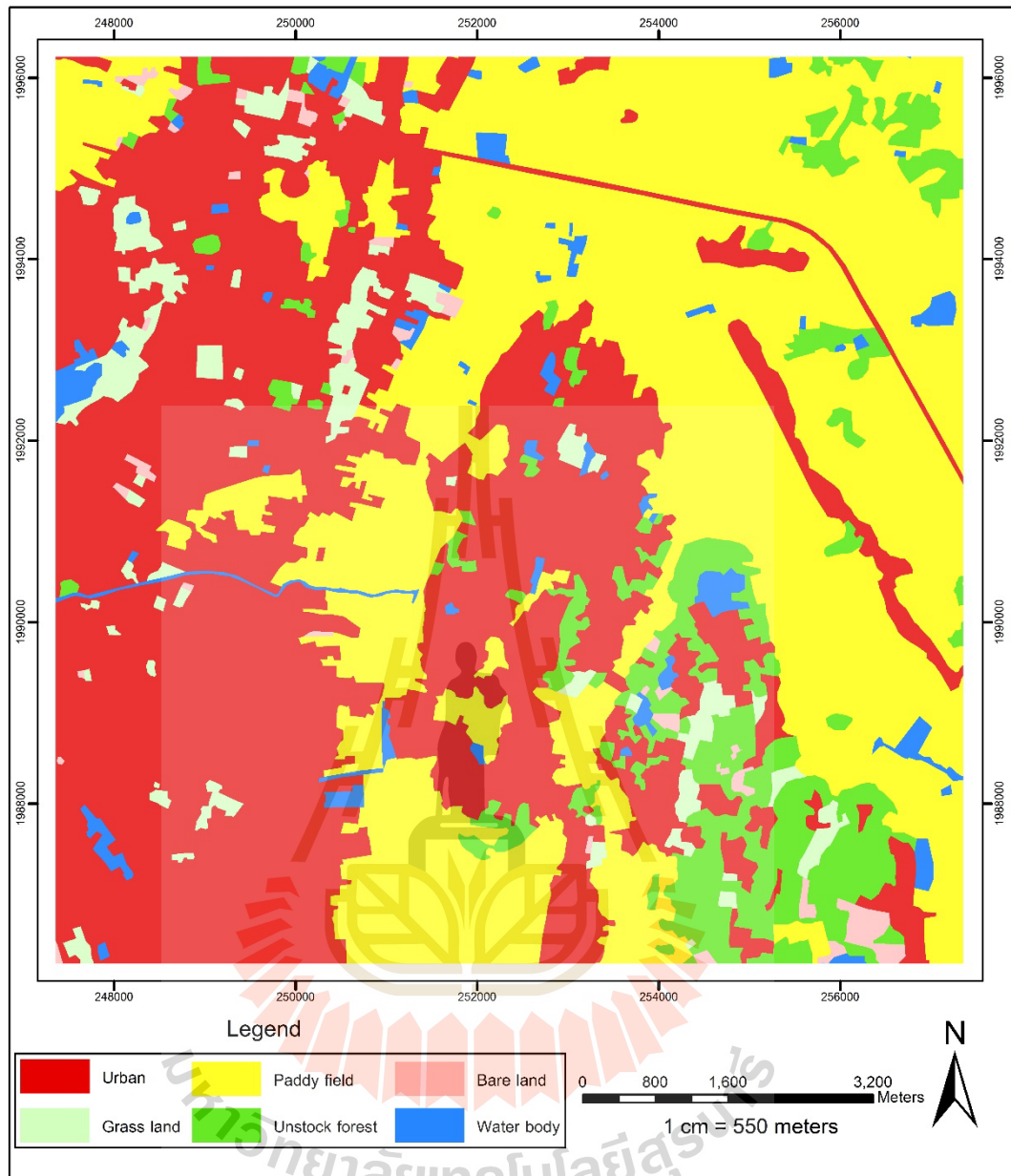


Figure 4.1 Prototype area of urban class.

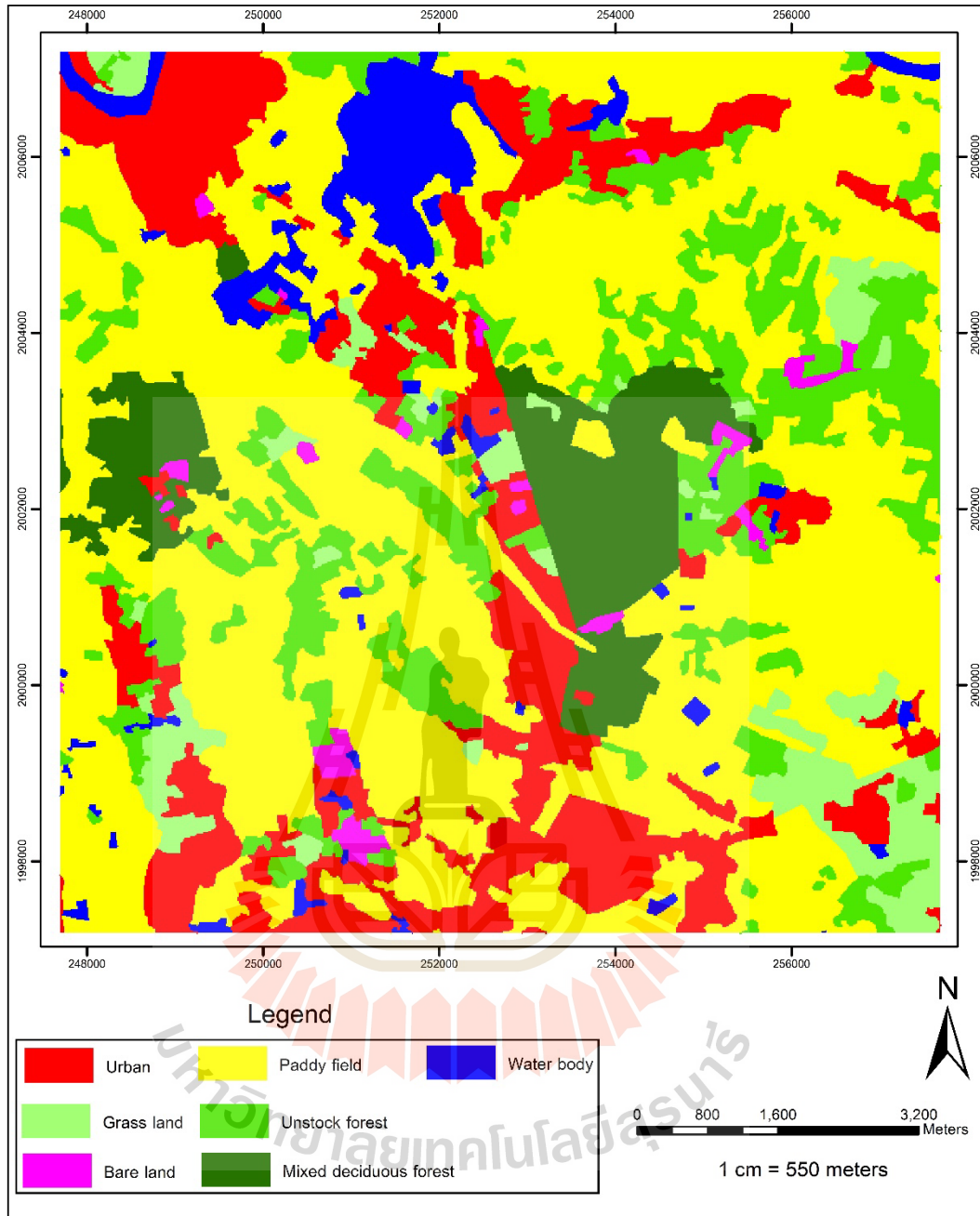


Figure 4.2 Prototype area of paddy field class.

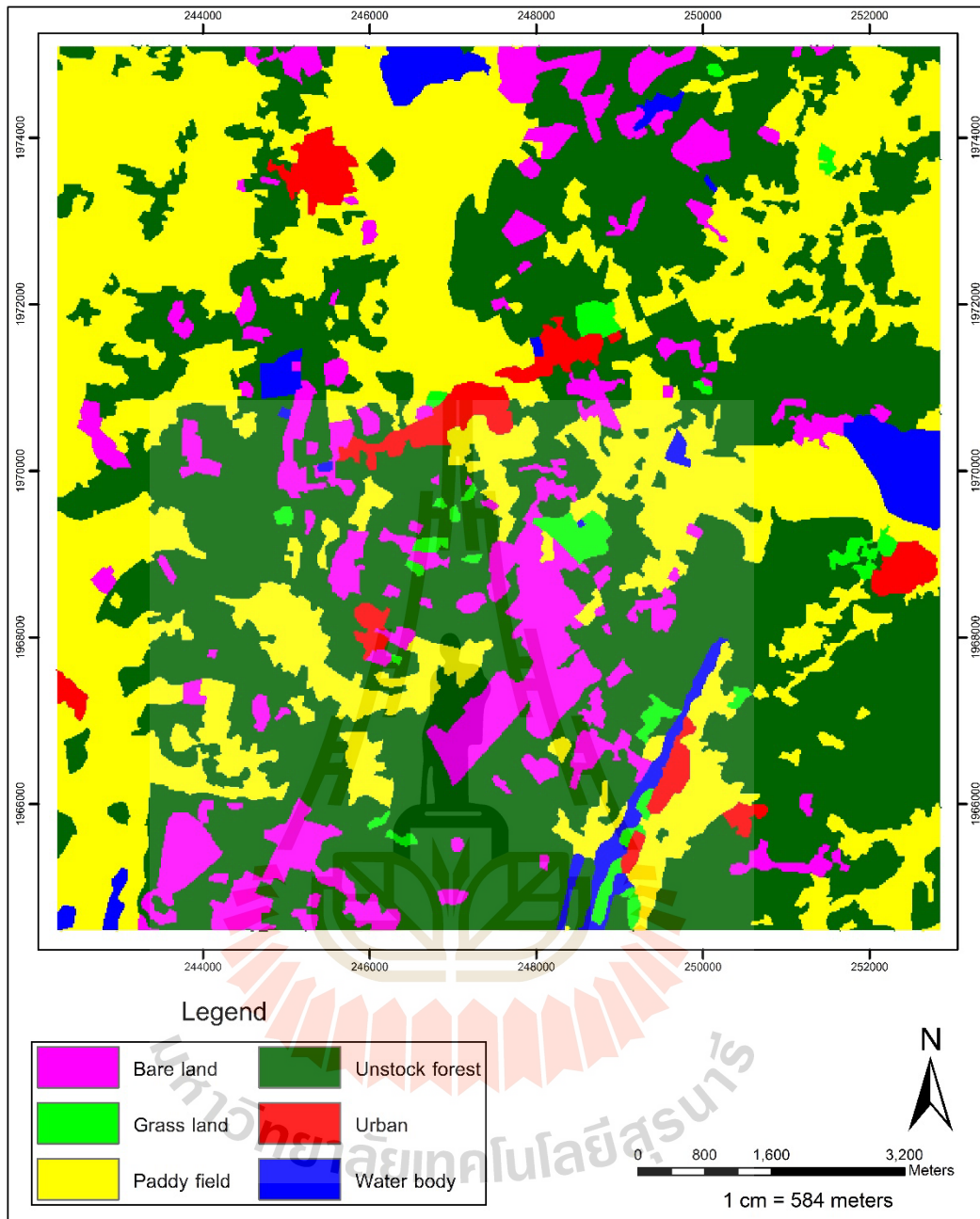


Figure 4.3 Prototype area of unstock forest class.

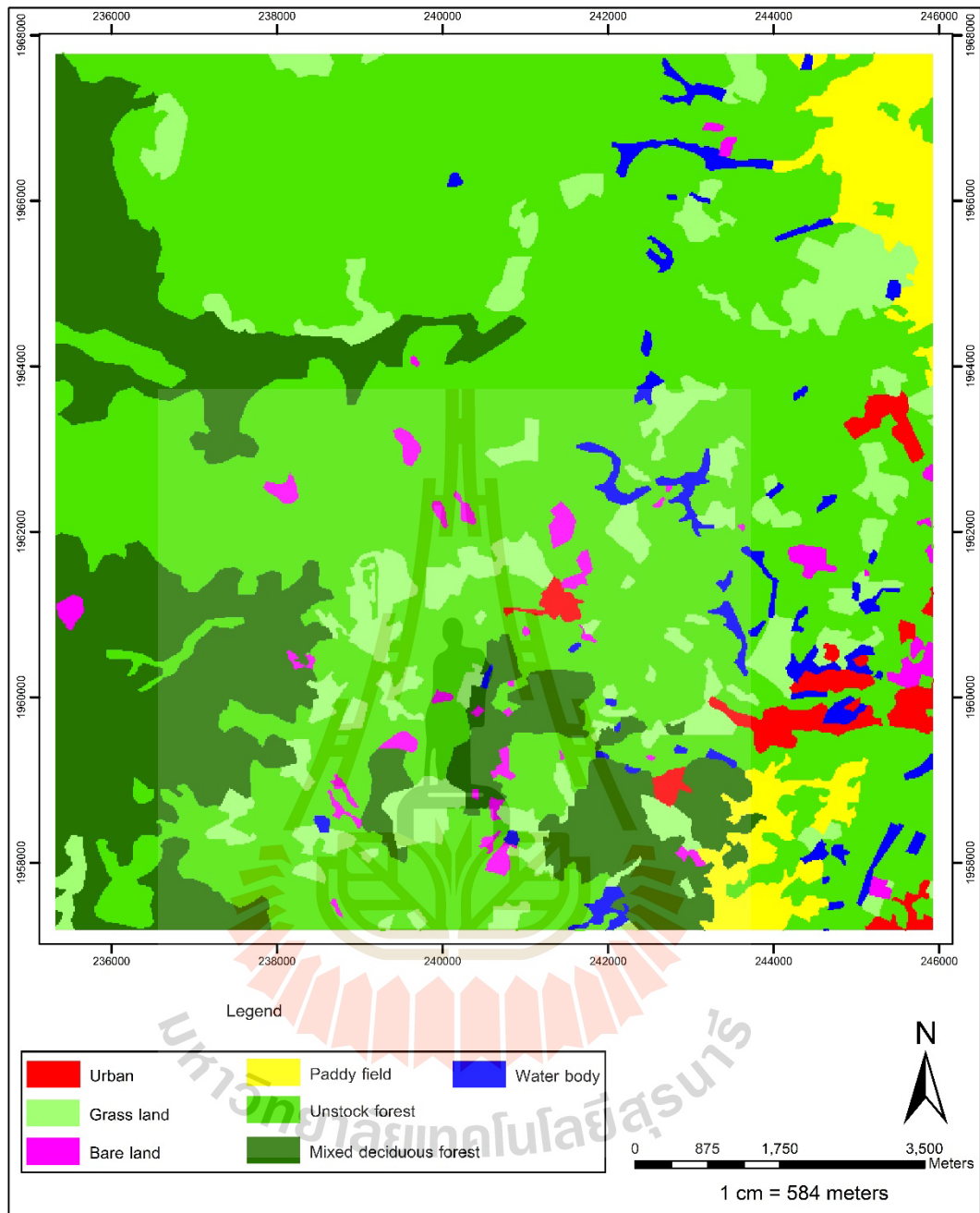


Figure 4.4 Prototype area of mixed deciduous forest class.

Table 4.1 Area and percentage of LULC classes in urban prototype area.

No.	LULC classes	Area in sq. km.	Percent
1	Urban	42.68	42.68
2	Water body	2.41	2.41
3	Unstock forest	8.21	8.20
4	Paddy field	42.24	42.24
5	Grass land	3.51	3.51
6	Bare land	0.95	0.95
Total		100.00	100.00

Table 4.2 Area and percentage of LULC classes in paddy field area.

No.	LULC classes	Area in sq. km.	Percent
1	Bare Land	1.11	1.11
2	Grass Land	4.99	4.99
3	Urban	16.97	16.98
4	Paddy field	50.04	50.07
5	Unstock Forest	14.31	14.32
6	Mixed Deciduous Forest	7.62	7.63
7	Water body	4.90	4.90
Total		99.96	100.00

Table 4.3 Area and percentage of LULC classes in unstock forest area.

No.	LULC classes	Area in sq. km.	Percent
1	Bare land	9.40	9.40
2	Grass land	1.37	1.37
3	Paddy field	35.45	35.47
4	Unstock forest	48.58	48.60
5	Urban	2.55	2.55
6	Water body	2.61	2.61
Total		99.96	100.00

Table 4.4 Area and percentage of LULC classes in mixed deciduous forest area.

No.	LULC classes	Area in sq. km.	Percent
1	Bare Land	1.40	1.40
2	Grass Land	9.50	9.51
3	Mixed Deciduous Forest	19.02	19.03
4	Paddy Field	4.24	4.24
5	Unstock Forest	61.97	61.99
6	Urban	1.69	1.69
7	Water body	2.14	2.14
Total		99.96	100.00

4.2 Pan-sharpening process

Results of pan-sharpening process of Landsat data in 2017 covering four prototype areas using five selected methods: (1) Ehlers fusion (EF), (2) Gram-Schmidt pan-sharpening (GS), (3) High Pass Filtering (HPF) (4) Modified IHS transformation (MIHS), and (5) Wavelet fusion (WT) are displayed in Figure 4.5.

4.3 Optimum pan-sharpening method identification

The derived results of pan-sharpening images were here applied to identify an optimum pan-sharpening image for OBCD using the UIQI (Eq. 3.1). In this study, UIQI were calculated using Model Builder module under ERDAS Imagine software as shown in Figure 4.6. As a result, it was found that HPF method can provides the highest average Q values and it is considered as an optimum pan-sharpening method (Table 4.5). The HPF pan-sharpened image is further used to create additional band under ERDAS Imagine for OBCD.

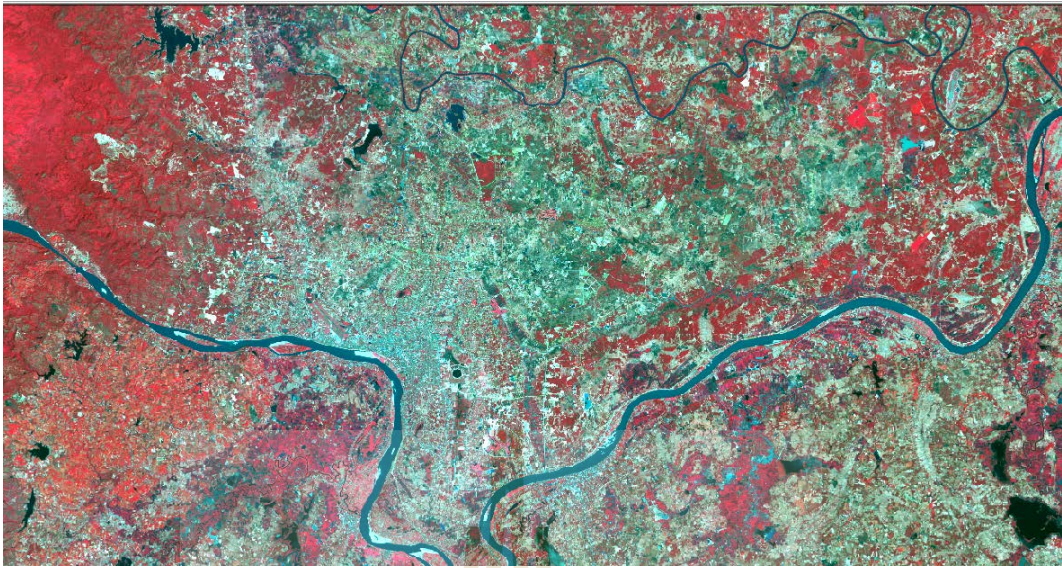


(a)

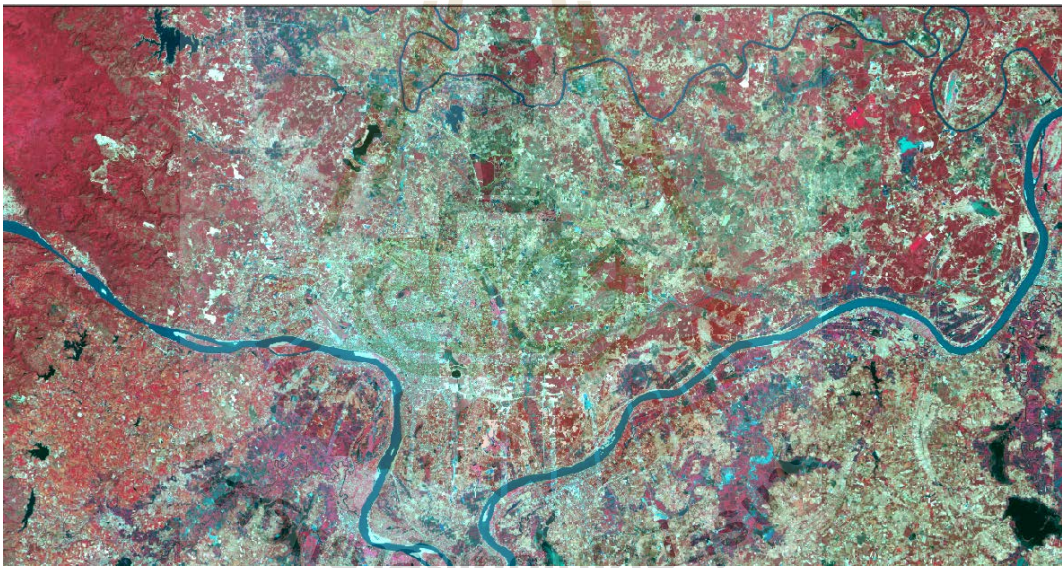


(b)

Figure 4.5 False color composite of original Landsat 8 image in 2012 and the pan-sharpened images, band 5, 4, 3 (RGB): (a) original image, (b) WT, (c) HPF, (d) MIHST, (e) EF, and (f) GS.



(c)

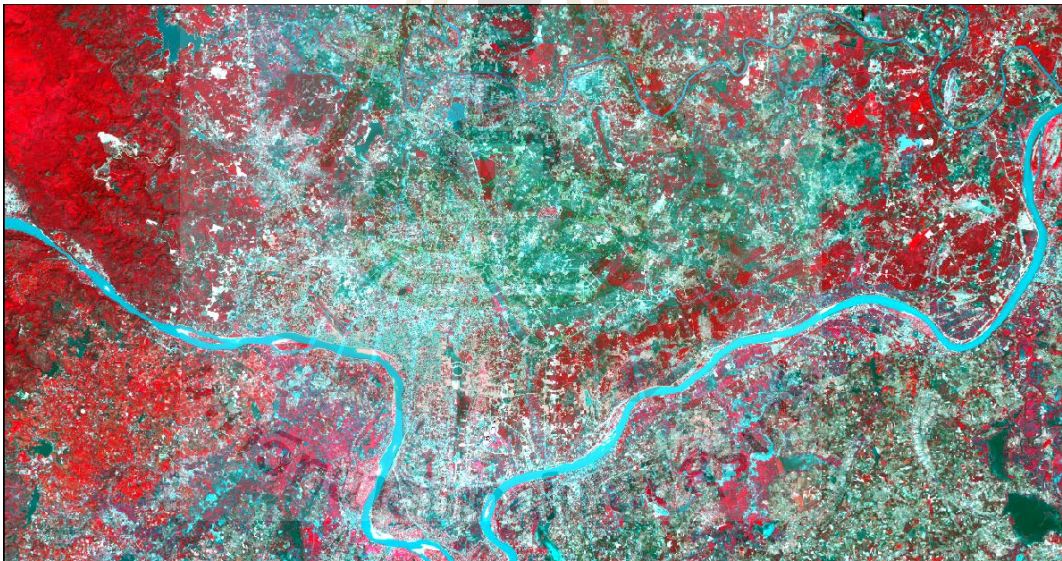


(d)

Figure 4.5 (Continued).



(e)



(f)

Figure 4.5 (Continued).

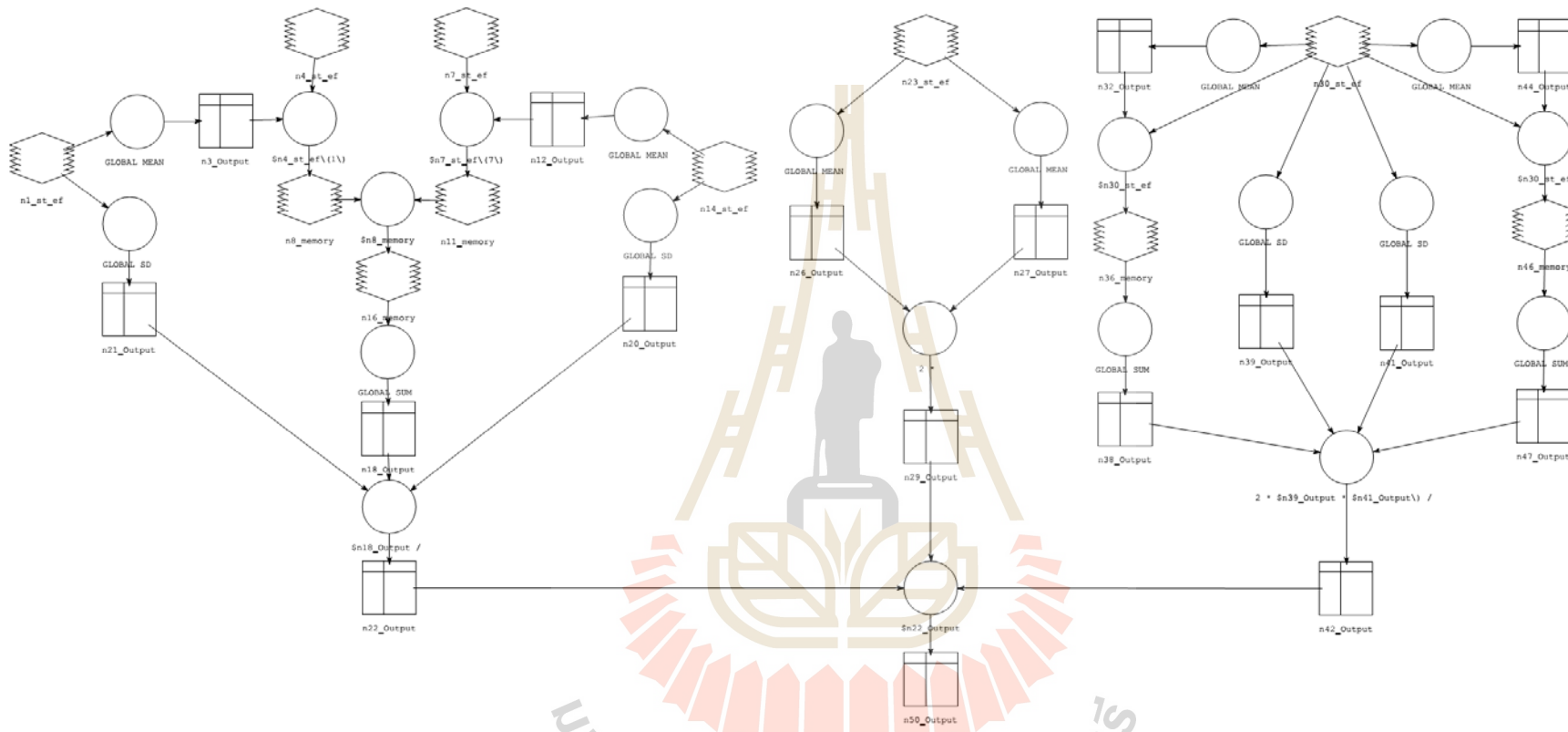


Figure 4.6 Structure of Model Builder model for Universal Image Quality Index calculation.

Table 4.5 Comparison of the image quality from different pan-sharpening methods for Landsat 8 data of 2012 based on Q-average value.

Landsat 8 data in 2017					
Band	Q and Q-average of various pan-sharpening methods				
	WT	HPF	MIHST	EF	GS
2	0.94031	0.91483	0.80007	0.82276	0.79516
3	0.93946	0.92424	0.87765	0.82199	0.81798
4	0.92578	0.93755	0.95283	0.87096	0.82963
5	0.96468	0.93281	0.90324	0.92472	0.82050
6	0.89335	0.94353	0.96817	0.93324	0.75575
7	0.90040	0.94477	0.97028	0.91514	0.78851
Sum	5.56396	5.59773	5.47224	5.28881	4.80753
Q-average	0.92733	0.93296	0.91204	0.88147	0.80125
Ranking	2	1	3	4	5

4.4 Additional band generation

Results of additional spectral band generation based on three selected indices which are related vegetation (NDVI), soil moisture (MNDWI) and urban (NDBI) are displayed Figures 4.7 to 4.9, respectively. The derived additional bands are further combined with pan-sharpened image as stacking layer for OBCD.

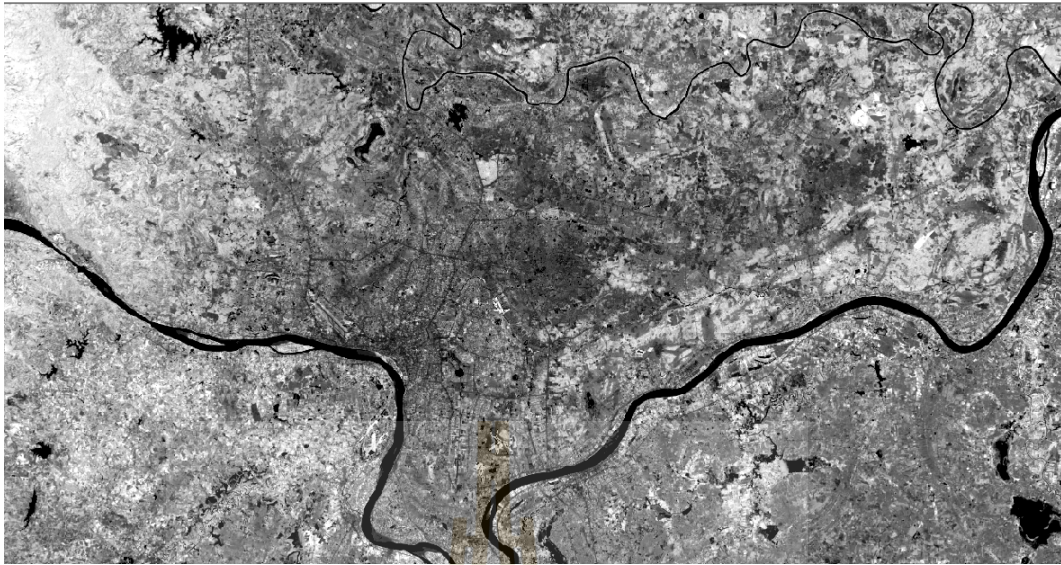


Figure 4.7 Normalized Different Vegetation Index (NDVI) image.



Figure 4.8 Modified Normalized Different Water Index (MNDWI) image.

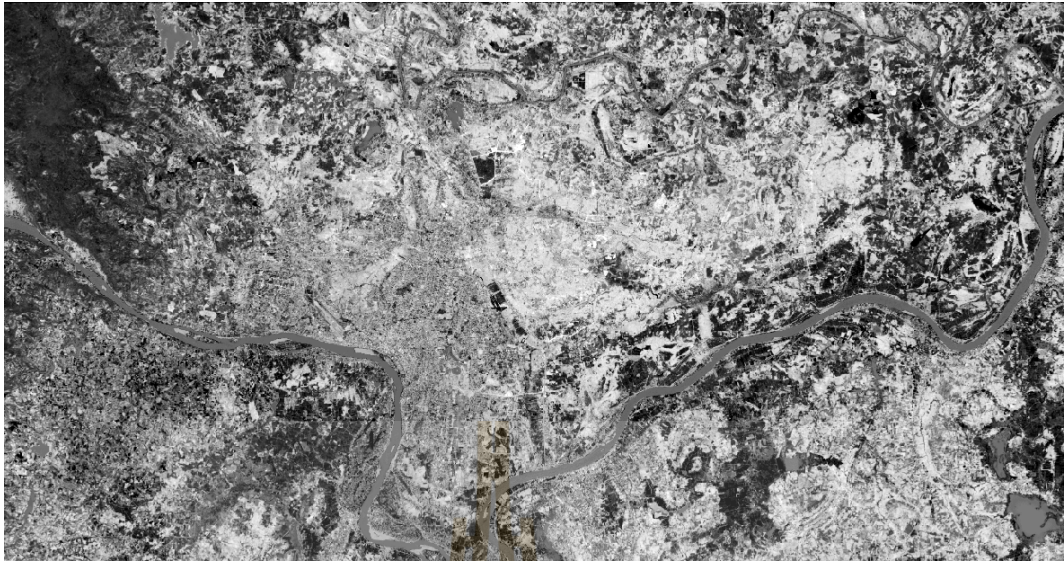


Figure 4.9 Normalized Different Built-Up Index (NDBI) image.



CHAPTER V

LULC UPDATING IN URBAN AREA

The main results of land use and land cover map updating in urban area include (1) development of rule set for LULC classification in urban area, (2) LULC in 2017 updating and (3) accuracy assessment.

5.1 Development of rule set for land use/land cover classification

Major results of rule set LULC classification development of urban area include (1) image segmentation by Multiresolution segmentation, (2) feature extraction by SEaTH analysis, and (3) semantic modelling and classification.

5.1.1 Image segmentation by Multiresolution segmentation

Two steps of image segmentation were here implemented for hierarchical object structure creation as parent and child relationship (object and its super object) for OBCD. Firstly, an optimum pan-sharpened image are segmented with thematic map of LULC data in 2012 as result shown in Figure 5.1. Secondly, the derived image objects at Level 2 are segmented again at Level 1 with thematic layer as child level as a result shown in Figure 5.2. The configuration of Multiresolution segmentation at Level 2 and Level 1 is summarized in Table 5.1.

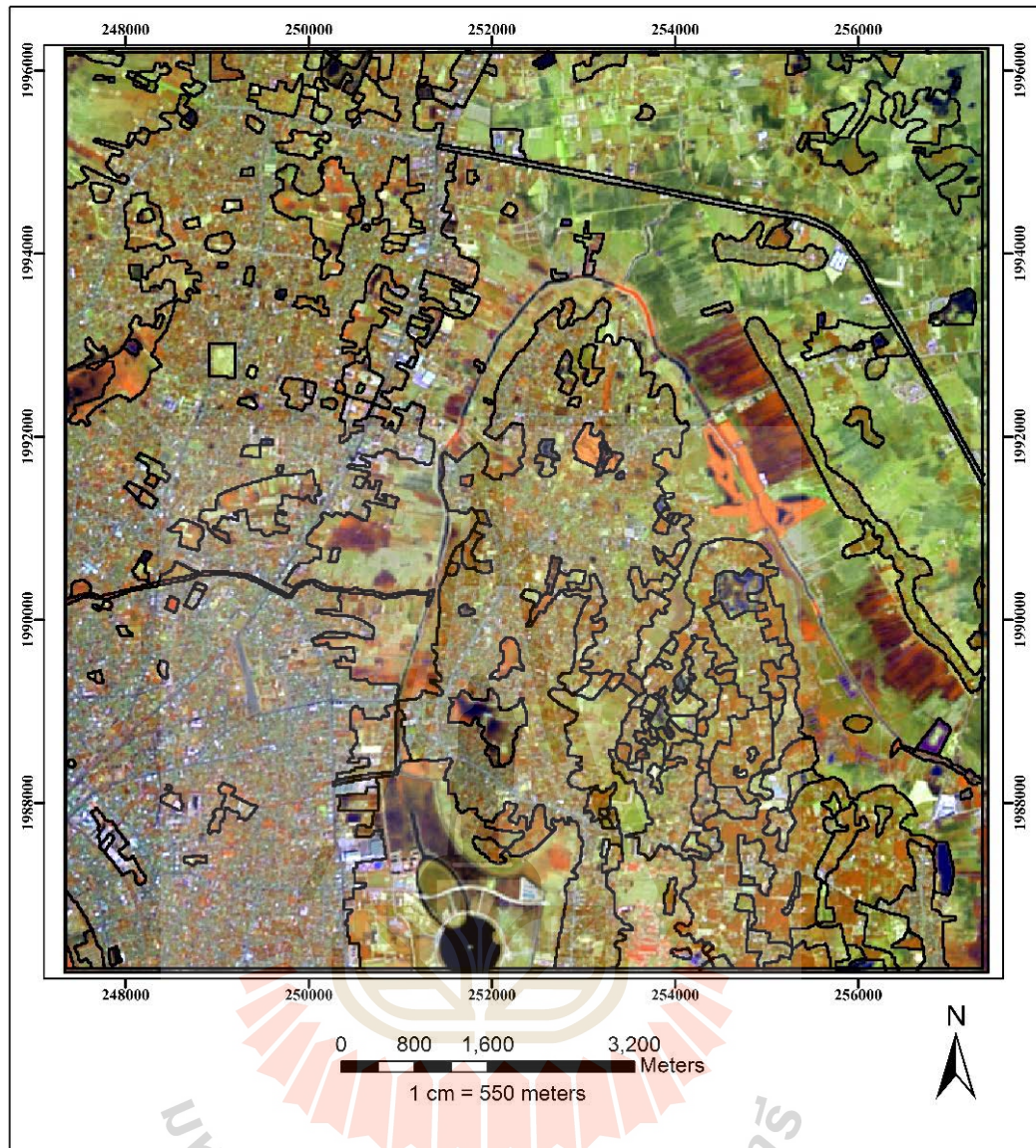


Figure 5.1 Image object of optimum pan-sharpened Landsat 8 data of 2012 by Multiresolution segmentation at level 2.

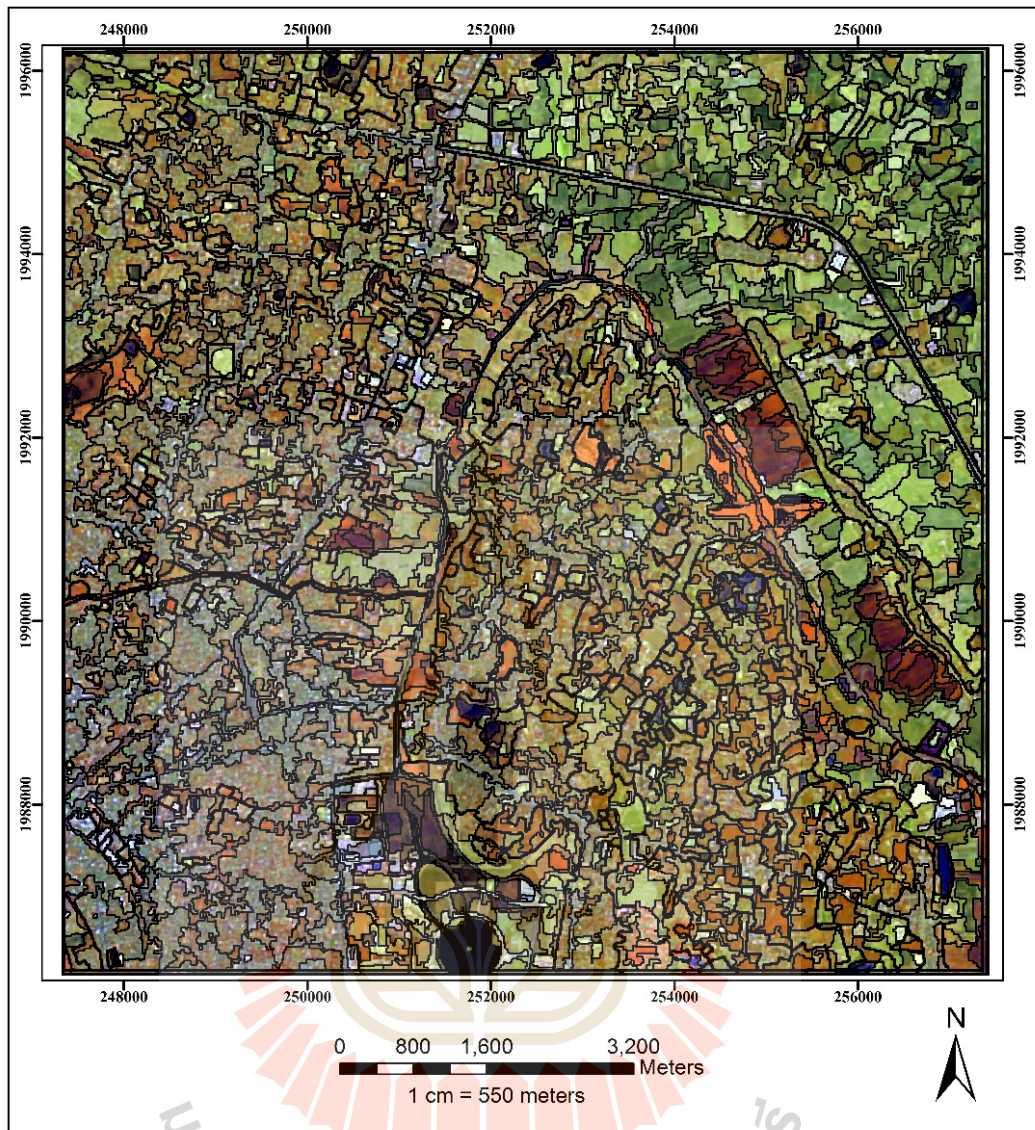


Figure 5.2 Image object of optimum pan-sharpened Landsat 8 data of 2017 by Multiresolution segmentation at level 1.

Table 5.1 Configuration of multiresolution segmentation at Level 2 and Level 1 with thematic layer.

Image object domain	Pixel level	Image object level
Level setting		
Level name	Level 2	Level 1
Segmentation setting		
Image layer weight	0, 0, 0, 0, 0, 0, 0, 0, 0	1, 1, 1, 1, 1, 1, 1, 1, 1
Thematic layer usage	Yes	YES
Scale parameters		
	20	20
Composition of homogeneity criterion		
Shape	0	0.1
Compactness	0	0.5

As results, it was found number of image object at Level 2 as parent level is 282 while number of image object at Level 1 as child level is 2,108. In fact, child objects that have similar spectral characteristics as parent objects are unchanged objects, while any deviation is an indicator of changed objects.

5.1.2 Feature extraction by SEaTH analysis

Parent-child relationship between image objects at Level 2 and Level 1 is applied to quantify changed and unchanged objects between 2012 and 2017. In this study, two main steps are required for feature extraction by SEaTH analysis.

At the first step, existence of LULC class from 2012 at Level 2 as parent level is created under class-related feature property of image objects as shown in Figure 5.3. Herein, the created existence LULC classes in urban area include bare land, grass land, paddy field, unstock forest, urban and water body are applied as super-object (parent) of Level 1 as child level. This image property is applied to create super-object class hierarchy under Level 2 including LULC in 2012 and LULC change between 2012 and 2017 as shown in Figure 5.4. This structure can directly

apply to classify LULC map in 2012 according to class description as shown in figure 5.5. It consists of LULC code of each LULC class and Level number (Level 2).

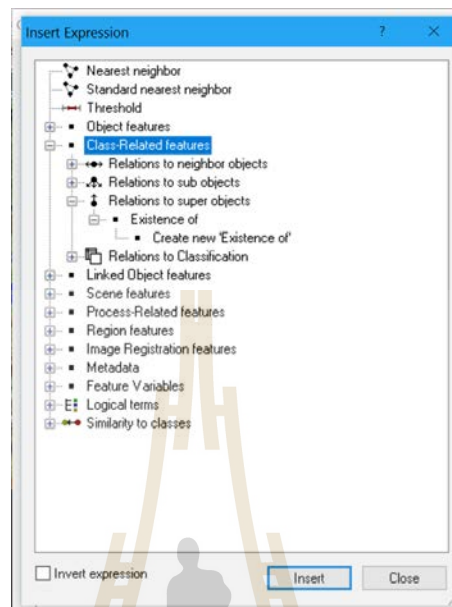


Figure 5.3 Class-related feature properties: Existence of.

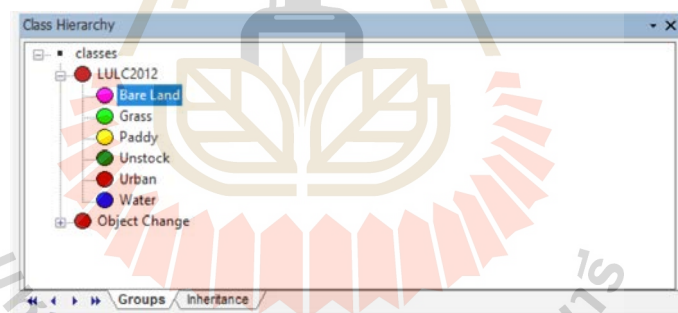


Figure 5.4 Class hierarchy structure of Super-object at Level 2.

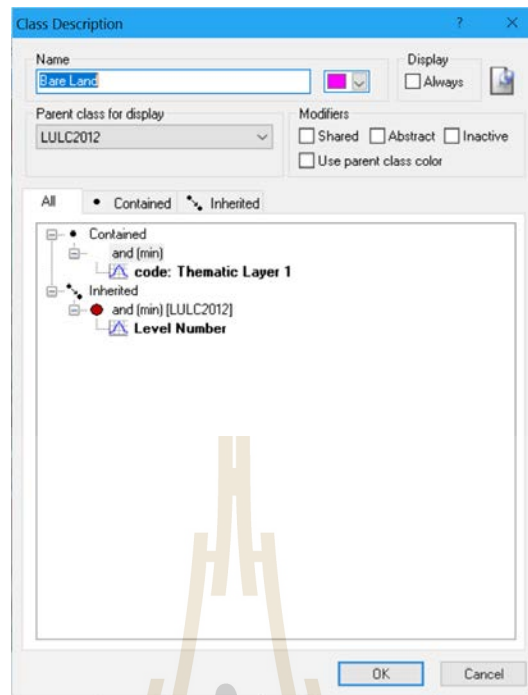


Figure 5.5 Class description of Super-object at Level 2.

At the second step, mean diff to super-object function under To super-object property of layers values are applied to identify changed objects of Level 1 as child level as shown in Figure 5.6. In practice, mean value of each layer from 5 training areas are extracted and exported to MS-Excel spreadsheet software for SEaTH analysis. Examples of training areas for LULC changed objects in 2017 are displayed in Figure 5.7. Meanwhile, the results of SEaTH analysis for separability test and threshold value extraction for rule-based development of urban among other classes using Equation 2.1, 2.2 and 2.6 are displayed in Tables 5.2 to 5.6.

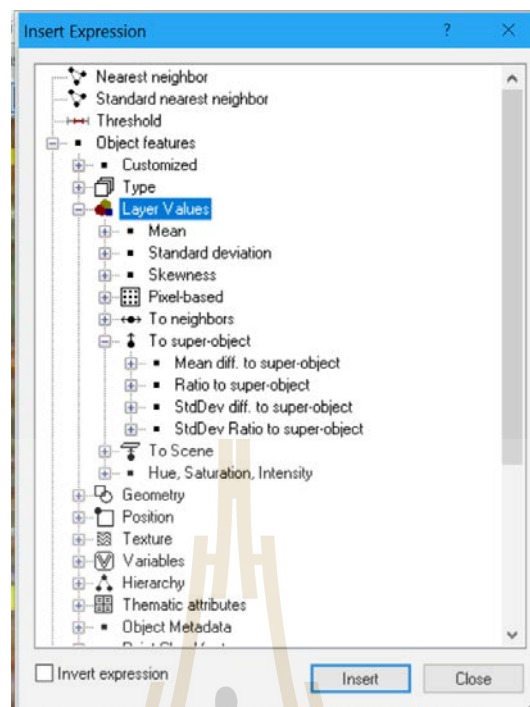


Figure 5.6 Structure of Mean diff to super-object parameter for changed object identification.

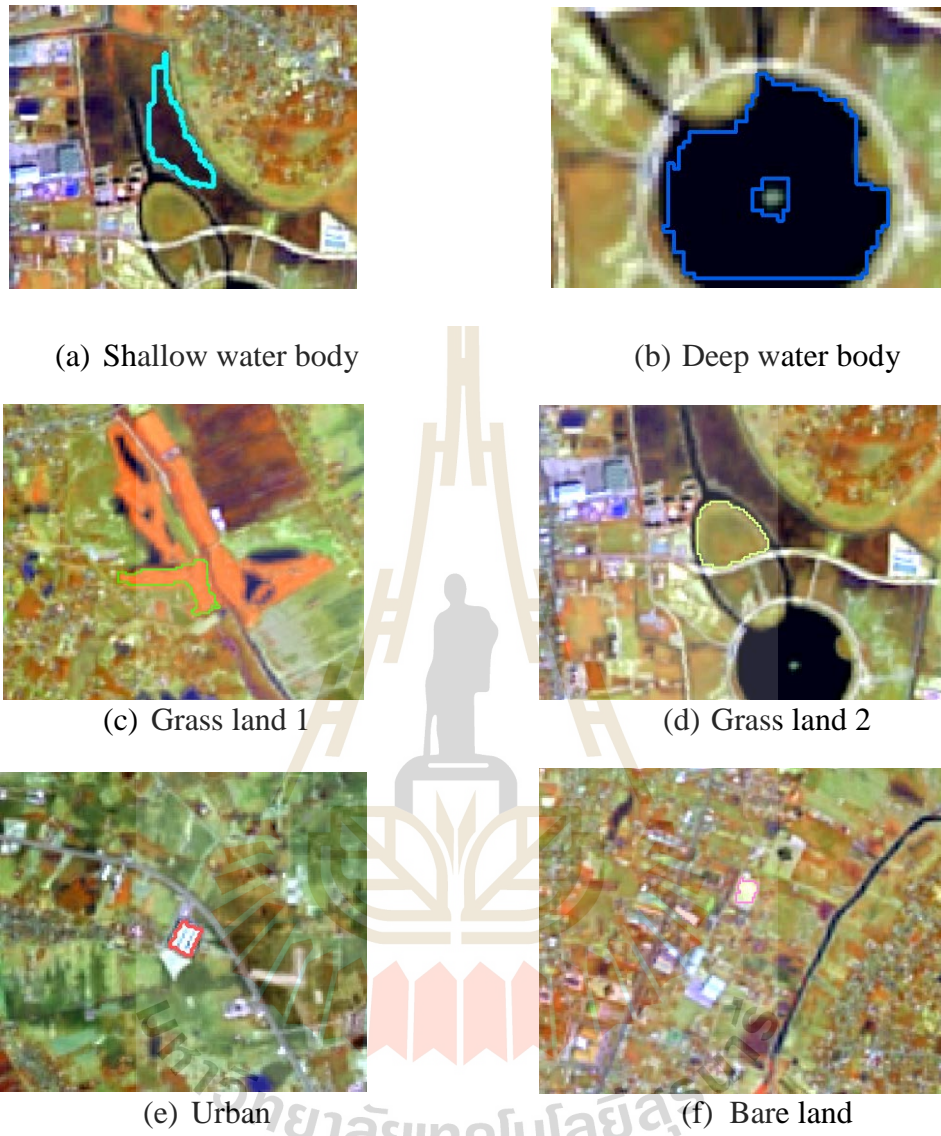


Figure 5.7 Training areas of changed objects in 2017 for SEaTH analysis.

Table 5.2 Pairwise of mean and variance between urban and bare land for threshold value calculation.

Feature	Mean	Variance	Mean	Variance	J Value	Membership	LEFT	RIGHT
	Urban	Urban	Bare land	Bare land				
Layer 1 (1)	41.7350	635.9084	16.2890	39.5638	0.9215	Ascending	24.43	117.39
NDVI (1)	-15.7630	944.0892	-20.4175	29.8304	0.8324	Descending	-107.94	-27.42
Layer 2 (1)	38.8948	1073.7891	24.3925	78.9240	0.6420	Ascending	33.95	137.20
Layer 6 (1)	52.8475	857.5831	31.4325	105.0278	0.5980	Ascending	41.94	140.70
NDBI (1)	52.8150	216.6087	35.2450	80.1798	0.5468	Ascending	43.44	96.97
Layer 3 (1)	43.0278	1244.6990	41.1725	122.7050	0.4889	Descending	-62.81	29.25
MNDWI (1)	-35.1500	573.0257	-35.8200	57.0168	0.4853	Descending	-106.96	-43.86
Layer 5 (1)	45.4375	447.6589	36.9825	84.9501	0.3450	Ascending	44.82	108.91
Layer 4 (1)	31.1775	350.9180	29.3000	80.7389	0.2374	Descending	-25.02	20.48

Table 5.3 Pairwise of mean and variance between urban and grass land (2) for threshold value calculation.

Feature	Mean	Variance	Mean	Variance	J Value	Membership	LEFT	RIGHT
	Urban	Urban	Grass land (2)	Grass land (2)				
Layer 1 (1)	41.7350	635.9084	-3.3287	3.9555	1.6418	Ascending	1.03	117.39
Layer 2 (1)	38.8948	1073.7891	-4.2000	6.0071	1.4982	Ascending	0.47	137.20
Layer 3 (1)	43.0278	1244.6990	-6.0203	14.4501	1.4275	Ascending	0.95	148.87
Layer 6 (1)	52.8475	857.5831	-0.3695	50.2852	1.3798	Ascending	12.23	140.70
Layer 5 (1)	45.4375	447.6589	3.9006	53.5291	1.3352	Ascending	16.21	108.91
NDBI (1)	52.8150	216.6087	7.8338	328.8499	1.2173	Ascending	32.13	96.97
Layer 4 (1)	31.1775	350.9180	3.7775	38.5657	1.0453	Ascending	12.46	87.38
NDVI (1)	-15.7630	944.0892	23.0475	62.9839	1.0424	Descending	-107.94	11.87
MNDWI (1)	-35.1500	573.0257	-23.6318	225.3378	0.1797	Descending	-106.96	-33.26

Table 5.4 Pairwise of mean and variance between urban and grass land (1) for threshold value calculation.

Feature	Mean	Variance	Mean	Variance	J Value	Membership	LEFT	RIGHT
	Urban	Urban	Grass land (1)	Grass land (1)				
NDBI (1)	52.8150	216.6087	-96.8000	50.2855	2.0000	Ascending	-47.93	96.97
NDVI (1)	-15.7630	944.0892	93.0350	7.3055	1.9627	Descending	-107.94	83.46
Layer 1 (1)	41.7350	635.9084	-4.7740	0.4686	1.8008	Ascending	-3.06	117.39
Layer 6 (1)	52.8475	857.5831	-13.2700	3.4173	1.8007	Ascending	-8.46	140.70
Layer 5 (1)	45.4375	447.6589	-4.8494	11.2391	1.7196	Ascending	3.09	108.91
Layer 3 (1)	43.0278	1244.6990	-11.7820	2.2088	1.6824	Ascending	-8.50	148.87
Layer 2 (1)	38.8948	1073.7891	-0.7488	3.1873	1.5423	Ascending	2.71	137.20
MNDWI (1)	-35.1500	573.0257	7.9381	30.3489	1.3873	Descending	-106.96	-1.92
Layer 4 (1)	31.1775	350.9180	45.4825	10.5131	0.9935	Descending	-25.02	41.13

Table 5.5 Pairwise of mean and variance between urban and deep water body for threshold value calculation.

Feature	Mean		Variance		J Value	Membership	LEFT	RIGHT
	Urban	Urban	Deep water body	Deep water body				
MNDWI (1)	-35.1500	573.0257	101.5150	104.7116	1.9983	Descending	-106.96	59.93
NDBI (1)	52.8150	216.6087	-26.4050	64.4409	1.9931	Ascending	1.95	96.97
Layer 5 (1)	45.4375	447.6589	-34.8650	4.3966	1.9750	Ascending	-27.09	108.91
Layer 4 (1)	31.1775	350.9180	-39.9575	14.9339	1.9604	Ascending	-27.11	87.38
Layer 6 (1)	52.8475	857.5831	-27.6675	3.7758	1.8892	Ascending	-21.88	140.70
Layer 1 (1)	41.7350	635.9084	-4.6420	11.2239	1.5548	Ascending	2.23	117.39
Layer 3 (1)	43.0278	1244.6990	-13.2900	15.8825	1.4964	Ascending	-5.53	148.87
NDVI (1)	-15.7630	944.0892	-71.3325	101.5391	1.2644	Ascending	-55.07	76.42
Layer 2 (1)	38.8948	1073.7891	-4.5929	35.8572	1.2232	Ascending	4.97	137.20

Table 5.6 Pairwise of mean and variance between urban and shallow water body for threshold value calculation.

Feature	Mean		Variance		J Value	Membership	LEFT	RIGHT
	Urban	Urban	Shallow water body	Shallow water body				
MNDWI (1)	-35.15	573.0257	72.2625	159.8211	1.9645	Descending	-106.96	34.36
Layer 5 (1)	45.4375	447.6589	-28.92	8.7774	1.9493	Ascending	-19.09	108.91
NDBI (1)	52.815	216.6087	-55.31	763.9651	1.9075	Ascending	14.22	96.97
Layer 1 (1)	41.735	635.9084	-7.00025	0.3796	1.8262	Ascending	-5.40	117.39
Layer 6 (1)	52.8475	857.5831	-23.27	11.9611	1.8175	Ascending	-14.07	140.70
Layer 4 (1)	31.1775	350.9180	-23.615	28.7625	1.7985	Ascending	-10.45	87.38
Layer 3 (1)	43.027775	1244.6990	-12.05	1.3857	1.7190	Ascending	-9.38	148.87
Layer 2 (1)	38.89475	1073.7891	-8.851	2.5920	1.6312	Ascending	-5.46	137.20
NDVI (1)	-15.763	944.0892	-23.929	212.3509	0.2652	Descending	-107.94	-40.53

The derived optimum threshold value of changed object are added to class description for rule set of LULC change class as an example of urban change in Figure 5.8. Herein, an optimum threshold value and the membership function (ascending or descending) is assigned for each feature under rule set as an example shown in Figure 5.9 for mean diff to super-object of layer 1 (Band 2) with ascending membership.

Class hierarchy of LULC2012 and Object change (LULC changes between 2012 and 2017) of urban area is displayed in Figure 5.10. All rule set of object change were applied to create semantic model for classification in the next section.

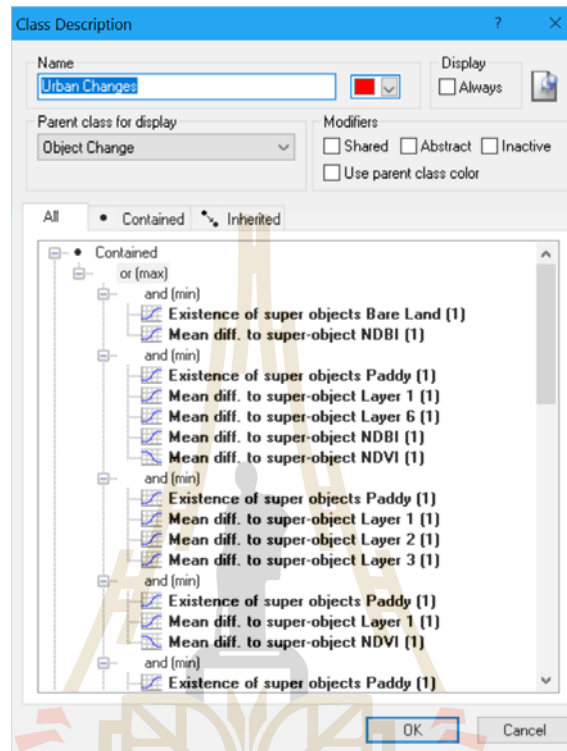


Figure 5.8 Rule set of urban change under class description.

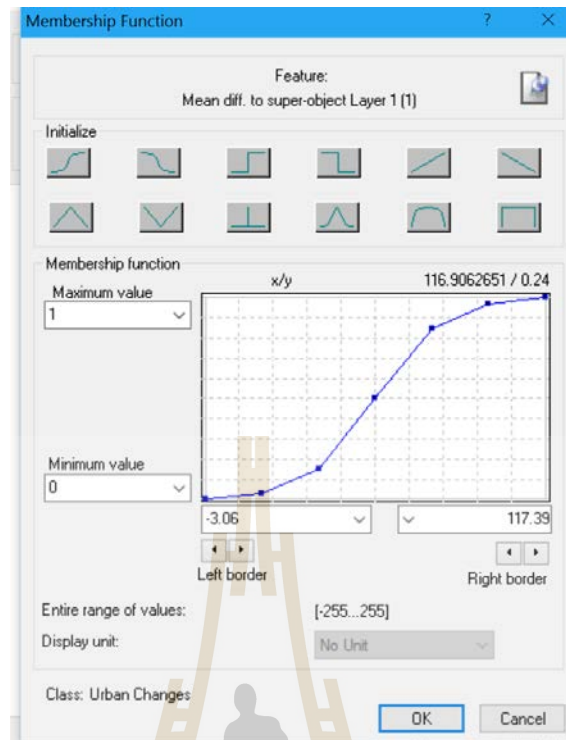


Figure 5.9 Membership function and assigned value of mean diff to-super object of layer 1.

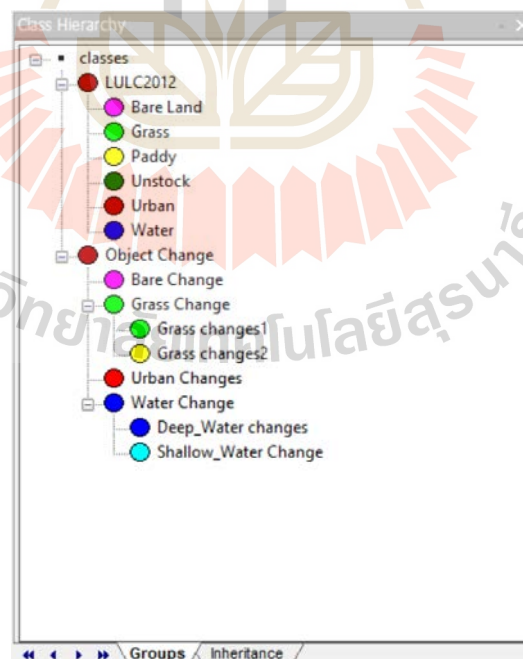


Figure 5.10 Class hierarchy of LULC2012 and Object Change.

5.1.3 Semantic modelling and classification

The developed semantic models for OBCD in urban with pan-sharpened Landsat 8 data of 2017 for Layer 1 (Band 2), Layer 2 (Band 3), Layer 4 (Band 5), Layer 5 (Band 6), Layer 6 (Band 7), MNDWI, NDBI, and NDVI are presented in Tables 5.7 to 5.12. All rule sets were directly applied to classify LULC change between 2012 and 2017 as result shown in Figure 5.11.



Table 5.7 Semantic model for bare land change between 2012 and 2017 in urban area.

LULC classes	Membership function and threshold value		
	Membership function	Left border	Right border
Bare land and Deep water body			
Existence of super-object unstock forest (1)	Ascending	0	1
Mean Diff to super-object layer 4 (1)	Ascending	-7.1	22.28
Mean Diff to super-object layer 5 (1)	Ascending	-6.77	29.22
Mean Diff to super-object MNDWI (1)	Descending	-49.9	20.28
Mean Diff to super-object NDVI (1)	Ascending	-12.5	9.8
Bare land and Urban			
Existence of super-object paddy field (1)	Ascending	0	1
Mean Diff to super-object layer 1 (1)	Ascending	-2.58	24.43
Mean Diff to super-object layer 2 (1)	Descending	-2.26	33.95
Mean Diff to super-object layer 3 (1)	Descending	7.94	52.69
Mean Diff to super-object layer 6 (1)	Descending	0.69	41.94
Mean Diff to super-object NDBI (1)	Descending	8.38	43.44
Mean Diff to super-object NDVI (1)	Ascending	-36.8	-13.72
Bare land and Urban			
Existence of super-object unstock forest (1)	Ascending	0	1
Mean Diff to super-object layer 1 (1)	Descending	-1.37	6.01
Mean Diff to super-object layer 2 (1)	Descending	-1.54	7.87
Mean Diff to super-object layer 3 (1)	Descending	-3.18	11.78
Mean Diff to super-object layer 4 (1)	Ascending	5.48	22.28
Mean Diff to super-object layer 5 (1)	Descending	-6.88	15.71
Mean Diff to super-object layer 6 (1)	Descending	-6.39	16.06
Mean Diff to super-object MNDWI (1)	Descending	-49.9	-19.87
Mean Diff to super-object NDBI (1)	Descending	-6.94	21.49
Mean Diff to super-object NDVI (1)	Ascending	-5.34	9.8
Bare land and Urban			
Existence of super-object water body (1)	Ascending	0	1
Mean Diff to super-object layer 1 (1)	Descending	-3.23	3.18
Mean Diff to super-object layer 2 (1)	Descending	-3.6	4.5
Mean Diff to super-object NDVI (1)	Ascending	8.29	53.88

Table 5.8 Semantic model for grass land change (1) between 2012 and 2017 in urban area.

LULC classes	Membership function and threshold value		
	Membership function	Left border	Right border
Grass land (1) and Urban			
Existence of super-object paddy field (1)	Ascending	0	1
Mean Diff to super-object layer 1 (1)	Descending	-6.83	-3.06
Mean Diff to super-object layer 5 (1)	Descending	-14.91	3.09
Mean Diff to super-object layer 6 (1)	Descending	-18.82	-8.46
Mean Diff to super-object NDBI (1)	Descending	-118.07	-47.93
Mean Diff to super-object NDVI (1)	Ascending	83.46	101.14
Grass land (1) and Bare land			
Existence of super-object paddy field (1)	Ascending	0	1
Mean Diff to super-object layer 1 (1)	Descending	-6.83	-2.52
Mean Diff to super-object layer 2 (1)	Descending	-6.1	3.88
Mean Diff to super-object layer 3 (1)	Descending	-16.24	-5.25
Mean Diff to super-object layer 5 (1)	Descending	-14.91	6.63
Mean Diff to super-object layer 6 (1)	Descending	-18.82	-6.13
Mean Diff to super-object MNDWI (1)	Ascending	-10.65	24.47
Mean Diff to super-object NDBI (1)	Descending	-118.07	-38.39
Mean Diff to super-object NDVI (1)	Ascending	55.44	101.14
Grass land(1) and Grass land(2)			
Existence of super-object paddy field (1)	Ascending	0	1
Mean Diff to super-object layer 4 (1)	Ascending	31.04	55.21
Mean Diff to super-object NDBI (1)	Descending	-118.07	-66.89
Mean Diff to super-object NDVI (1)	Ascending	75.11	101.14

Table 5.9 Semantic model for grass land change (2) between 2012 and 2017 in urban.

LULC classes	Membership function and threshold value		
	Membership function	Left border	Right border
Grass land (2) and Bare land			
Existence of super-object paddy field (1)	Ascending	0	1
Mean Diff to super-object layer 1 (1)	Descending	-9.3	1.7
Mean Diff to super-object layer 2 (1)	Descending	-11.55	2.4
Mean Diff to super-object layer 3 (1)	Descending	-17.42	6.45
Mean Diff to super-object layer 5 (1)	Descending	-18.05	18.74
Mean Diff to super-object NDVI (1)	Ascending	-2.54	46.86
Grass land (2) and Urban			
Existence of super-object unstock forest (1)	Ascending	0	1
Mean Diff to super-object layer 1 (1)	Descending	-18.07	1.34
Mean Diff to super-object layer 2 (1)	Descending	-26.21	1.61
Mean Diff to super-object layer 3 (1)	Descending	-39.09	2.56
Mean Diff to super-object layer 4 (1)	Descending	-21.6	0.88
Mean Diff to super-object layer 5 (1)	Descending	-37.43	3.28
Mean Diff to super-object layer 6 (1)	Descending	-42.05	2.84
Mean Diff to super-object MNDWI (1)	Ascending	-6.9	37.61
Mean Diff to super-object NDBI (1)	Descending	-56.84	9.31
Mean Diff to super-object NDVI (1)	Ascending	-2.87	36.93
Grass land (2) and Bare land			
Existence of super-object unstock forest (1)	Ascending	0	1
Mean Diff to super-object layer 1 (1)	Descending	-18.07	1.45
Mean Diff to super-object layer 2 (1)	Descending	-26.21	2.16
Mean Diff to super-object layer 3 (1)	Descending	-39.09	2.97
Mean Diff to super-object layer 4 (1)	Descending	-21.6	2.88
Mean Diff to super-object layer 5 (1)	Descending	-37.43	4.03
Mean Diff to super-object layer 6 (1)	Descending	-42.05	3.81
Mean Diff to super-object MNDWI (1)	Ascending	-6.81	37.61
Mean Diff to super-object NDBI (1)	Descending	-56.84	5.44
Mean Diff to super-object NDVI (1)	Ascending	3.47	36.93
Grass land(2) and Deep water body			
Existence of super-object unstock forest (1)	Ascending	0	1
Mean Diff to super-object layer 4 (1)	Ascending	-13.44	15.9
Mean Diff to super-object layer 5 (1)	Ascending	-16.04	25.34
Mean Diff to super-object MNDWI (1)	Descending	-30.24	31.85
Mean Diff to super-object NDVI (1)	Ascending	-16.57	36.93

Table 5.10 Semantic model for urban change between 2012 and 2017 in urban area.

LULC classes	Membership function and threshold value		
	Membership function	Left border	Right border
Urban change and Grass land(1)			
Existence of super-object paddy field (1)	Ascending	0	1
Mean Diff to super-object layer 1 (1)	Ascending	-3.06	117.39
Mean Diff to super-object layer 6 (1)	Ascending	-8.46	140.7
Mean Diff to super-object NDBI (1)	Ascending	-47.93	96.97
Mean Diff to super-object NDVI (1)	Descending	-107.94	83.46
Urban change and Grass land(2)			
Existence of super-object paddy field (1)	Ascending	0	1
Mean Diff to super-object layer 1 (1)	Ascending	1.03	117.39
Mean Diff to super-object layer 2 (1)	Ascending	0.47	137.2
Mean Diff to super-object layer 3 (1)	Ascending	0.95	148.87
Urban change and Bare land			
Existence of super-object paddy field (1)	Ascending	0	1
Mean Diff to super-object layer 1 (1)	Ascending	24.43	117.39
Mean Diff to super-object NDVI (1)	Descending	-107.94	-27.42
Urban change and Deep water body			
Existence of super-object paddy field (1)	Ascending	0	1
Mean Diff to super-object layer 4 (1)	Ascending	-27.11	87.38
Mean Diff to super-object layer 5 (1)	Ascending	-27.09	108.91
Mean Diff to super-object layer 6 (1)	Ascending	-21.88	140.7
Mean Diff to super-object MNDWI (1)	Descending	-106.96	59.93
Mean Diff to super-object NDBI (1)	Ascending	1.95	96.97
Urban change and Shallow water body			
Existence of super-object paddy field (1)	Ascending	0	1
Mean Diff to super-object layer 1 (1)	Ascending	-5.4	117.39
Mean Diff to super-object layer 4 (1)	Ascending	-10.45	87.38
Mean Diff to super-object layer 5 (1)	Ascending	-19.09	108.91
Mean Diff to super-object layer 6 (1)	Ascending	-14.07	140.7
Mean Diff to super-object MNDWI (1)	Descending	-106.96	34.36
Mean Diff to super-object NDBI (1)	Ascending	14.22	96.97
Urban change and Bare land			
Existence of super-object unstock forest(1)	Ascending	0	1
Mean Diff to super-object layer 1 (1)	Ascending	6.01	32.99
Mean Diff to super-object layer 2 (1)	Ascending	7.87	35.28

Table 5.10 (Continued).

LULC classes	Membership function and threshold value		
	Membership function	Left border	Right border
Mean Diff to super-object layer 3 (1)	Ascending	11.78	47.75
Mean Diff to super-object layer 6 (1)	Descending	-24.05	4.84
Mean Diff to super-object NDBI (1)	Ascending	21.49	81.55
Mean Diff to super-object NDVI (1)	Descending	-58.23	-5.34
Urban change and Deep water body			
Existence of super-object unstock forest(1)	Ascending	0	1
Mean Diff to super-object layer 4 (1)	Ascending	-10.27	23.32
Mean Diff to super-object layer 5 (1)	Ascending	-10.34	44.11
Mean Diff to super-object MNDWI (1)	Descending	-37.5	14.22
Mean Diff to super-object NDBI (1)	Ascending	-7.11	81.55
Urban change and Deep water body			
Existence of super-object grass land (1)	Ascending	0	1
Mean Diff to super-object layer 4 (1)	Ascending	-1.6	37.67
Mean Diff to super-object layer 6 (1)	Ascending	-5.32	53.2
Urban change and Bare land			
Existence of super-object water body (1)	Ascending	0	1
Mean Diff to super-object layer 1 (1)	Ascending	3.18	38.99
Mean Diff to super-object layer 2 (1)	Descending	4.5	43.05
Mean Diff to super-object NDVI (1)	Ascending	-51.88	8.29

Table 5.11 Semantic model for deep water body change between 2012 and 2017 in urban area.

LULC classes	Membership function and threshold value		
	Membership function	Left border	Right border
Deep water body and Urban			
Existence of super-object paddy field (1)	Ascending	0	1
Mean Diff to super-object layer 4 (1)	Descending	-51.55	-27.11
Mean Diff to super-object layer 5 (1)	Descending	-41.16	-27.09
Mean Diff to super-object layer 6 (1)	Descending	-33.5	-21.88
Mean Diff to super-object MNDWI (1)	Ascending	59.93	132.21
Mean Diff to super-object NDBI (1)	Descending	-50.49	1.95
Deep water body and Bare land			
Existence of super-object paddy field (1)	Ascending	0	1
Mean Diff to super-object layer 1 (1)	Descending	-14.69	2.91
Mean Diff to super-object layer 3 (1)	Descending	-25.25	1.48
Mean Diff to super-object layer 4 (1)	Descending	-51.55	-18.95
Mean Diff to super-object layer 5 (1)	Descending	-41.16	-21.38
Mean Diff to super-object layer 6 (1)	Descending	-33.5	-18.01
Mean Diff to super-object MNDWI (1)	Ascending	22.57	132.21
Mean Diff to super-object NDBI (1)	Descending	-50.49	2.79
Mean Diff to super-object NDVI (1)	Descending	-101.56	-38.6
Deep water body and Grass land(1)			
Existence of super-object paddy field (1)	Ascending	0	1
Mean Diff to super-object layer 4 (1)	Descending	-51.55	6.49
Mean Diff to super-object layer 5 (1)	Descending	-41.16	-26.02
Mean Diff to super-object layer 6 (1)	Descending	-33.5	-21.52
Mean Diff to super-object MNDWI (1)	Ascending	50.58	132.21
Mean Diff to super-object NDVI (1)	Descending	-101.56	58.18
Deep water body and Grass land(2)			
Existence of super-object paddy field (1)	Ascending	0	1
Mean Diff to super-object layer 4 (1)	Descending	-51.55	-23.07
Mean Diff to super-object layer 5 (1)	Descending	-41.16	-26.02
Mean Diff to super-object layer 6 (1)	Descending	-33.5	-21.52
Mean Diff to super-object MNDWI (1)	Ascending	50.58	132.21
Mean Diff to super-object NDVI (1)	Descending	-101.56	-18.62

Table 5.11 (Continued).

LULC classes	Membership function and threshold value		
	Membership function	Left border	Right border
Deep water body and Bare land			
Existence of super-object unstock forest (1)	Ascending	0	1
Mean Diff to super-object layer 4 (1)	Descending	-35.91	-7.1
Mean Diff to super-object MNDWI (1)	Ascending	20.28	99.77
Mean Diff to super-object NDVI (1)	Descending	-52.64	-12.5
Deep water body and Urban			
Existence of super-object grass land (1)	Ascending	0	1
Mean Diff to super-object layer 4 (1)	Descending	-38.17	-1.6
Mean Diff to super-object layer 5 (1)	Descending	-33.3	-6.48
Mean Diff to super-object layer 6 (1)	Descending	-22.56	-5.32

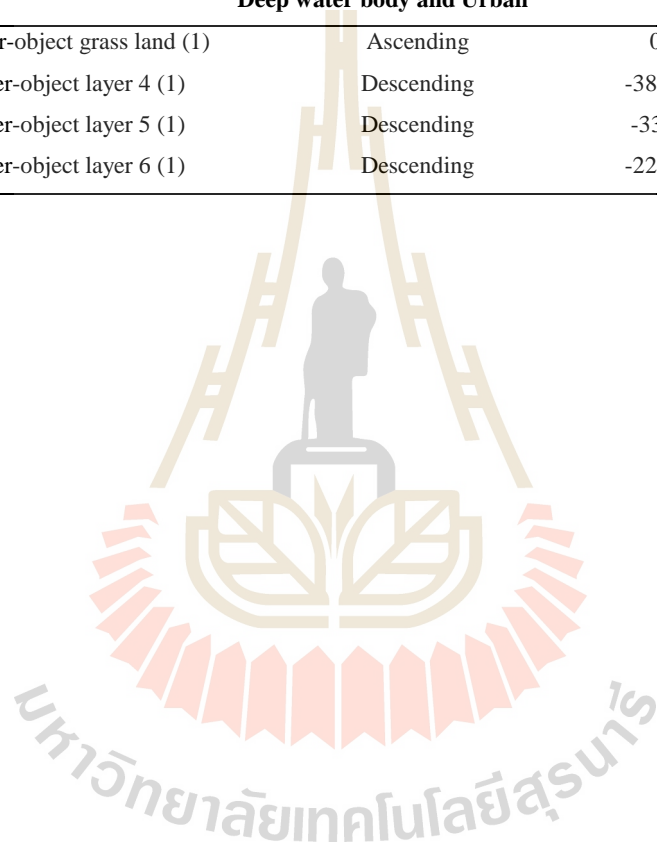


Table 5.12 Semantic model for shallow water body change between 2012 and 2017 in urban.

LULC classes	Membership function and threshold value		
	Membership function	Left border	Right border
Shallow water body and Deep water body			
Existence of super-object paddy field (1)	Ascending	0	1
Mean Diff to super-object layer 4 (1)	Descending	-32.93	-7.53
Mean Diff to super-object MNDWI (1)	Ascending	34.34	88.02
Mean Diff to super-object NDVI (1)	Descending	-51.46	19.79
Shallow water body and Grass land (1)			
Existence of super-object paddy field (1)	Ascending	0	1
Mean Diff to super-object layer 2 (1)	Descending	-13.68	-4.99
Mean Diff to super-object layer 4 (1)	Descending	-39.7	19.39
Mean Diff to super-object layer 5 (1)	Descending	-37.81	-17.61
Mean Diff to super-object MNDWI (1)	Ascending	27.85	110.19
Mean Diff to super-object NDVI (1)	Descending	-67.65	74.49
Shallow water body and Grass land(2)			
Existence of super-object paddy field (1)	Ascending	0	1
Mean Diff to super-object layer 4 (1)	Descending	-39.7	-10.84
Mean Diff to super-object layer 5 (1)	Descending	-37.81	-19.2
Mean Diff to super-object layer 6 (1)	Descending	-33.65	-15.43
Mean Diff to super-object MNDWI (1)	Ascending	28.28	110.19
Mean Diff to super-object NDVI (1)	Descending	-67.65	5.84
Shallow water body and Bare land			
Existence of super-object paddy field (1)	Ascending	0	1
Mean Diff to super-object layer 1 (1)	Descending	-8.85	-4.76
Mean Diff to super-object layer 2 (1)	Descending	-13.68	-3.44
Mean Diff to super-object layer 3 (1)	Descending	-15.58	-6.7
Mean Diff to super-object layer 4 (1)	Descending	-39.7	-3.63
Mean Diff to super-object layer 5 (1)	Descending	-37.81	12.69
Mean Diff to super-object layer 6 (1)	Descending	-33.65	-9.16
Mean Diff to super-object MNDWI (1)	Ascending	4.79	110.19
Mean Diff to super-object NDBI (1)	Descending	-138.23	11.78
Shallow water body and Urban			
Existence of super-object paddy field (1)	Ascending	0	1
Mean Diff to super-object layer 1 (1)	Descending	-8.85	-5.4
Mean Diff to super-object layer 4 (1)	Descending	-39.7	-10.45
Mean Diff to super-object layer 5 (1)	Descending	-37.81	19.09
Mean Diff to super-object layer 6 (1)	Descending	-33.65	-14.07
Mean Diff to super-object MNDWI (1)	Ascending	34.36	110.19
Mean Diff to super-object NDBI (1)	Descending	-138.23	14.22

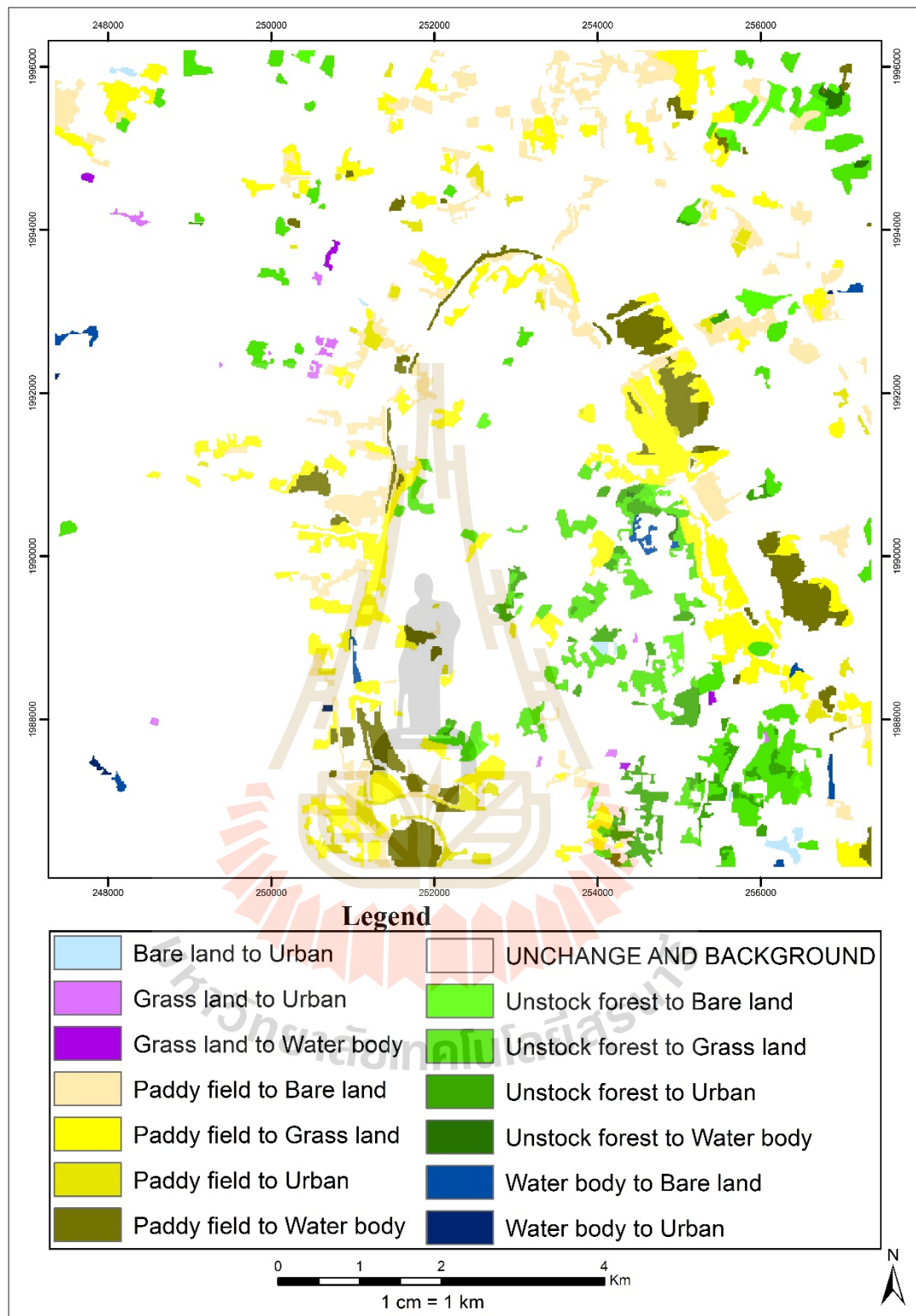


Figure 5.11 LULC change between 2012 and 2017 in urban area.

5.2 Land use and land cover in 2017 updating

The derived LULC change data is applied to update LULC map in 2012 for final LULC map in 2017 as a result shown in Figure 5.12. Comparison of area and percentage of LULC data in 2012 and 2017 is presented in Table 5.13 and the change matrix of LULC classes between 2012 and 2017 is reported in Table 5.14.

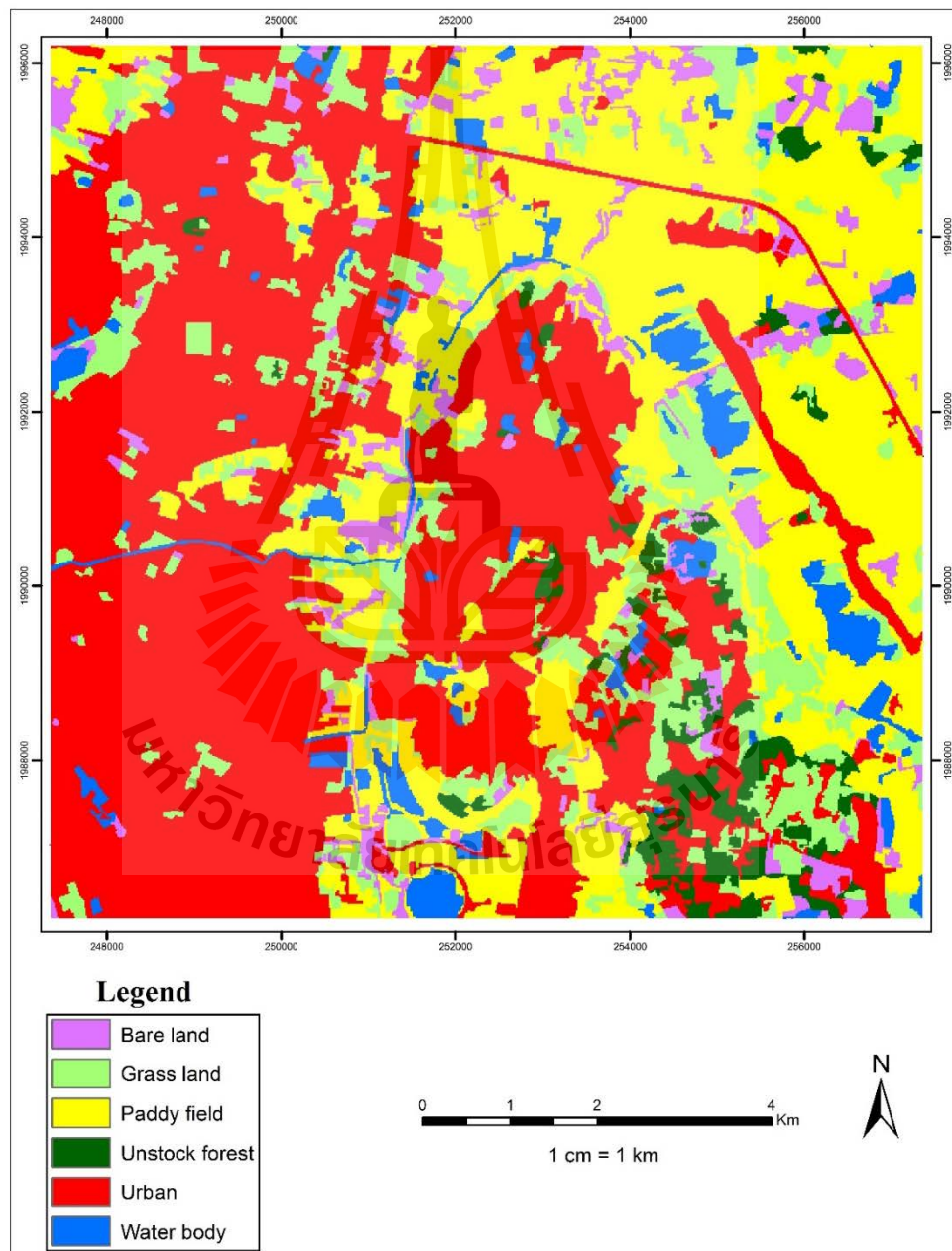


Figure 5.12 Final LULC map in 2017 in urban area.

Table 5.13 Comparison of area and percent of LULC in 2012 and 2017 in urban area.

LULC class	LULC in 2012		LULC in 2017	
	Area (Sq. Km)	%	Area (Sq. Km)	%
Urban	42.68	42.68	44.83	44.83
Water body	2.41	2.41	4.73	4.73
Unstock forest	8.21	8.20	3.12	3.12
Paddy field	42.24	42.24	29.31	29.31
Grass land	3.51	3.51	12.67	12.67
Bare land	0.95	0.95	5.34	5.34
Total	100.00	100.00	100.00	100.00

Table 5.14 Change matrix of LULC classes between 2012 and 2017.

LULC classes in 2012	LULC classes in 2017 (Unit: sq. km)						Total
	Urban	Water body	Grass land	Unstock forest	Bare land	Paddy field	
Urban	42.74						42.74
Water body	0.03	2.16			0.23		2.43
Grass land	0.14	0.06	3.29				3.49
Unstock forest	1.05	0.08	3.37	3.13	0.59		8.22
Bare land	0.13				0.82		0.95
Paddy field	0.77	2.46	6.04		3.72	29.29	42.28
Total	44.86	4.76	12.70	3.13	5.36	29.29	

As result, it was found that urban area between 2012 and 2017 was increased about 2.12 sq. km. The increased urban area in 2017 came from unstock forest (1.05 sq. km.), paddy field (0.77 sq. km.), grass land (0.14 sq. km.), bare land (0.13 sq. km.) and water body (0.03 sq. km.) in 2012. On contrary, paddy field between 2012 and 2017 was dramatic decreased about 12.99 sq. km. Paddy field in 2012 was changed to be grass land (6.04 sq. km.), bare land (3.72 sq. km.), water body (2.46 sq. km.) and urban (0.77 sq. km.) in 2017.

5.3 Accuracy assessment

The extracted LULC change map between 2012 and 2017 is further assess accuracy based on 144 stratified random sampling points with reference image from Google Earth in 2017. Error matrix and accuracy assessment is presented in Table 5.15.

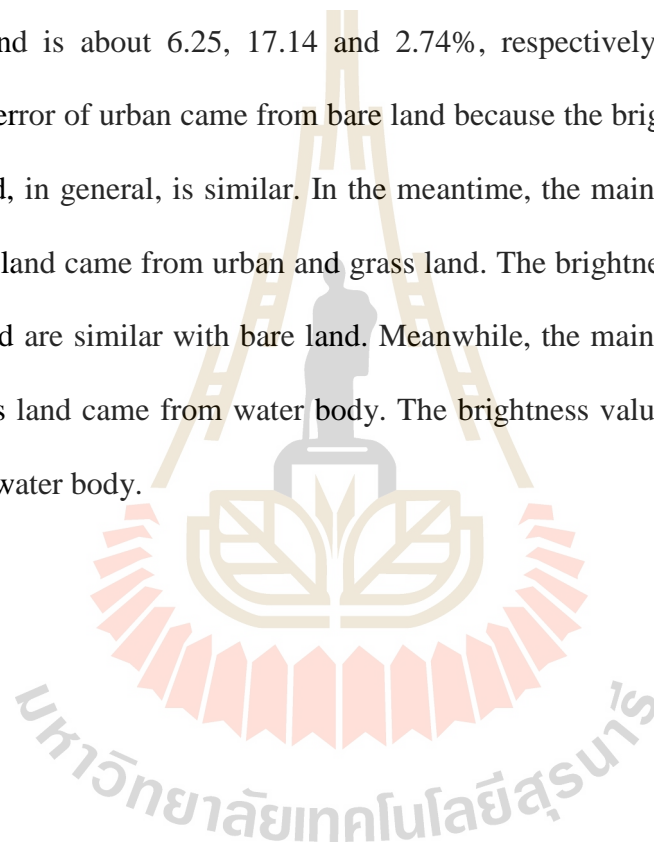
As a result it reveals that overall accuracy and Kappa hat coefficient is 93.75% and 90.45%, respectively. Meanwhile producer's accuracy of LULC change class varies between 78.95% for urban and 100.00% for bare land while user's accuracy of LULC change class varies between 82.86% for bare land and 100.00% for water body. Based on Fitzpatrick-Lins (1981), Kappa hat coefficient more than 80% represents strong agreement or accuracy between the predicted map and the reference map.

Table 5.15 Error matrix and accuracy assessment of LULC change between 2012 and 2017.

Class Name	Reference Data				Row Total	PA	UA
	Urban	Water body	Bare Land	Grass Land			
Urban	15			1	16	78.95	93.75
Water body		20			20	90.91	100.00
Bare Land	4		29	2	35	100.00	82.86
Grass Land		2		71	73	95.95	97.26
Column Total	19	22	29	74	144		
Overall accuracy	93.75						
Kappa hat coefficient	90.45						

In addition, it can be observed that omission error of urban area and water body is about 21.05 and 9.09%, respectively. The main cause of omission error of urban came from bare land because the brightness value of urban and bare land, in general, is similar. Meanwhile, the main cause of omission error of water body came from grass land because the appearance of wet grass land is similar water body.

Likewise, it can be observed that commission error of urban area, bare land and grass land is about 6.25, 17.14 and 2.74%, respectively. The main cause of commission error of urban came from bare land because the brightness value of urban and bare land, in general, is similar. In the meantime, the main cause of commission error of bare land came from urban and grass land. The brightness value of urban and dry grass land are similar with bare land. Meanwhile, the main cause of commission error of grass land came from water body. The brightness value of wet grass land is similar with water body.



CHAPTER VI

LULC UPDATING IN PADDY FIELD

The main results of land use and land cover updating in paddy field area include (1) the development of rule set for LULC classification in paddy field, (2) land use and land cover in 2017 updating and (3) accuracy assessment.

6.1 Development of rule set for land use/land cover classification

Major results of rule set for LULC classification development of paddy field area includes (1) the image segmentation by Multiresolution segmentation, (2) the feature extraction by SEaTH analysis, and (3) the semantic modelling and classification.

6.1.1 Image segmentation by Multiresolution segmentation

Two steps of image segmentation were here implemented for hierarchical object structure creation as parent and child relationship (object and its super object) for OBCD. Firstly, an optimum pan-sharpened image are segmented with thematic map of LULC data in 2012 as result shown in Figure 6.1. Secondly, the derived image objects at Level 2 are segmented again at Level 1 with thematic layer as child level as a result shown in Figure 6.2. The configuration of Multiresolution segmentation at Level 2 and Level 1 is summarized in Table 6.1.

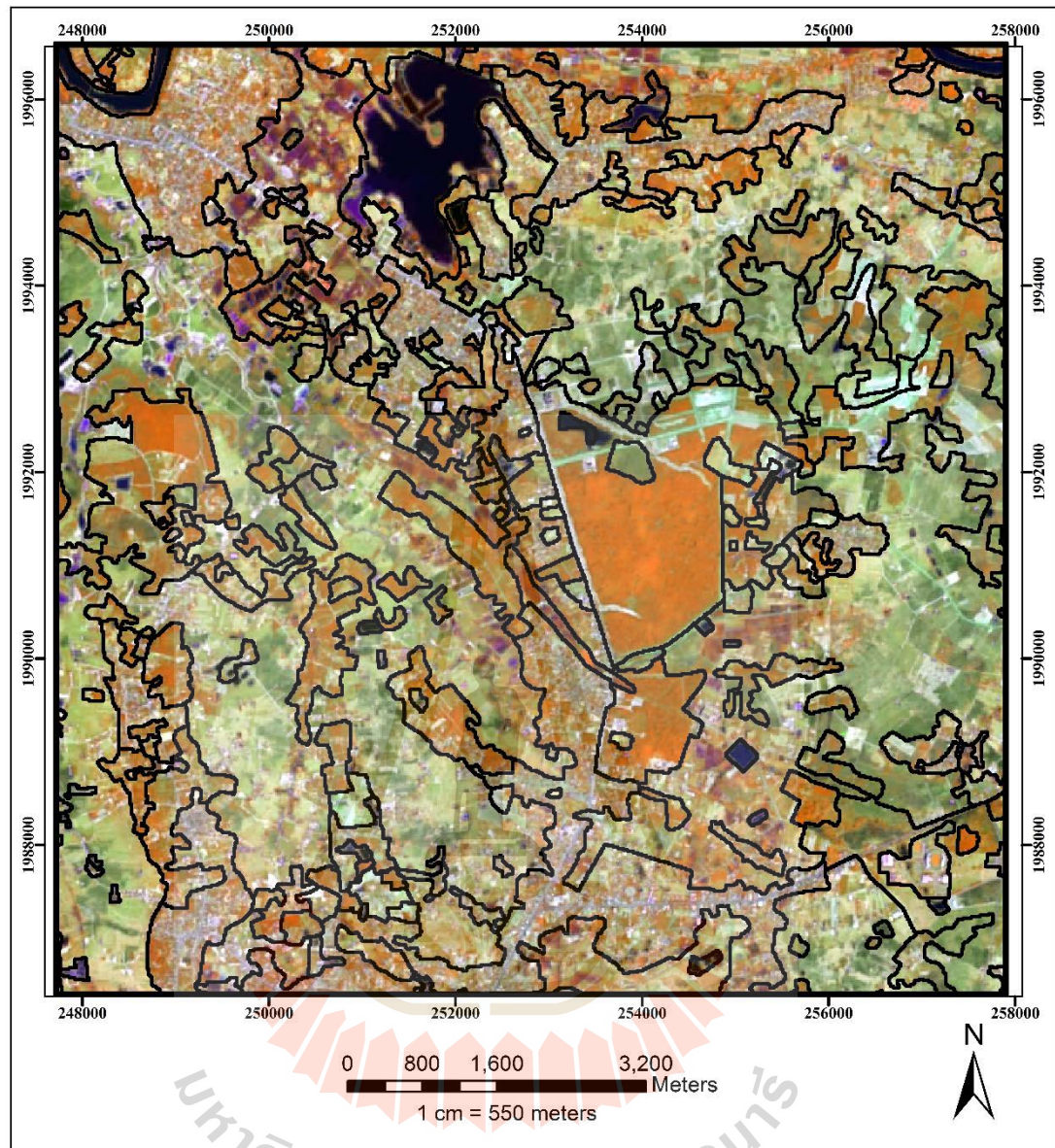


Figure 6.1 Image object of optimum pan-sharpened Landsat 8 data of 2012 by Multiresolution segmentation at level 2.

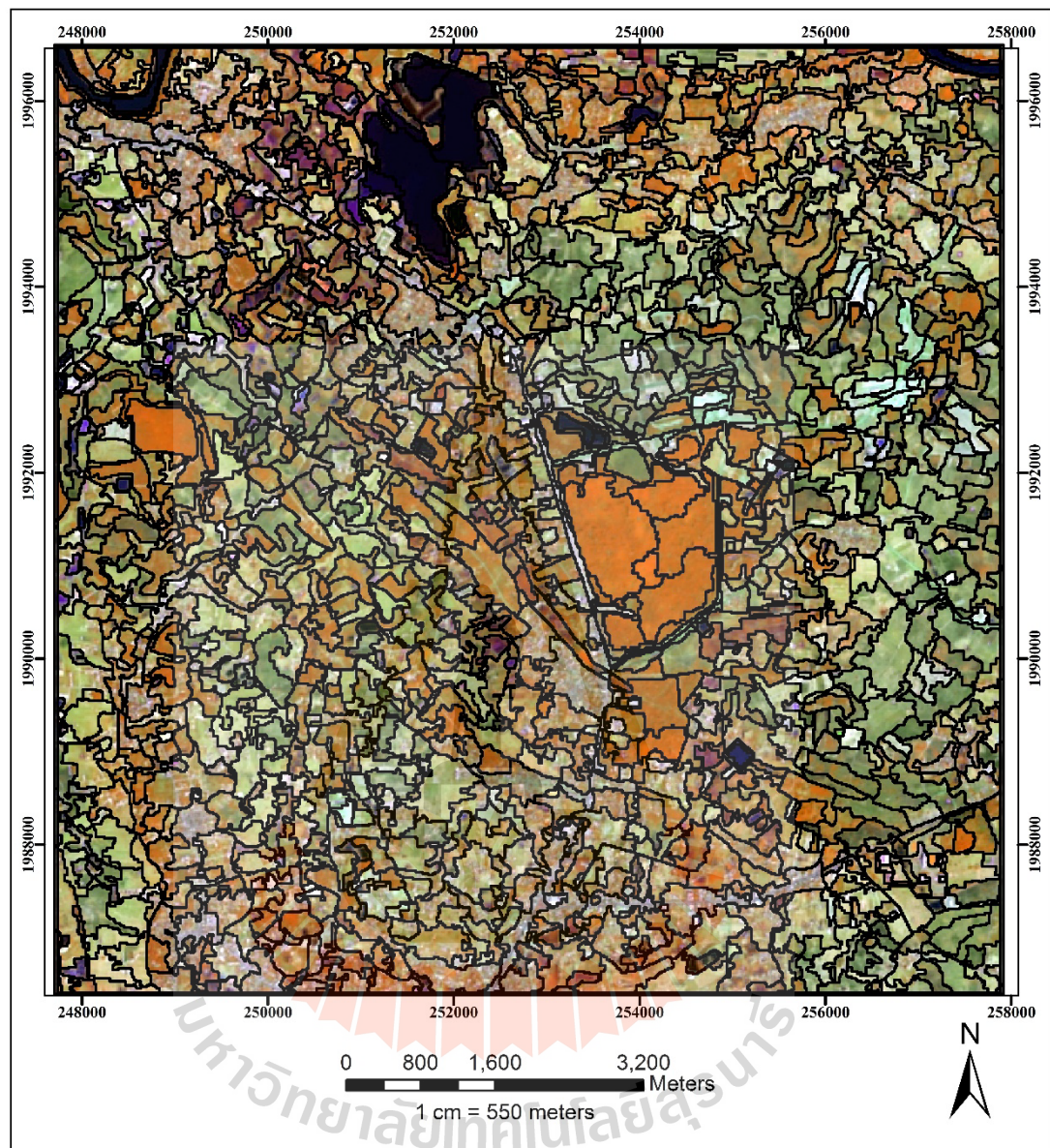


Figure 6.2 Image object of optimum pan-sharpened Landsat 8 data of 2017 by Multiresolution segmentation at level 1.

Table 6.1 Configuration of multiresolution segmentation at Level 2 and Level 1 with thematic layer.

Image object domain	Pixel level	Image object level
Level setting		
Level name	Level 2	Level 1
Segmentation setting		
Image layer weight	0, 0, 0, 0, 0, 0, 0, 0, 0	1, 1, 1, 1, 1, 1, 1, 1, 1
Thematic layer usage	Yes	YES
Scale parameters		
	20	20
Composition of homogeneity criterion		
Shape	0	0.1
Compactness	0	0.5

As results, it was found number of image object at Level 2 as parent level is 266 while number of image object at Level 1 as child level is 1,447. In principle, child objects that have similar spectral characteristics as parent objects are unchanged objects, while any deviation is an indicator of changed objects.

6.1.2 Feature extraction by SEaTH analysis

Parent-child relationship between image objects at Level 2 and Level 1 is applied to extract changed and unchanged objects between 2012 and 2017. In this study, two main steps are required for feature extraction by SEaTH analysis.

At the first step, existence of LULC class from 2012 at Level 2 as parent level is created under class-related feature properties as shown in Figure 6.3. Herein, the created existence LULC classes in paddy field area include bare land, grass land, mixed deciduous forest, paddy field, unstock forest, urban and water body are applied as super-object (parent) of Level 1 as child level. This image property is applied to create super-object class hierarchy under Level 2 including LULC in 2012 and LULC change between 2012 and 2017 as shown in Figure 6.4. This structure can

directly apply to classify LULC map in 2012 according to class description as shown in Figure 6.5. It consists of LULC code of each LULC class and Level number (Level 2).

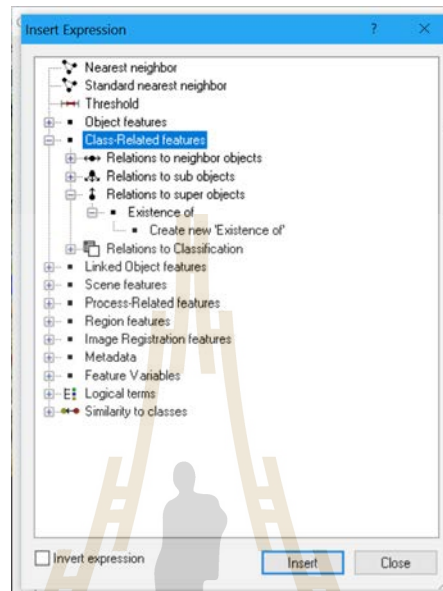


Figure 6.3 Class-related feature properties: Existence of.

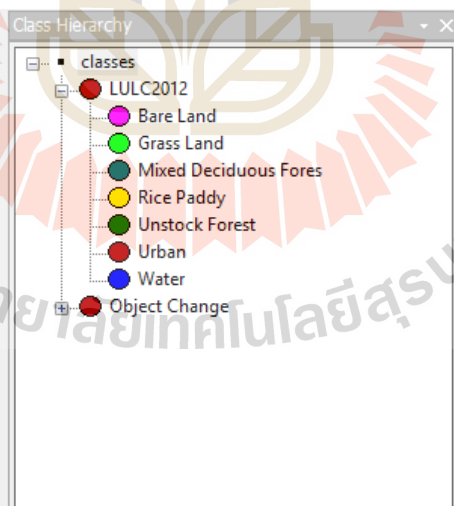


Figure 6.4 Class hierarchy structure of Super-object at Level 2.

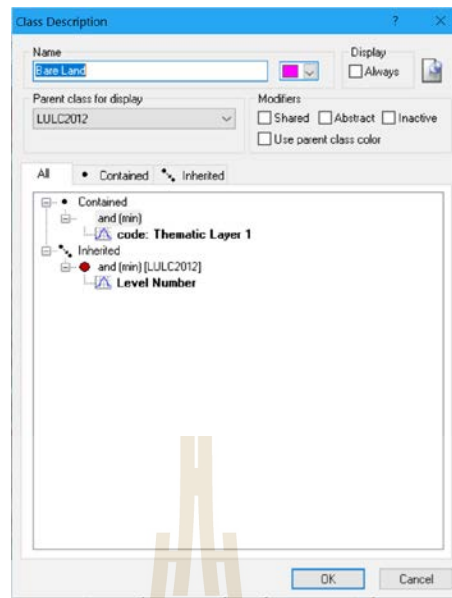


Figure 6.5 Class description of Super-object at Level 2.

At the second step, mean diff to super-object under To super-object property of layers values are applied to identify changed objects of Level 1 as child level as shown in Figure 6.6. In practice, mean value of each layer from 5 training areas are extracted and exported to MS-Excel spreadsheet software for SEaTH analysis. Examples of training areas for LULC changed object in 2017 are displayed in Figure 6.7. Meanwhile results of SEaTH analysis for separability test and threshold value extraction for rule-based development of paddy field among other classes using Equation 2.1, 2.2 and 2.6 are displayed in Tables 6.2 to 6.5.

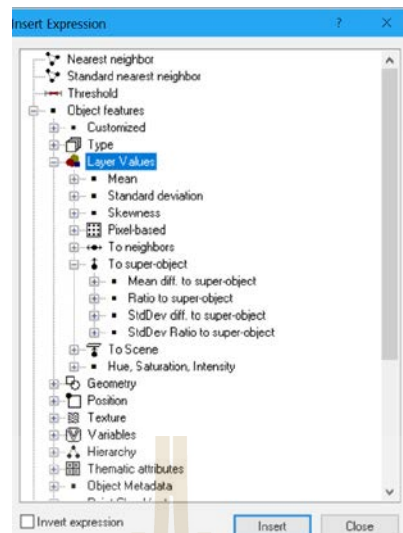


Figure 6.6 Structure of Mean diff to super-object parameter for changed object identification.

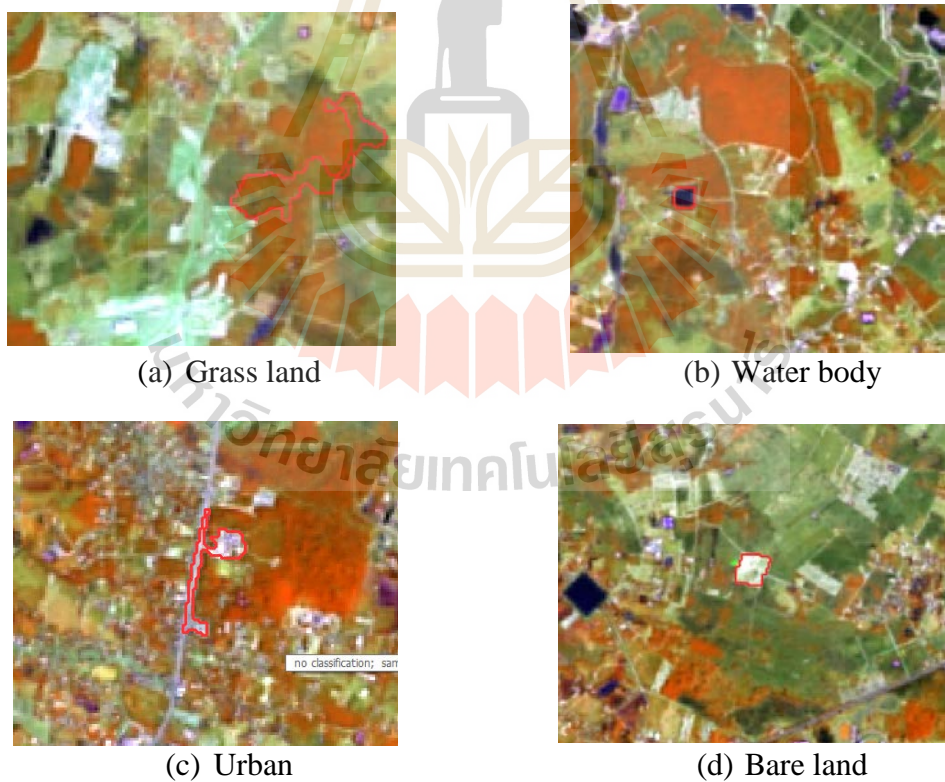


Figure 6.7 Training areas of changed objects in 2017 for SEaTH analysis.

Table 6.2 Pairwise of mean and variance between water body and urban for threshold value calculation.

Feature	Mean	Variance	Mean	Variance	J Value	Membership	LEFT	RIGHT
	Water body	Water body	urban	urban				
MNDWI (1)	52.96	109.38	-3.70	53.91	1.99	Ascending	19.88	84.34
NDVI (1)	-32.98	24.48	-1.40	41.82	1.95	Descending	-47.82	-19.17
Layer 4 (1)	-27.06	21.25	16.93	435.92	1.55	Descending	-40.89	-17.75
Layer 5 (1)	-29.42	27.20	17.74	843.61	1.38	Descending	-45.07	-20.11
Layer 6 (1)	-19.54	13.49	16.61	765.43	1.33	Descending	-30.56	-13.27
Layer 1 (1)	0.02	8.21	15.50	585.47	1.13	Descending	-8.58	4.14
Layer 3 (1)	-7.31	30.40	21.05	685.06	1.04	Descending	-23.85	0.44
Layer 2 (1)	0.71	22.46	19.32	737.52	0.96	Descending	-13.50	6.94
NDBI (1)	-12.37	20.92	0.64	69.18	0.85	Descending	-26.09	-7.02

Table 6.3 Pairwise of mean and variance between bare land and water body for threshold value calculation.

Feature	Mean	Variance	Mean	Variance	J Value	Membership	LEFT	RIGHT
	Bare land	Bare land	Water body	Water body				
Layer 5 (1)	20.24	16.16	-29.42	27.20	2.00	Ascending	-1.42	32.30
MNDWI (1)	-10.90	1.35	52.96	109.38	2.00	Descending	-14.38	-4.34
Layer 6 (1)	16.37	20.75	-19.54	13.49	2.00	Ascending	-3.47	30.04
Layer 4 (1)	16.59	39.70	-27.06	21.25	2.00	Ascending	-8.52	35.49
NDVI (1)	-4.60	6.44	-32.98	24.48	2.00	Ascending	-14.35	3.02
Layer 3 (1)	23.69	39.12	-7.31	30.40	1.94	Ascending	7.28	42.46
NDBI (1)	6.39	12.94	-12.37	20.92	1.85	Ascending	-1.96	17.18
Layer 1 (1)	10.76	10.61	0.02	8.21	1.57	Ascending	5.09	20.53
Layer 2 (1)	17.69	24.57	0.71	22.46	1.57	Ascending	9.04	32.56

Table 6.4 Pairwise of mean and variance between grass land and urban for threshold value calculation.

Feature	Mean	Variance	Mean	Variance	J Value	Membership	LEFT	RIGHT
	Grass land	Grass land	urban	urban				
Layer 1 (1)	-4.67	1.14	15.50	585.47	1.50	Descending	-7.87	-2.74
Layer 2 (1)	-6.03	1.88	19.32	737.52	1.49	Descending	-10.14	-3.54
Layer 4 (1)	1.24	1.79	16.93	435.92	1.38	Descending	-2.78	3.48
Layer 3 (1)	-8.75	8.58	21.05	685.06	1.32	Descending	-17.54	-3.85
Layer 6 (1)	-8.93	7.79	16.61	765.43	1.28	Descending	-17.31	-4.46
NDVI (1)	12.14	12.54	-1.40	41.82	1.21	Ascending	6.91	22.76
Layer 5 (1)	-8.10	20.17	17.74	843.61	1.09	Descending	-21.58	-1.65
NDBI (1)	-12.95	39.82	0.64	69.18	0.71	Descending	-31.88	-6.63
MNDWI (1)	6.04	35.30	-3.70	53.91	0.48	Ascending	1.27	23.86

Table 6.5 Pairwise of mean and variance between urban and water body for threshold value calculation.

Feature	Mean	Variance	Mean	Variance	J Value	Membership	LEFT	RIGHT
	Urban	Urban	Water body	Water body				
MNDWI (1)	-3.70	53.91	52.96	109.38	1.99	Descending	-25.73	19.88
NDVI (1)	-1.40	41.82	-32.98	24.48	1.95	Ascending	-19.17	18.00
Layer 4 (1)	16.93	435.92	-27.06	21.25	1.55	Ascending	-17.75	79.57
Layer 5 (1)	17.74	843.61	-29.42	27.20	1.38	Ascending	-20.11	104.88
Layer 6 (1)	16.61	765.43	-19.54	13.49	1.33	Ascending	-13.27	99.61
Layer 1 (1)	15.50	585.47	0.02	8.21	1.13	Ascending	4.14	88.09
Layer 3 (1)	21.05	685.06	-7.31	30.40	1.04	Ascending	0.44	99.58
Layer 2 (1)	19.32	737.52	0.71	22.46	0.96	Ascending	6.94	100.79
NDBI (1)	0.64	69.18	-12.37	20.92	0.85	Ascending	-7.02	25.59

The derived optimum threshold value of changed object are added to class description for rule set of LULC change class as an example of urban change in Figure 6.8. Herein, an optimum threshold value and the membership function (ascending or descending) is assigned for each feature under rule set as an example shown in Figure 6.9 for mean diff to super-object of layer 1 (Band 2) with ascending membership.

Class hierarchy of LULC2012 and Object change (LULC change between 2012 and 2017) of urban area is displayed in Figure 6.10. All rule set of object change are then applied to create semantic model for classification in the next section.

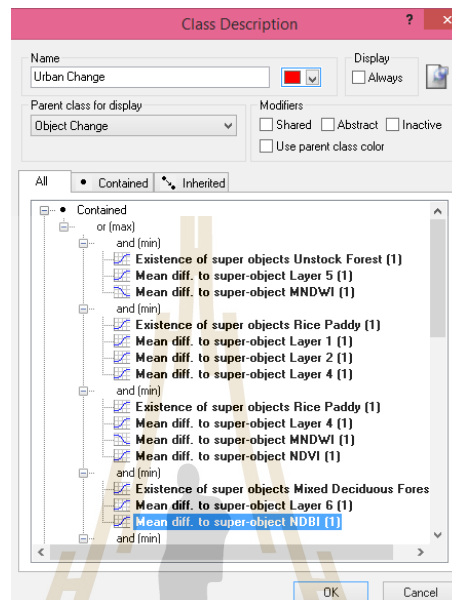


Figure 6.8 Rule set of urban change under class description.

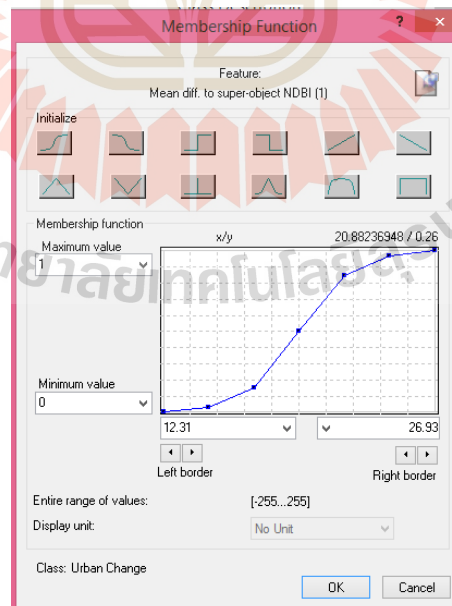


Figure 6.9 Membership function and assigned value of mean diff to-super object of layer 1.

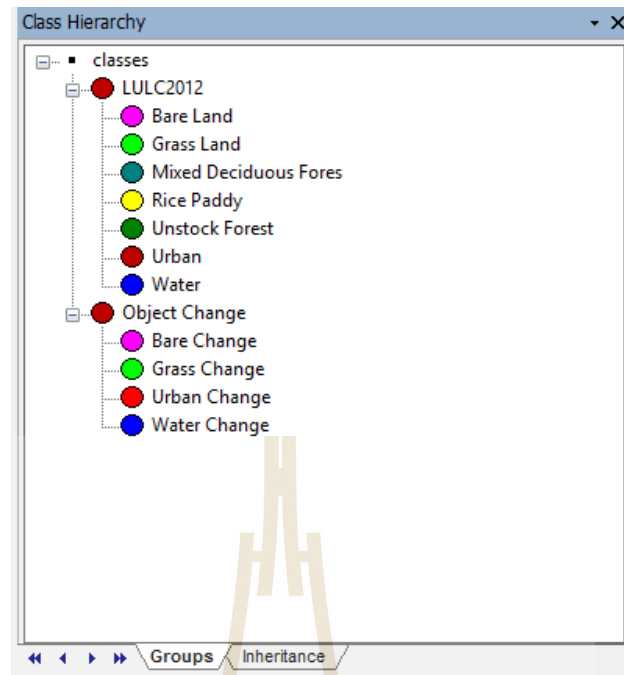


Figure 6.10 Class hierarchy of LULC2012 and Object Change.

6.1.3 Semantic modelling and classification

The developed semantic models for OBCD in paddy field with pan-sharpened Landsat 8 data of 2017 for Layer 1 (Band 2), Layer 2 (Band 3), Layer 4 (Band 5), Layer 5 (Band 6), Layer 6 (Band 7), MNDWI, NDBI, and NDVI are presented in Tables 6.6 to 6.9. All rule set is directly applied to classify LULC change between 2012 and 2017 as result shown in Figure 6.11.

Table 6.6 Semantic model for bare land change between 2012 and 2017 in paddy field area.

LULC classes	Membership function and threshold value		
	Membership function	Left border	Right border
Bare land and Grass land			
Existence of super-object unstock forest (1)	Ascending	0	1
Mean Diff to super-object NDVI (1)	Descending	-13.7	-0.78
Bare land and Urban			
Existence of super-object paddy field (1)	Ascending	0	1
Mean Diff to super-object layer 1 (1)	Descending	0.99	15.06
Mean Diff to super-object layer 2 (1)	Descending	2.82	23.77
Mean Diff to super-object layer 3 (1)	Descending	4.93	31.06
Mean Diff to super-object layer 4 (1)	Descending	-2.31	23.3
Mean Diff to super-object layer 5 (1)	Descending	8.18	25.62
Mean Diff to super-object layer 6 (1)	Descending	2.7	22.14
Mean Diff to super-object MNDWI (1)	Descending	-14.38	-9.19
Mean Diff to super-object NDBI (1)	Ascending	3.14	17.18
Mean Diff to super-object NDVI (1)	Descending	-12.21	-2.28
Bare land and Water body			
Existence of super-object paddy field (1)	Ascending	0	1
Mean Diff to super-object layer 3 (1)	Ascending	7.28	42.46
Mean Diff to super-object layer 4 (1)	Ascending	-8.52	35.49
Mean Diff to super-object layer 5 (1)	Ascending	-1.42	32.3
Mean Diff to super-object layer 6 (1)	Ascending	-3.47	30.04
Mean Diff to super-object MNDWI (1)	Descending	-14.38	-4.34
Mean Diff to super-object NDBI (1)	Ascending	-1.96	17.18
Mean Diff to super-object NDVI (1)	Ascending	-14.35	3.02
Bare land and Water body			
Existence of super-object mixed deciduous forest (1)	Ascending	0	1
Mean Diff to super-object MNDWI (1)	Descending	-27.88	7.87
Mean Diff to super-object NDVI (1)	Ascending	-15.56	-0.6
Bare land and Grass land			
Existence of super-object paddy field (1)	Ascending	0	1
Mean Diff to super-object layer 1 (1)	Ascending	-0.75	20.53
Mean Diff to super-object layer 2 (1)	Ascending	-0.73	32.56
Mean Diff to super-object layer 3 (1)	Ascending	1.78	42.46

Table 6.6 (Continued).

LULC classes	Membership function and threshold value		
	Membership function	Left border	Right border
Mean Diff to super-object layer 5 (1)	Ascending	6.82	32.3
Mean Diff to super-object layer 6 (1)	Ascending	0.79	30.04
Mean Diff to super-object MNDWI (1)	Descending	-14.38	-7.85
Mean Diff to super-object NDVI (1)	Descending	-12.21	2.47
Bare land and Urban			
Existence of super-object unstock forest (1)	Ascending	0	1
Mean Diff to super-object MNDWI (1)	Descending	-26.34	-8.02
Bare land and Water body			
Existence of super-object water body (1)	Ascending	0	1
Mean Diff to super-object NDVI (1)	Ascending	-3.53	56.01



Table 6.7 Semantic model for grass land change between 2012 and 2017 in paddy field area.

LULC classes	Membership function and threshold value		
	Membership function	Left border	Right border
Grass land and Urban			
Existence of super-object unstock forest (1)	Ascending	0	1
Mean Diff to super-object NDBI (1)	Descending	-11.63	1.5
Mean Diff to super-object NDVI (1)	Ascending	0.09	10.06
Grass land and Water body			
Existence of super-object paddy field (1)	Ascending	0	1
Mean Diff to super-object layer 1 (1)	Descending	-7.87	-3.14
Mean Diff to super-object layer 2 (1)	Descending	-10.14	-4.05
Mean Diff to super-object layer 3 (1)	Descending	-17.54	-6.54
Mean Diff to super-object layer 4 (1)	Ascending	-5.24	5.26
Mean Diff to super-object layer 5 (1)	Ascending	-18.04	5.37
Mean Diff to super-object layer 6 (1)	Ascending	-13.63	-0.56
Mean Diff to super-object MNDWI (1)	Descending	-11.79	23.36
Mean Diff to super-object NDBI (1)	Descending	-31.88	-15.35
Mean Diff to super-object NDVI (1)	Ascending	-6.74	22.76
Grass land and Bare land			
Existence of super-object paddy field (1)	Ascending	0	1
Mean Diff to super-object layer 1 (1)	Descending	-7.87	-0.75
Mean Diff to super-object layer 2 (1)	Descending	-10.14	-0.73
Mean Diff to super-object layer 3 (1)	Descending	-17.54	1.78
Mean Diff to super-object layer 4 (1)	Descending	-2.78	4.28
Mean Diff to super-object layer 5 (1)	Descending	-21.58	6.82
Mean Diff to super-object layer 6 (1)	Descending	-17.31	0.79
Mean Diff to super-object MNDWI (1)	Ascending	-7.85	23.86
Mean Diff to super-object NDBI (1)	Descending	-31.88	-0.91
Mean Diff to super-object NDVI (1)	Descending	2.47	22.76
Grass land and Urban			
Existence of super-object paddy field (1)	Ascending	0	1
Mean Diff to super-object layer 1 (1)	Descending	-7.87	-2.74
Mean Diff to super-object layer 2 (1)	Descending	-10.14	-3.54
Mean Diff to super-object layer 3 (1)	Descending	-17.54	-3.85
Mean Diff to super-object layer 4 (1)	Descending	-2.78	3.48
Mean Diff to super-object layer 5 (1)	Descending	-21.58	-1.65

Table 6.7 (Continued).

LULC classes	Membership function and threshold value		
	Membership function	Left border	Right border
Mean Diff to super-object layer 6 (1)	Descending	-17.31	-4.46
Mean Diff to super-object MNDWI (1)	Ascending	1.27	23.86
Mean Diff to super-object NDBI (1)	Descending	-31.88	-6.63
Mean Diff to super-object NDVI (1)	Ascending	6.91	22.76
Grass land and Bare land			
Existence of super-object unstock forest (1)	Ascending	0	1
Mean Diff to super-object MNDWI (1)	Ascending	-1.29	6.78

Table 6.8 Semantic model for urban change between 2012 and 2017 in paddy field.

LULC classes	Membership function and threshold value		
	Membership function	Left border	Right border
Urban and Grass land			
Existence of super-object unstock forest (1)	Ascending	0	1
Mean Diff to super-object layer 5 (1)	Ascending	1.28	17.26
Mean Diff to super-object MNDWI (1)	Descending	-10.74	-2.94
Urban and Grass land			
Existence of super-object paddy field (1)	Ascending	0	1
Mean Diff to super-object layer 1 (1)	Ascending	-2.74	88.09
Mean Diff to super-object layer 2 (1)	Ascending	-3.54	100.79
Mean Diff to super-object layer 4 (1)	Ascending	3.48	79.57
Urban and Water body			
Existence of super-object paddy field (1)	Ascending	0	1
Mean Diff to super-object layer 4 (1)	Ascending	-17.75	79.57
Mean Diff to super-object MNDWI (1)	Descending	-25.73	19.88
Mean Diff to super-object NDVI (1)	Ascending	-19.17	18
Urban and Water body			
Existence of super-object mixed deciduous forest (1)	Ascending	0	1
Mean Diff to super-object layer 6 (1)	Ascending	2.4	33.99
Mean Diff to super-object NDBI (1)	Ascending	12.31	26.93
Urban and Water body			
Existence of super-object bare land (1)	Ascending	0	1
Mean Diff to super-object layer 2 (1)	Ascending	-2.11	2.24
Mean Diff to super-object layer 3 (1)	Ascending	-3.46	8.6
Mean Diff to super-object layer 4 (1)	Ascending	-4.68	13.21

Table 6.8 (Continued).

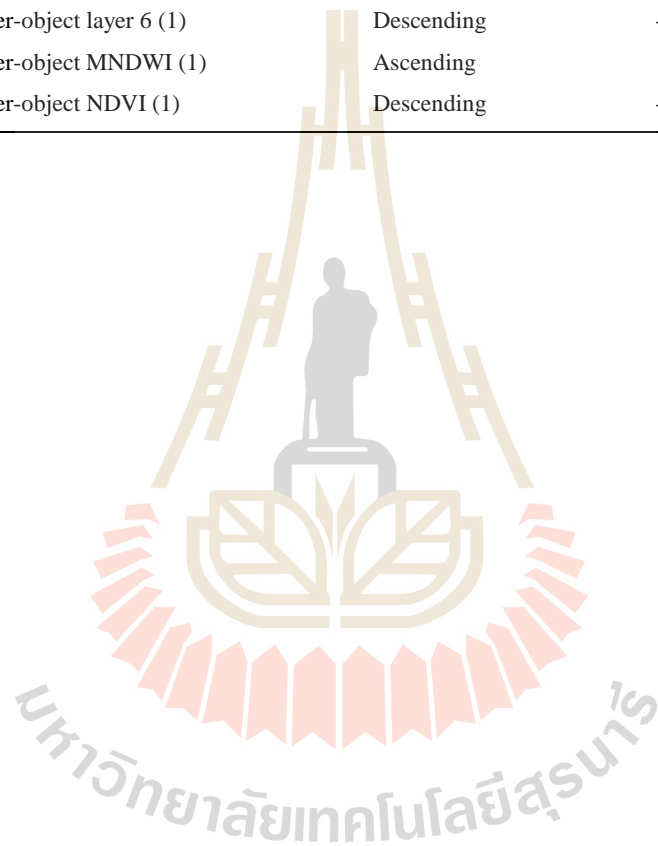
LULC classes	Membership function and threshold value		
	Membership function	Left border	Right border
Mean Diff to super-object layer 5 (1)	Ascending	-4.92	13.81
Mean Diff to super-object layer 6 (1)	Ascending	-3.47	10.13
Mean Diff to super-object MNDWI (1)	Descending	-18.48	5.45
Mean Diff to super-object NDBI (1)	Ascending	-0.78	4.56
Urban and Water Body			
Existence of super-object grass land (1)	Ascending	0	1
Mean Diff to super-object layer 3 (1)	Ascending	-3.69	27.24
Mean Diff to super-object layer 5 (1)	Ascending	1.31	21.81
Mean Diff to super-object layer 6 (1)	Ascending	-0.16	20.07
Urban and Bare land			
Existence of super-object mixed deciduous forest (1)	Ascending	0	1
Mean Diff to super-object layer 1 (1)	Ascending	6.45	18.26
Mean Diff to super-object layer 2 (1)	Ascending	7.77	26.37
Urban and Bare land			
Existence of super-object paddy field (1)	Ascending	0	1
Mean Diff to super-object layer 1 (1)	Ascending	15.06	88.09
Mean Diff to super-object layer 5 (1)	Descending	-69.39	14.96
Mean Diff to super-object MNDWI (1)	Ascending	-9.19	18.33
Urban and Bare land			
Existence of super-object unstock forest (1)	Ascending	0	1
Mean Diff to super-object MNDWI (1)	Descending	-10.74	-4.39

Table 6.9 Semantic model for water change between 2012 and 2017 in paddy field area.

LULC classes	Membership function and threshold value		
	Membership function	Left border	Right border
Water change and Urban			
Existence of super-object paddy field (1)	Ascending	0	1
Mean Diff to super-object layer 4 (1)	Descending	-40.89	-17.75
Mean Diff to super-object MNDWI (1)	Ascending	19.88	84.34
Mean Diff to super-object NDVI (1)	Descending	-47.82	-19.17
Water change and Bare land			
Existence of super-object mixed deciduous forest (1)	Ascending	0	1
Mean Diff to super-object layer 5 (1)	Descending	-41.29	-4.43
Mean Diff to super-object MNDWI (1)	Ascending	7.87	80.09
Mean Diff to super-object NDVI (1)	Descending	-75.29	-15.56
Water change and Urban			
Existence of super-object grass land (1)	Ascending	0	1
Mean Diff to super-object layer 3 (1)	Descending	-5.71	-3.69
Mean Diff to super-object layer 5 (1)	Descending	-41.4	1.31
Mean Diff to super-object layer 6 (1)	Descending	-21.33	-0.16
Water change and Urban			
Existence of super-object bare land (1)	Ascending	0	1
Mean Diff to super-object layer 2 (1)	Descending	-19.67	-2.1
Mean Diff to super-object layer 3 (1)	Descending	-30.59	-3.46
Mean Diff to super-object layer 4 (1)	Descending	-38.94	-4.68
Mean Diff to super-object layer 5 (1)	Descending	-43.97	-4.92
Mean Diff to super-object layer 6 (1)	Descending	-28.06	-3.47
Mean Diff to super-object MNDWI (1)	Ascending	5.45	63.97
Mean Diff to super-object NDBI (1)	Descending	-27.8	-0.78
Water change and Urban			
Existence of super-object mixed deciduous forest (1)	Ascending	0	1
Mean Diff to super-object layer 1 (1)	Descending	-4.35	9.25
Mean Diff to super-object layer 5 (1)	Descending	-41.29	-3.77
Mean Diff to super-object layer 6 (1)	Descending	-24.78	2.4
Mean Diff to super-object MNDWI (1)	Ascending	15.96	80.09
Mean Diff to super-object NDBI (1)	Descending	-6.59	12.31

Table 6.9 (Continued).

LULC classes	Membership function and threshold value		
	Membership function	Left border	Right border
Water change and Bare land			
Existence of super-object paddy field (1)	Ascending	0	1
Mean Diff to super-object layer 3 (1)	Descending	-23.85	7.28
Mean Diff to super-object layer 4 (1)	Descending	-40.89	-8.52
Mean Diff to super-object layer 5 (1)	Descending	-45.07	-1.42
Mean Diff to super-object layer 6 (1)	Descending	-30.56	-3.47
Mean Diff to super-object MNDWI (1)	Ascending	-4.34	84.34
Mean Diff to super-object NDVI (1)	Descending	-47.82	-14.35



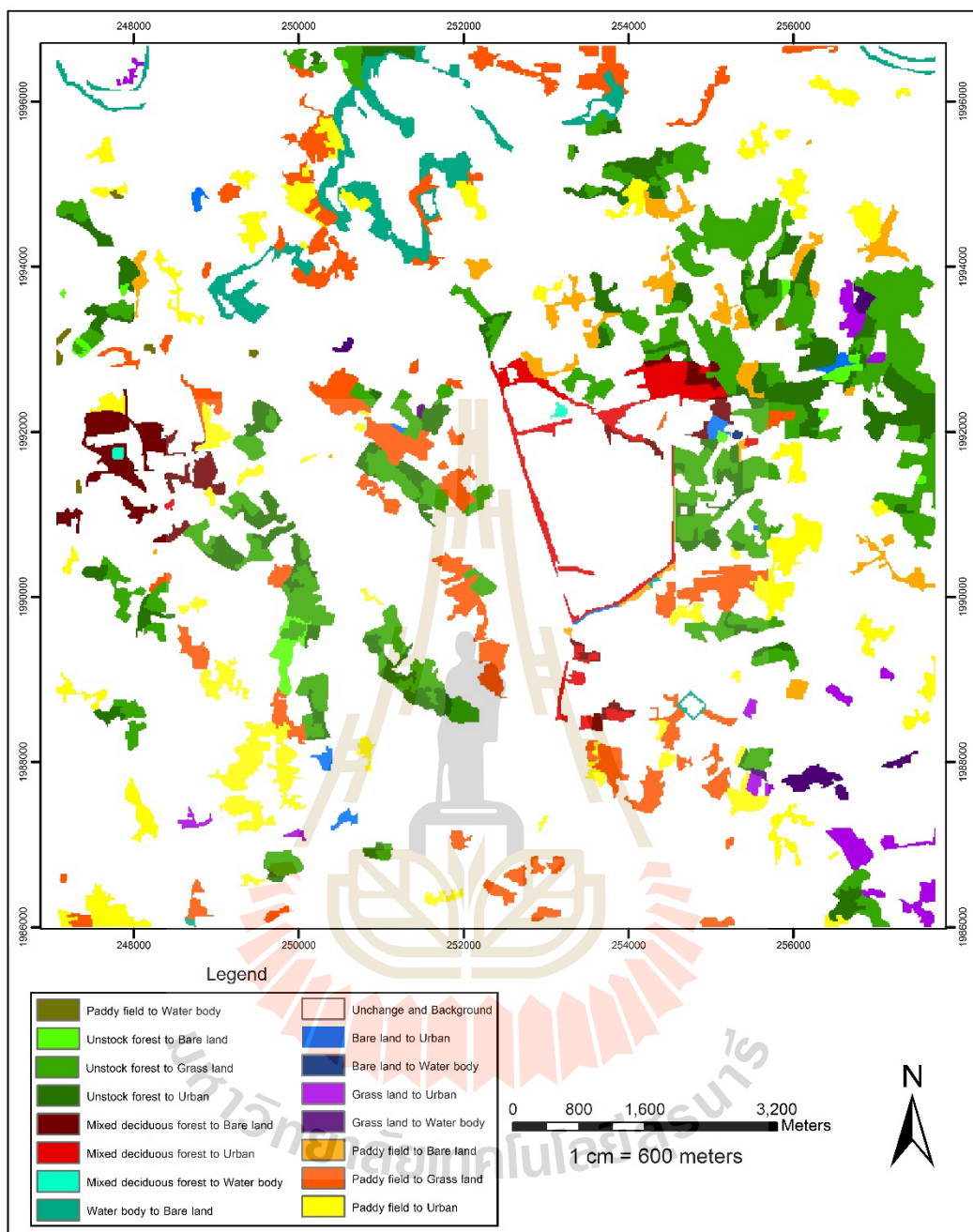


Figure 6.11 LULC change between 2012 and 2017 in paddy field area.

6.2 Land use and land cover in 2017 updating

In addition, the LULC change data is applied to update LULC map in 2012 for final LULC map in 2017 as a result shown in Figure 6.12. Comparison of area and percentage of LULC data in 2012 and 2017 is presented in Table 6.10 and the change matrix of LULC classes between 2012 and 2017 is reported in Table 6.11.

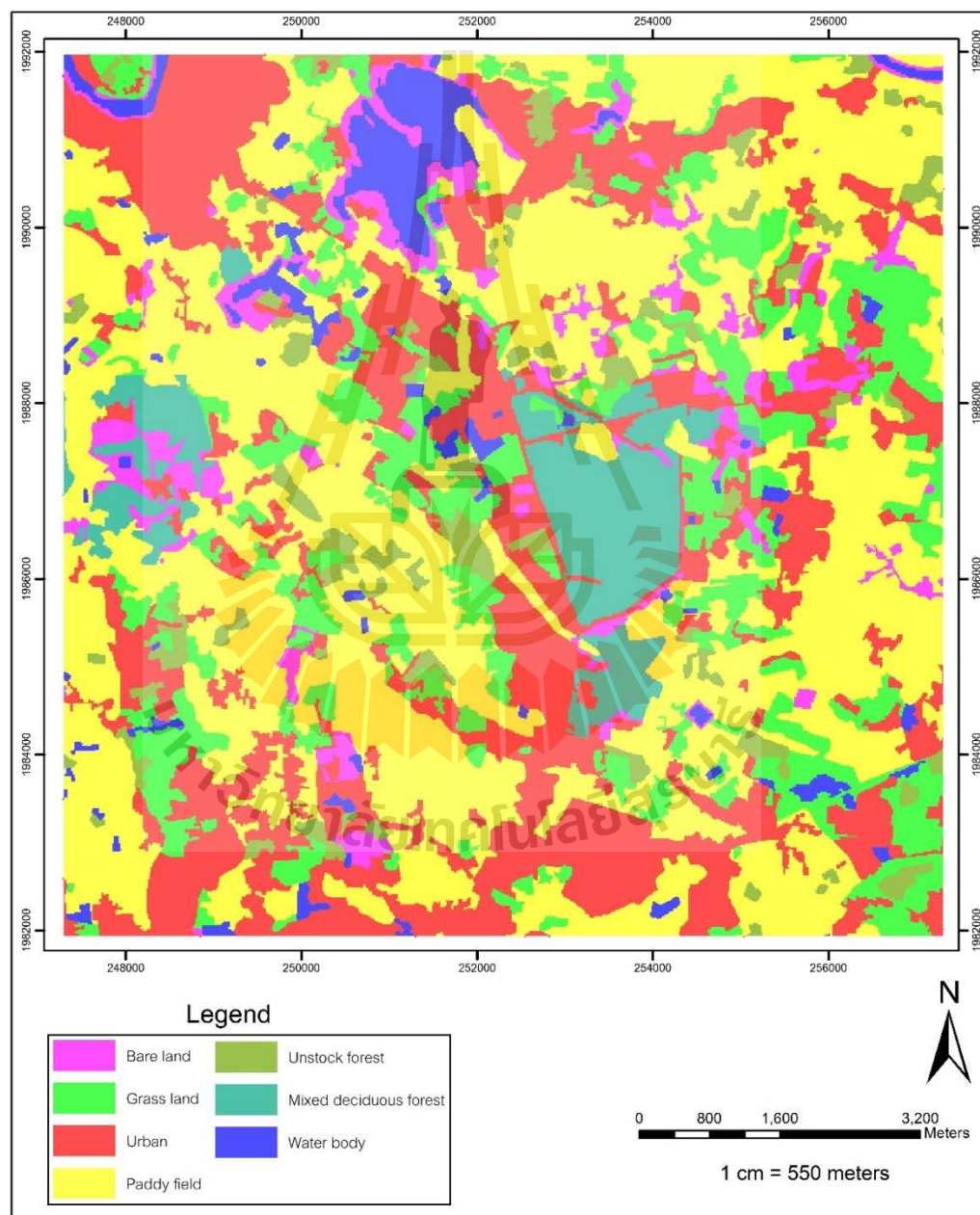


Figure 6.12 Final LULC map in 2017 in paddy field area.

Table 6.10 Comparison of area and percent of LULC in 2012 and 2017 in paddy field area.

LULC class	LULC in 2012		LULC in 2017	
	Area (Sq. Km.)	%	Area (Sq. Km.)	%
Bare land	1.11	1.11	4.66	4.66
Grass land	4.99	4.99	14.34	14.35
Urban	16.97	16.98	25.53	25.55
Paddy field	50.04	50.07	41.64	41.65
Unstock forest	14.31	14.32	4.22	4.22
Mixed deciduous forest	7.62	7.63	5.70	5.70
Water body	4.90	4.90	3.86	3.86
Total	99.96	100.00	99.96	100.00

Table 6.11 Change matrix of LULC classes between 2012 and 2017.

LULC classes in 2012	LULC classes in 2017 (Unit: sq. km)							Total
	Bare Land	Grass Land	Urban	Paddy field	Unstock Forest	Mixed Deciduous Forest	water body	
Bare land	0.90		0.20				0.01	1.11
Grass land		4.14	0.60				0.25	4.99
Urban			16.97					16.97
Paddy field	1.07	3.72	3.54	41.64			0.08	50.04
Unstock forest	0.29	6.49	3.31		4.22			14.31
Mixed deciduous forest	0.98		0.91			5.70	0.04	7.62
Water body	1.41						3.49	4.90
Total	4.66	14.34	25.53	41.64	4.22	5.70	3.86	

As result, it was found that paddy field area between 2012 and 2017 was decreased about 8.40 sq. km. The paddy field in 2012 was changed to be urban (3.54 sq. km.), grass land (3.72 sq. km.), bare land (1.07 sq. km.) and water body (0.08 sq. km.) in 2017. On contrary, grass land between 2012 and 2017 was increased about 9.35 sq. km. The increased grass land in 2017 came from unstock forest (6.49 sq. km.) and paddy field (3.72 sq. km.) in 2012. Likewise, urban between 2012 and 2017 was increased about 8.56 sq. km. The increased urban in 2017 came from paddy field (3.51 sq. km.), unstock forest (3.51 sq. km.), mixed deciduous forest (0.91 sq. km.), grass land (0.60 sq. km.) and bare land (0.20 sq. km.) in 2012.

6.3 Accuracy assessment

The extracted LULC change map between 2012 and 2017 was further assessed accuracy based on 144 stratified random sampling points with reference image from Google Earth in 2017. Error matrix and accuracy assessment is presented in Table 6.12.

As a result it reveals that overall accuracy and Kappa hat coefficient is 95.14% and 92.36%, respectively. Meanwhile producer's accuracy of LULC change class varies between 88.89% for bare land and 100.00% for urban while user's accuracy of LULC change class varies between 87.04% for urban and 100.00% for bare land. Based on Fitzpatrick-Lins (1981), Kappa hat coefficient more than 80% represents strong agreement or accuracy between the predicted map and the reference map.

In addition, it can be observed that omission error of bare land and grass land is about 11.11 and 5.88%, respectively. The main cause of omission error of bare land from urban because the brightness value of bare land and urban, in general, is similar.

Meanwhile, the main cause of omission error of grass land came from urban because the appearance of dry grass land is similar urban.

Likewise, it can be observed that commission error of urban area is about 12.96%. The main cause of commission error of urban came from bare land and grass land because its brightness value is similar with bare land or dry grass land.

Table 6.12 Error matrix and accuracy assessment of LULC change between 2012 and 2017.

Class Name	Reference Data				Row Total	PA	UA
	Bare land	Grass land	Urban	Water body			
Bare land	24				24	88.89	100.00
Grass land		64			64	94.12	100.00
Urban	3	4	47		54	100.00	87.04
Water body				2	2	100.00	100.00
Column Total	27	68	47	2	144		
Overall accuracy	95.14						
Kappa hat coefficient	92.36						

CHAPTER VII

LULC UPDATING IN UNSTOCK FOREST

The main results of land use map updating in unstock forest include (1) development of rule set for LULC classification in unstock forest, (2) land use and land cover in 2017 updating and (3) accuracy assessment.

7.1 Development of rule set for land use/land cover classification

Major results of rule set for LULC classification development of unstock forest area includes (1) image segmentation by Multiresolution segmentation, (2) feature extraction by SEaTH analysis and (3) semantic modelling and classification.

7.1.1 Image segmentation by Multiresolution segmentation

Two steps of image segmentation were here implemented for hierarchical object structure creation as parent and child relationship (object and its super object) for OBCD. Firstly, an optimum pan-sharpened image are segmented with thematic map of LULC data in 2012 as result shown in Figure 7.1. Secondly, the derived image objects at Level 2 are segmented again at Level 1 with thematic layer as child level as a result shown in Figure 7.2. The configuration of Multiresolution segmentation at Level 2 and Level 1 is summarized in Table 7.1.

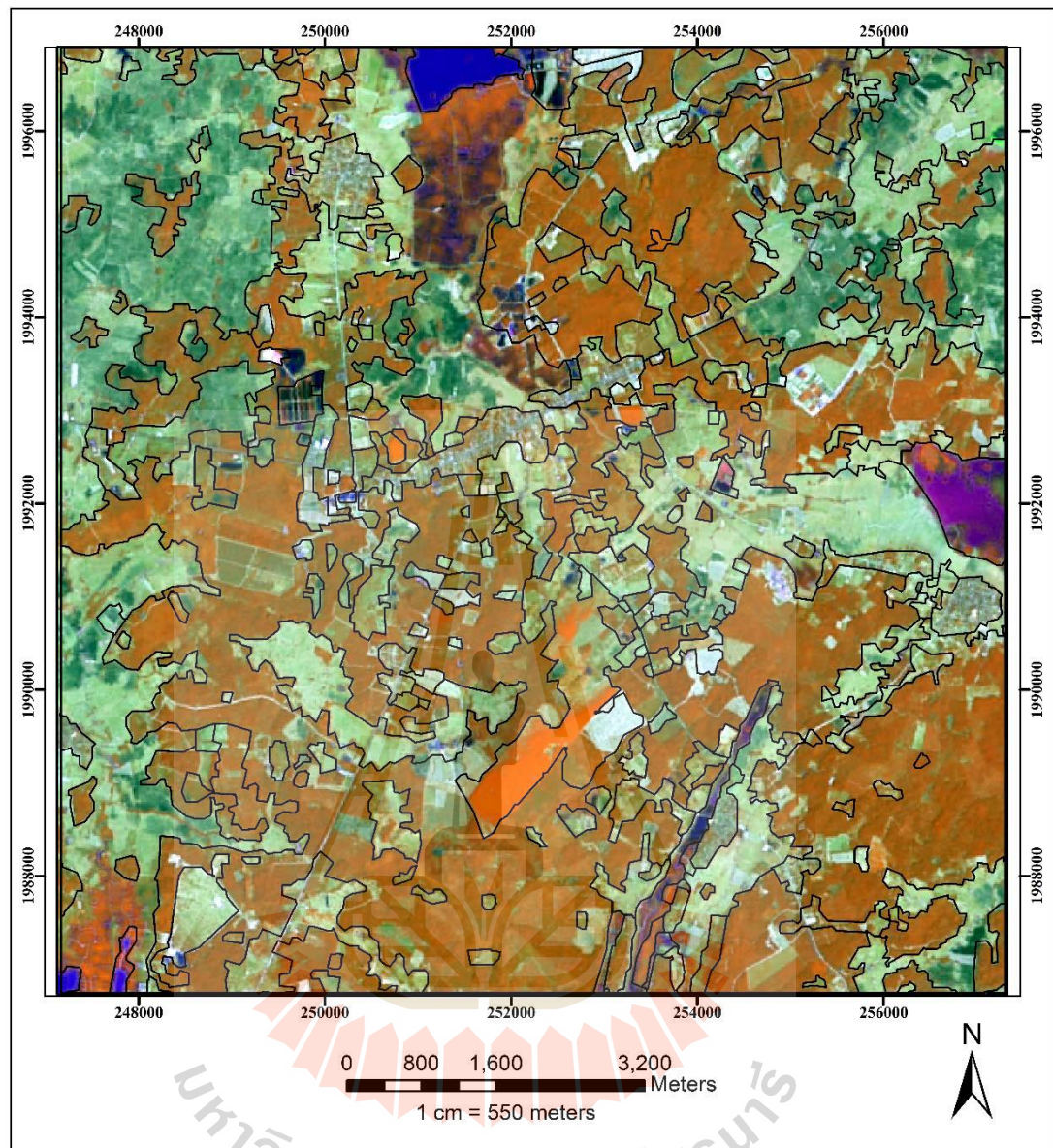


Figure 7.1 Image object of optimum pan-sharpened Landsat 8 data of 2012 by Multiresolution segmentation at level 2.

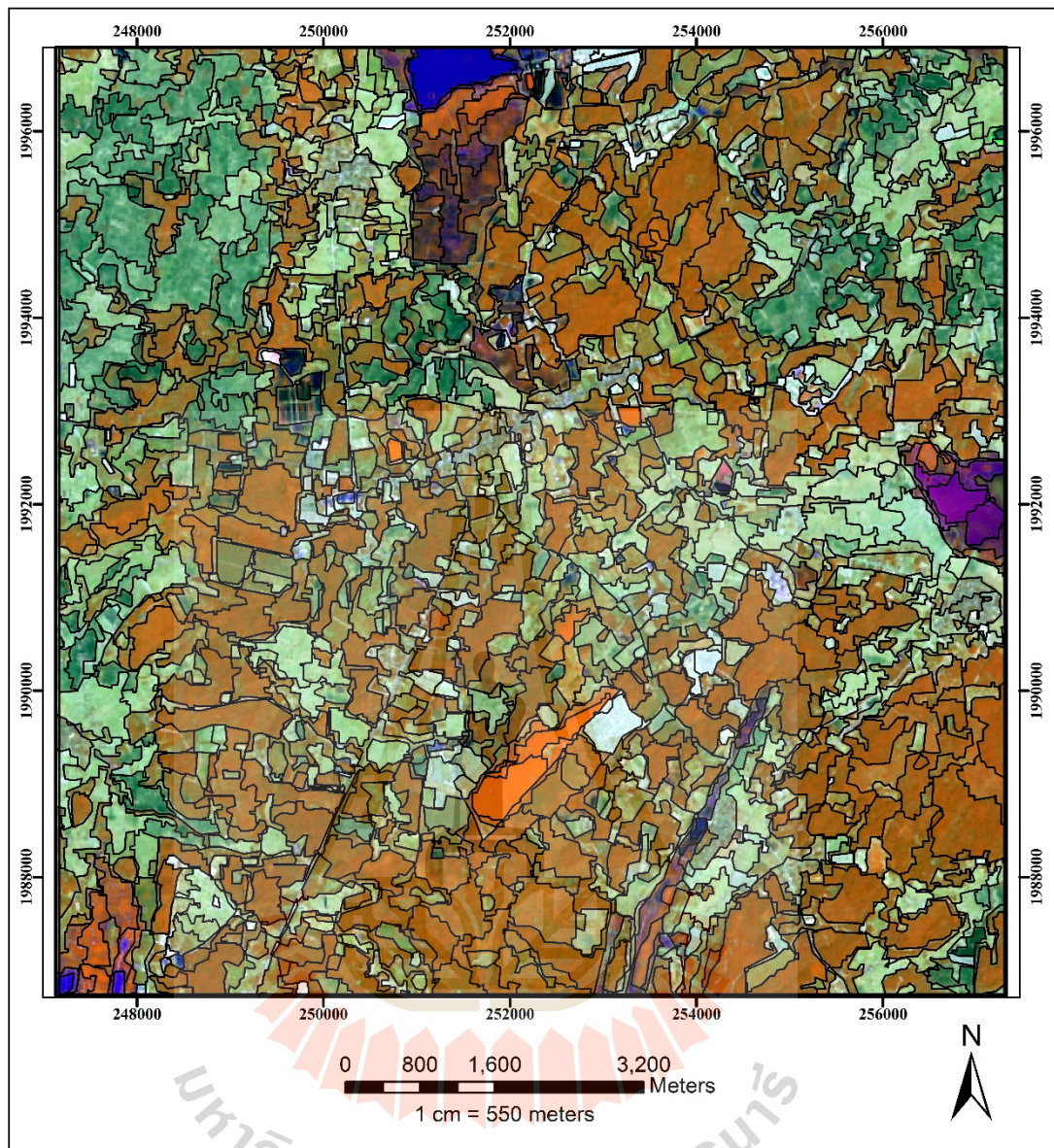


Figure 7.2 Image object of optimum pan-sharpened Landsat 8 data of 2017 by Multiresolution segmentation at level 1.

Table 7.1 Configuration of multiresolution segmentation at Level 2 and Level 1 with thematic layer.

Image object domain	Pixel level	Image object level
Level setting		
Level name	Level 2	Level 1
Segmentation setting		
Image layer weight	0, 0, 0, 0, 0, 0, 0, 0, 0	1, 1, 1, 1, 1, 1, 1, 1, 1
Thematic layer usage	Yes	YES
Scale parameters		
	20	20
Composition of homogeneity criterion		
Shape	0	0.1
Compactness	0	0.5

As results, it was found number of image object at Level 2 as parent level is 309 while number of image object at Level 1 as child level is 1,511. In fact, child objects that have similar spectral characteristics as parent objects are unchanged objects while any deviation is an indicator of changed objects.

7.1.2 Feature extraction by SEaTH analysis

Parent–child relationship between image objects at Level 2 and Level 1 is applied to extract changed and unchanged objects between 2012 and 2017. In this study, two main steps are required for feature extraction by SEaTH analysis.

At the first step, existence of LULC class from 2012 at Level 2 as parent level is created under class-related features property shown in Figure 7.3. Herein, the created existence LULC classes in unstock forest area include bare land, grass land, paddy field, unstock forest, urban and water body are applied as super-object (parent) of Level 1 as child level. This image property is applied to create super-object class hierarchy under Level 2 including LULC in 2012 and LULC change between 2012 and 2017 as shown in Figure 7.4. This structure can directly

apply to classify LULC map in 2012 according to class description as shown in Figure 7.5. It consists of LULC code of each LULC class and Level number (Level 2).

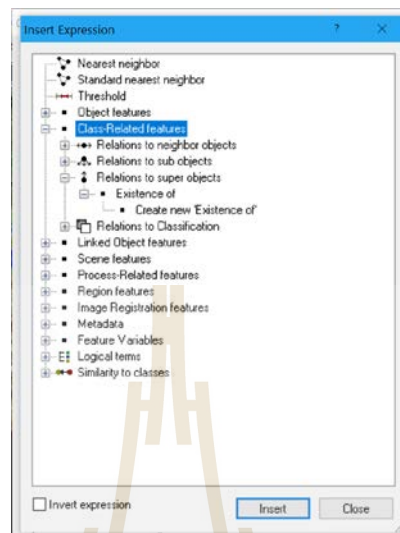


Figure 7.3 Class-related feature properties: Existence of.

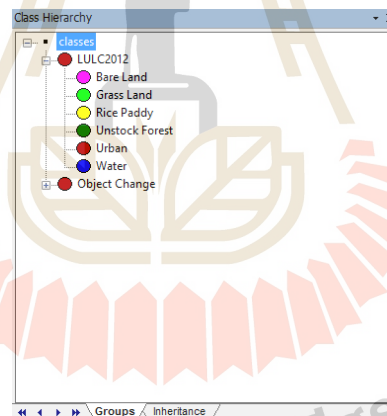


Figure 7.4 Class hierarchy structure of Super-object at Level 2.



Figure 7.5 Class description of Super-object at Level 2.

At the second step, mean diff to super-object under To super-object property of layers values are applied to identify changed objects of Level 1 as child level as shown in Figure 7.6. In practice, mean value of each layer from 5 training areas are extracted and exported to MS-Excel spreadsheet software for SEaTH analysis. Examples of training areas for LULC changed object in 2017 are displayed in Figure 7.7. Meanwhile results of SEaTH analysis for separability test and threshold value extraction for rule-based development of unstock forest among other classes using Equation 2.1, 2.2 and 2.6 are displayed in Tables 7.2 to 7.5.

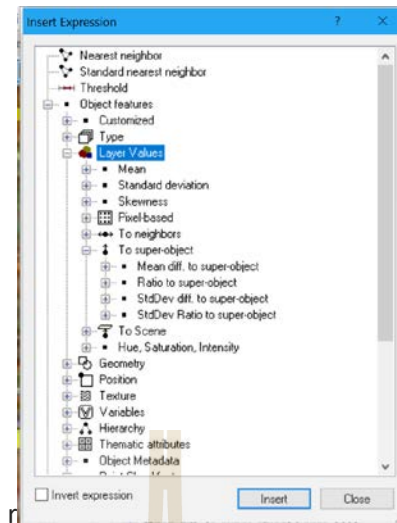


Figure 7.6 Structure of Mean diff to super-object parameter for changed object identification.

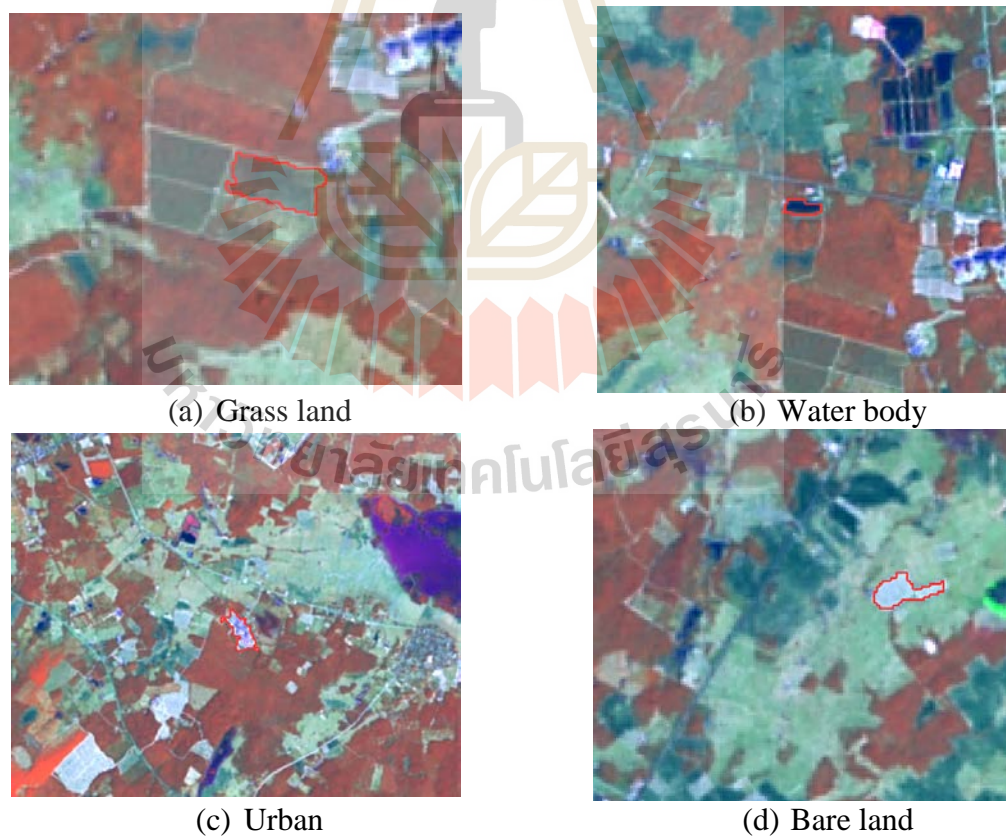


Figure 7.7 Training areas of changed objects in 2017 for SEaTH analysis.

Table 7.2 Pairwise of mean and variance between water body and urban for threshold value calculation.

Feature	Mean	Variance	Mean	Variance	J Value	Membership	LEFT	RIGHT
	water body	water body	urban	urban				
Layer 5 (1)	-10.71	42.77	29.21	48.00	1.98	Descending	-30.33	8.70
Layer 6 (1)	-4.76	17.87	26.73	40.22	1.97	Descending	-17.44	7.99
Layer 4 (1)	-21.29	45.20	9.93	29.22	1.93	Descending	-41.46	-4.10
Layer 3 (1)	2.00	11.38	32.85	104.77	1.80	Descending	-8.12	10.17
MNDWI (1)	23.03	150.79	-17.57	39.30	1.79	Ascending	-3.30	59.87
NDBI (1)	6.81	55.98	28.54	13.87	1.67	Descending	-15.64	20.94
Layer 2 (1)	2.74	5.13	27.10	102.60	1.67	Descending	-4.05	7.78
Layer 1 (1)	1.74	4.39	21.99	71.36	1.65	Descending	-4.55	6.27
NDVI (1)	-31.00	110.82	-25.06	22.95	0.37	Descending	-62.58	-29.11

Table 7.3 Pairwise of mean and variance between bare land and water body for threshold value calculation.

Feature	Mean	Variance	Mean	Variance	J Value	Membership	LEFT	RIGHT
	Bare land	Bare land	water body	water body				
MNDWI (1)	-23.70	4.65	23.03	150.79	1.97	Descending	-30.17	-16.30
Layer 5 (1)	26.33	97.58	-10.71	42.77	1.83	Ascending	4.35	55.97
Layer 4 (1)	7.44	71.33	-21.29	45.20	1.66	Ascending	-8.36	32.77
Layer 6 (1)	20.41	78.51	-4.76	17.87	1.66	Ascending	3.84	46.99
NDBI (1)	27.67	17.31	6.81	55.98	1.58	Ascending	19.84	40.16
Layer 3 (1)	21.16	196.67	2.00	11.38	1.13	Ascending	7.05	63.23
Layer 2 (1)	15.62	154.97	2.74	5.13	1.08	Ascending	6.01	52.97
Layer 1 (1)	12.09	75.84	1.74	4.39	1.03	Ascending	4.68	38.21
NDVI (1)	-16.20	29.93	-31.00	110.82	0.77	Ascending	-22.32	0.21

Table 7.4 Pairwise of mean and variance between grass land and urban for threshold value calculation.

Feature	Mean	Variance	Mean	Variance	J Value	Membership	LEFT	RIGHT
	Grass land	Grass land	urban	Urban				
Layer 6 (1)	3.15	2.19	26.73	40.22	1.95	Descending	-1.28	7.86
Layer 5 (1)	4.92	4.17	29.21	48.00	1.91	Descending	-1.21	10.75
Layer 3 (1)	2.34	2.74	32.85	104.77	1.87	Descending	-2.63	7.01
Layer 2 (1)	0.07	0.69	27.10	102.60	1.86	Descending	-2.42	2.42
Layer 1 (1)	0.24	0.38	21.99	71.36	1.85	Descending	-1.60	1.97
NDBI (1)	15.74	6.67	28.54	13.87	1.74	Descending	7.99	21.10
Layer 4 (1)	-6.57	7.72	9.93	29.22	1.71	Descending	-14.91	-0.71
NDVI (1)	-10.82	7.22	-25.06	22.95	1.66	Ascending	-16.16	-2.76
MNDWI (1)	-8.98	8.74	-17.57	39.30	0.80	Ascending	-12.40	-0.11

Table 7.5 Pairwise of mean and variance between urban and water body for threshold value calculation.

Feature	Mean	Variance	Mean	Variance	J Value	Membership	LEFT	RIGHT
	urban	urban	water body	water body				
Layer 5 (1)	29.21	48.00	-10.71	42.77	1.98	Ascending	8.70	49.99
Layer 6 (1)	26.73	40.22	-4.76	17.87	1.97	Ascending	7.99	45.76
Layer 4 (1)	9.93	29.22	-21.29	45.20	1.93	Ascending	-4.10	26.14
Layer 3 (1)	32.85	104.77	2.00	11.38	1.80	Ascending	10.17	63.56
MNDWI (1)	-17.57	39.30	23.03	150.79	1.79	Descending	-36.38	-3.30
NDBI (1)	28.54	13.87	6.81	55.98	1.67	Ascending	20.94	39.72
Layer 2 (1)	27.10	102.60	2.74	5.13	1.67	Ascending	7.78	57.49
Layer 1 (1)	21.99	71.36	1.74	4.39	1.65	Ascending	6.27	47.33
NDVI (1)	-25.06	22.95	-31.00	110.82	0.37	Ascending	-29.11	-10.69

The derived optimum threshold value of changed object are added to class description for rule set of LULC change class as an example of urban change in Figure 7.8. Herein, an optimum threshold value and the membership function (ascending or descending) is assigned for each feature under rule set as an example shown in Figure 7.9 for mean diff to super-object of layer 1 (Band 2) with ascending membership.

Class hierarchy of LULC2012 and object change (LULC change between 2012 and 2017) of urban area is displayed in Figure 7.10. All rule set of object change are then applied to create semantic model for classification in the next section.

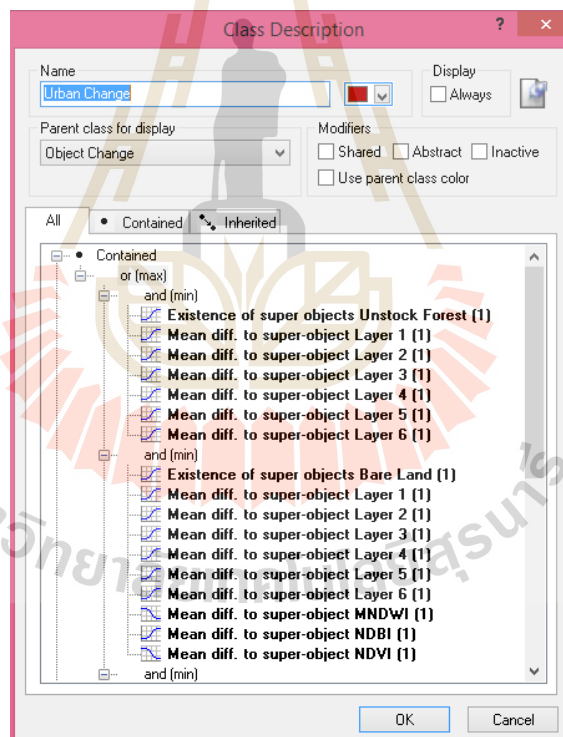


Figure 7.8 Rule set of urban change under class description.

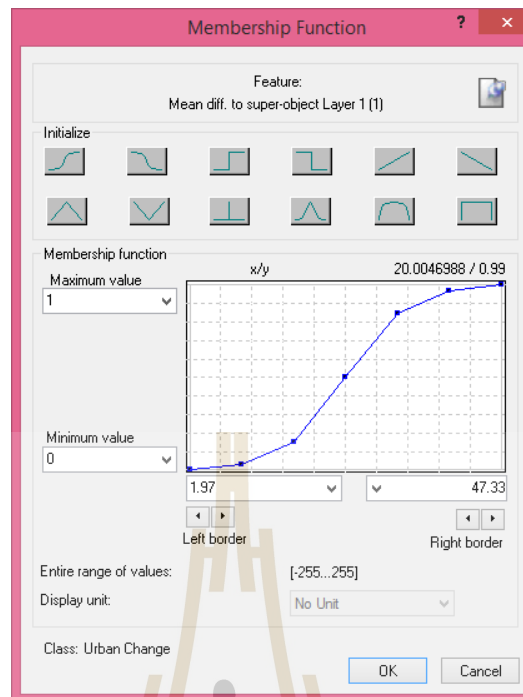


Figure 7.9 Membership function and assigned value of mean diff to-super object of layer 1.

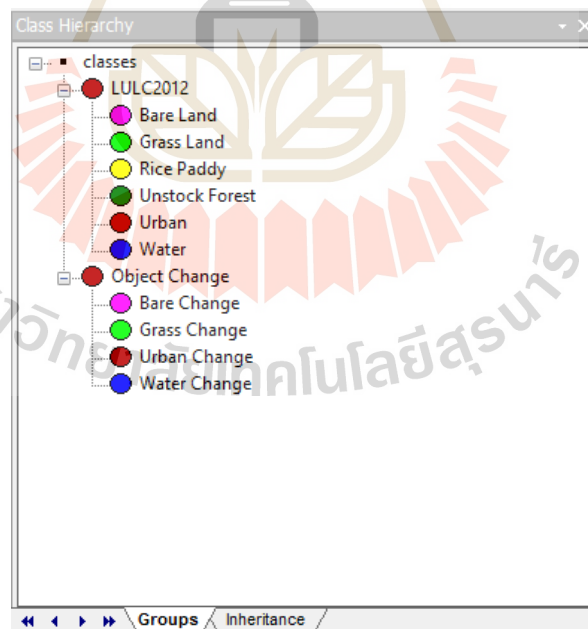


Figure 7.10 Class hierarchy of LULC2012 and Object Change.

7.1.3 Semantic modeling and classification

The developed semantic models for OBCD in unstock forest with pan-sharpened Landsat 8 data of 2017 for Layer 1 (Band 2), Layer 2 (Band 3), Layer 4 (Band 5), Layer 5 (Band 6), Layer 6 (Band 7), MNDWI, NDBI, and NDVI are presented in Tables 7.6 to 7.9. All rule set is directly applied to classify LULC change between 2012 and 2017 as result shown in Figure 7.11.

Table 7.6 Semantic model for bare land change between 2012 and 2017 in unstock forest area.

LULC classes	Membership function and threshold value		
	Membership function	Left border	Right border
Bare land and Water body			
Existence of super-object unstock forest(1)	Ascending	0	1
Mean Diff to super-object layer 5 (1)	Ascending	4.35	55.97
Mean Diff to super-object MNDWI (1)	Descending	-30.17	-16.30
Bare land and Grass land			
Existence of super-object unstock forest (1)	Ascending	0	1
Mean Diff to super-object MNDWI (1)	Descending	-30.17	-17.43
Bare land and Water body			
Existence of super-object Rice paddy field (1)	Ascending	0	1
Mean Diff to super-object layer 1 (1)	Ascending	4.69	31.34
Mean Diff to super-object layer 2 (1)	Ascending	7.94	46.59
Mean Diff to super-object layer 3 (1)	Ascending	7.98	57.41
Mean Diff to super-object layer 4 (1)	Ascending	4.41	42.12
Mean Diff to super-object layer 5 (1)	Ascending	-2.78	53.25
Mean Diff to super-object layer 6 (1)	Ascending	-3.69	49.97
Mean Diff to super-object MNDWI (1)	Descending	-28.53	8.53

Table 7.7 Semantic model for grass land change between 2012 and 2017 in unstock forest area.

LULC classes	Membership function and threshold value		
	Membership function	Left border	Right border
Grass land and Urban			
Existence of super-object Bare Land (1)	Ascending	0	1
Mean Diff to super-object layer 3 (1)	Descending	-16.12	-3.09
Mean Diff to super-object layer 5 (1)	Descending	-255	-3.89
Mean Diff to super-object layer 6 (1)	Descending	-14.83	-2.94
Mean Diff to super-object NDBI (1)	Descending	-47.83	-0.32
Grass land and Water body			
Existence of super-object Bare Land (1)	Ascending	0	1
Mean Diff to super-object MNDWI (1)	Descending	2.64	14.72
Mean Diff to super-object NDVI (1)	Ascending	1.58	48.56
Grass land and Urban			
Existence of super-object unstock forest (1)	Ascending	0	1
Mean Diff to super-object layer 1 (1)	Descending	-1.6	1.97
Mean Diff to super-object layer 2 (1)	Descending	-2.42	2.42
Mean Diff to super-object layer 3 (1)	Descending	-2.63	7.01
Mean Diff to super-object layer 4 (1)	Descending	-14.91	-0.71
Mean Diff to super-object layer 5 (1)	Descending	-1.21	10.75
Mean Diff to super-object layer 6 (1)	Descending	-1.28	7.86
Mean Diff to super-object NDBI (1)	Descending	7.99	21.1
Grass land and Bare land			
Existence of super-object unstock forest (1)	Ascending	0	1
Mean Diff to super-object layer 1 (1)	Descending	-1.6	1.44
Mean Diff to super-object layer 2 (1)	Descending	-2.42	1.64
Mean Diff to super-object layer 3 (1)	Descending	-2.63	5.27
Mean Diff to super-object layer 4 (1)	Descending	-14.91	-2.35
Mean Diff to super-object layer 5 (1)	Descending	-1.21	9.19
Mean Diff to super-object layer 6 (1)	Descending	-1.28	6.16
Mean Diff to super-object MNDWI (1)	Ascending	-17.43	-0.11
Mean Diff to super-object NDBI (1)	Descending	7.99	20.5
Grass land and Water body			
Existence of super-object unstock forest (1)	Ascending	0	1
Mean Diff to super-object layer 5 (1)	Ascending	0.78	11.04
Mean Diff to super-object MNDWI (1)	Descending	-17.85	-2.1
Mean Diff to super-object NDVI (1)	Ascending	-15.7	-2.76

Table 7.8 Semantic model for urban change between 2012 and 2017 in unstock forest area.

LULC classes	Membership function and threshold value		
	Membership function	Left border	Right border
Urban and Grass land			
Existence of super-object unstock forest (1)	Ascending	0	1
Mean Diff to super-object layer 1 (1)	Ascending	1.97	47.33
Mean Diff to super-object layer 2 (1)	Ascending	2.42	57.49
Mean Diff to super-object layer 3 (1)	Ascending	7.01	63.56
Mean Diff to super-object layer 4 (1)	Ascending	-4.1	26.14
Mean Diff to super-object layer 5 (1)	Ascending	10.75	49.99
Mean Diff to super-object layer 6 (1)	Ascending	7.86	45.76
Urban and Grass land			
Existence of super-object Bare Land (1)	Ascending	0	1
Mean Diff to super-object layer 1 (1)	Ascending	-2.74	57.13
Mean Diff to super-object layer 2 (1)	Ascending	-2.94	65.53
Mean Diff to super-object layer 3 (1)	Ascending	-3.09	57.62
Mean Diff to super-object layer 4 (1)	Ascending	8.36	31.68
Mean Diff to super-object layer 5 (1)	Ascending	-3.89	39.68
Mean Diff to super-object layer 6 (1)	Ascending	-2.94	41.26
Mean Diff to super-object MNDWI (1)	Descending	-34.9	5.9
Mean Diff to super-object NDBI (1)	Ascending	-0.32	28.75
Mean Diff to super-object NDVI (1)	Descending	-23.55	-3.12
Urban and Water body			
Existence of super-object Bare Land (1)	Ascending	0	1
Mean Diff to super-object layer 3 (1)	Ascending	6.01	57.62
Mean Diff to super-object layer 4 (1)	Ascending	0.83	31.68
Mean Diff to super-object layer 5 (1)	Ascending	1.6	39.68
Mean Diff to super-object layer 6 (1)	Ascending	0.33	41.26
Mean Diff to super-object MNDWI (1)	Descending	-34.9	8.61
Mean Diff to super-object NDBI (1)	Ascending	-1.3	28.75
Urban and Water body			
Existence of super-object unstock forest (1)	Ascending	0	1
Mean Diff to super-object layer 3 (1)	Ascending	10.17	63.56
Mean Diff to super-object layer 4 (1)	Ascending	-4.1	26.14
Mean Diff to super-object layer 5 (1)	Ascending	8.7	49.99
Mean Diff to super-object layer 6 (1)	Ascending	7.99	45.76
Mean Diff to super-object MNDWI (1)	Descending	-36.38	-3.3

Table 7.9 Semantic model for water body change between 2012 and 2017 in unstock forest area.

LULC classes	Membership function and threshold value		
	Membership function	Left border	Right border
Water body and Grass land			
Existence of super-object unstock forest (1)	Ascending	0	1
Mean Diff to super-object layer 4 (1)	Descending	-41.46	-11.35
Mean Diff to super-object layer 5 (1)	Descending	-30.33	0.78
Mean Diff to super-object layer 6 (1)	Descending	-17.44	0.76
Mean Diff to super-object MNDWI (1)	Ascending	-2.1	59.87
Mean Diff to super-object NDBI (1)	Descending	-62.58	-15.7
Water body and Bare land			
Existence of super-object unstock forest (1)	Ascending	0	1
Mean Diff to super-object layer 1 (1)	Descending	-4.55	4.68
Mean Diff to super-object layer 2 (1)	Descending	-4.05	6.01
Mean Diff to super-object layer 3 (1)	Descending	-8.12	7.05
Mean Diff to super-object layer 4 (1)	Descending	-41.46	-8.36
Mean Diff to super-object layer 5 (1)	Descending	-30.33	4.35
Mean Diff to super-object layer 6 (1)	Descending	-17.44	3.84
Mean Diff to super-object MNDWI (1)	Ascending	-16.3	59.87
Mean Diff to super-object NDBI (1)	Descending	-15.64	19.84
Water body and Urban			
Existence of super-object unstock forest (1)	Ascending	0	1
Mean Diff to super-object layer 1 (1)	Descending	-4.55	6.27
Mean Diff to super-object layer 2 (1)	Descending	-4.05	7.78
Mean Diff to super-object layer 3 (1)	Descending	-8.12	10.17
Mean Diff to super-object layer 4 (1)	Descending	-41.46	-4.1
Mean Diff to super-object layer 5 (1)	Descending	-30.33	8.7
Mean Diff to super-object layer 6 (1)	Descending	-17.44	7.99
Mean Diff to super-object MNDWI (1)	Ascending	-3.3	59.87
Mean Diff to super-object NDBI (1)	Descending	-15.64	20.94

Table 7.9 (Continued).

LULC classes	Membership function and threshold value		
	Membership function	Left border	Right border
Water body and Grass land			
Existence of super-object Bare Land (1)	Ascending	0	1
Mean Diff to super-object MNDWI (1)	Ascending	14.72	70.42
Mean Diff to super-object NDVI (1)	Descending	-51.14	1.58
Water body and Urban			
Existence of super-object Bare Land (1)	Ascending	0	1
Mean Diff to super-object layer 3 (1)	Descending	-30.39	6.01
Mean Diff to super-object layer 4 (1)	Descending	-47.27	0.83
Mean Diff to super-object layer 5 (1)	Descending	-42.35	1.6
Mean Diff to super-object layer 6 (1)	Descending	-27.07	0.33
Mean Diff to super-object NDBI (1)	Descending	-20.4	-1.3
Water body and Bare land			
Existence of super-object paddy field (1)	Ascending	0	1
Mean Diff to super-object layer 1 (1)	Descending	-8.73	4.69
Mean Diff to super-object layer 2 (1)	Descending	-8.91	7.94
Mean Diff to super-object layer 3 (1)	Descending	-20.22	7.98
Mean Diff to super-object layer 4 (1)	Descending	-35.3	4.41
Mean Diff to super-object layer 5 (1)	Descending	-39.57	-2.78
Mean Diff to super-object layer 6 (1)	Descending	-28.71	-3.69
Mean Diff to super-object MNDWI (1)	Ascending	8.53	61.28

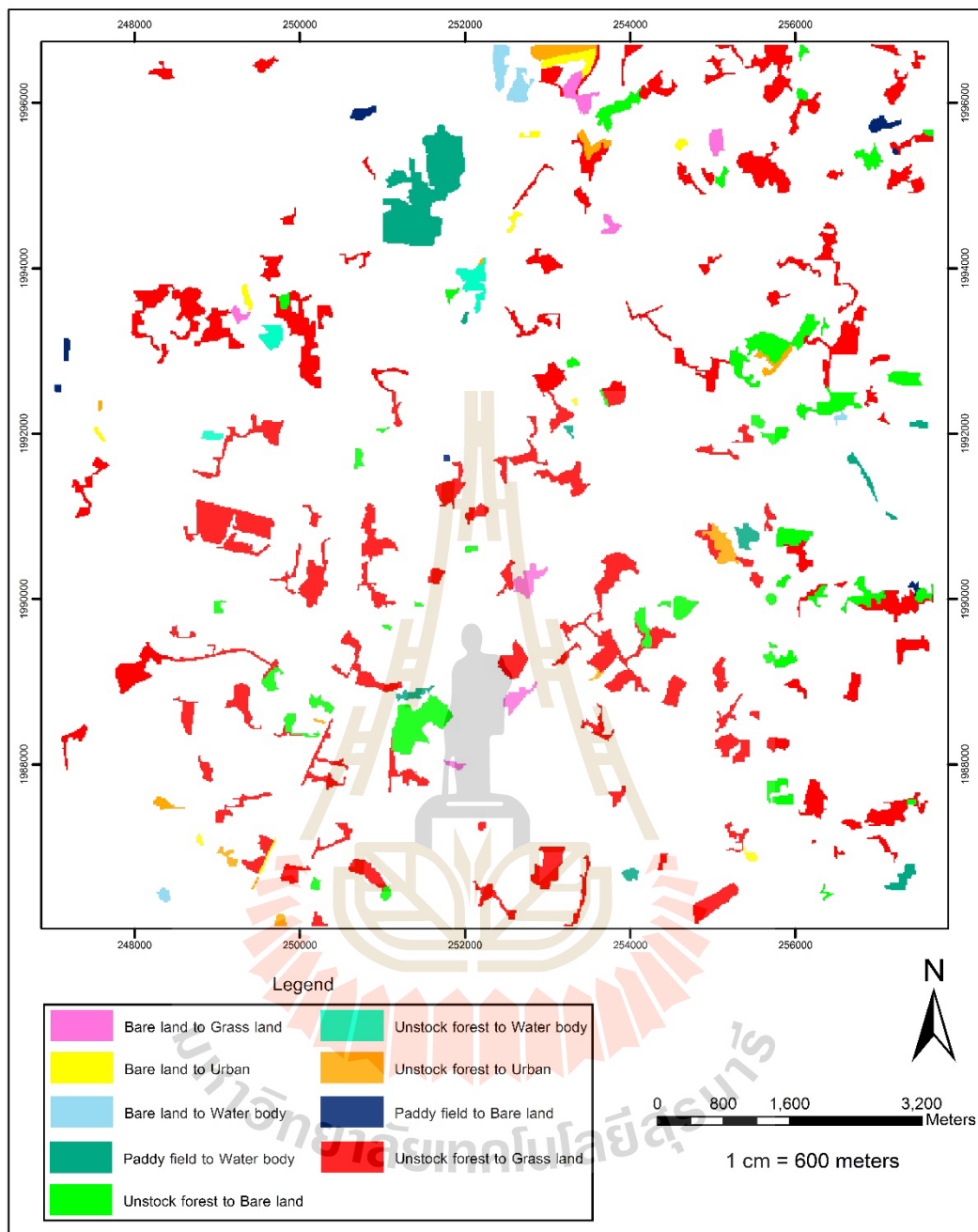


Figure 7.11 LULC change between 2012 and 2017 in unstock forest area.

7.2 Land use and land cover in 2017 updating

In addition, the LULC change data is applied to update LULC map in 2012 for final LULC map in 2017 as a result shown in Figure 7.12. Comparison of area and percentage of LULC data in 2012 and 2017 is presented in Table 7.10 and the change matrix of LULC classes between 2012 and 2017 is reported in Table 7.11.

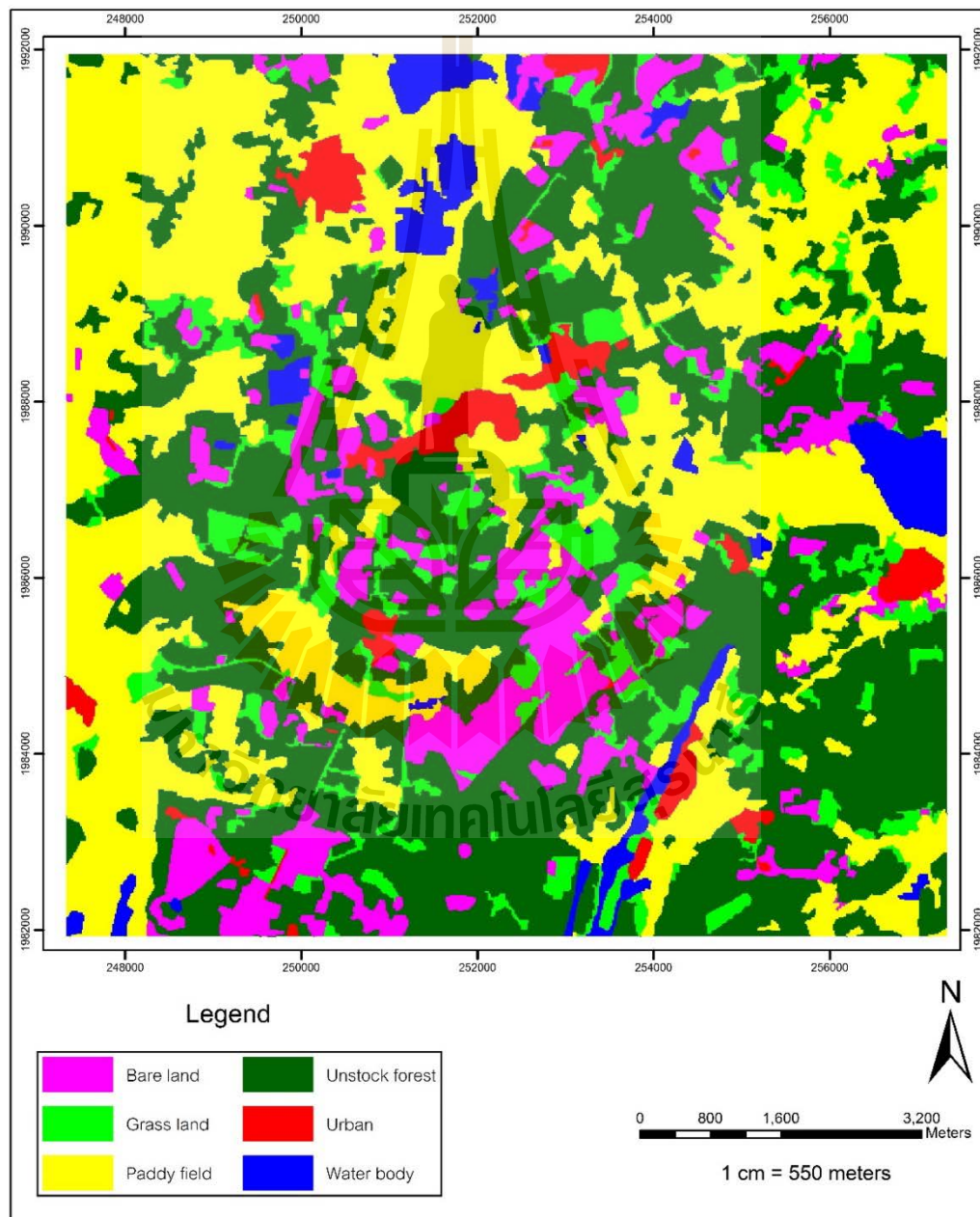


Figure 7.12 Final LULC map in 2017 in unstock forest area.

Table 7.10 Comparison of area and percentage of LULC in 2012 and 2017 in unstock forest area.

LULC class	LULC in 2012		LULC in 2017	
	Area (Sq. Km.)	%	Area (Sq. Km.)	%
Bare land	9.40	9.40	10.36	10.37
Grass land	1.37	1.37	7.90	7.90
Paddy field	35.45	35.47	34.43	34.44
Unstock forest	48.58	48.60	40.36	40.38
Urban	2.55	2.55	3.06	3.06
Water body	2.61	2.61	3.85	3.85
Total	99.96	100.00	99.96	100.00

Table 7.11 Change matrix of LULC classes between 2012 and 2017 in unstock forest area.

LULC classes in 2012	LULC classes in 2017 (Unit: sq. km.)						Total
	Bare land	Grass land	Paddy field	Unstock forest	Urban	Water body	
Bare land	8.75	0.31			0.18	0.16	9.40
Grass land		1.37					1.37
Paddy field	0.11		34.43			0.91	35.45
Unstock forest	1.50	6.22		40.36	0.33	0.17	48.58
Urban					2.55		2.55
Water body						2.61	2.61
Total	10.36	7.90	34.43	40.36	3.06	3.85	

As result, it was found that unstock forest area between 2012 and 2017 was decreased about 8.22 sq. km. The unstock forest in 2012 was changed to be grass land (6.22 sq. km.), bare land (1.50 sq. km.), urban (0.33 sq. km.) and water body (0.17 sq. km.) in 2017. On contrary, grass land between 2012 and 2017 was increased about 6.53 sq. km. Most of the increased grass land in 2017 came from unstock forest (6.22 sq. km.) in 2012. Likewise, bare land between 2012 and 2017 was increased about

0.96 sq. km. Most of the increased bare land in 2017 came from unstock forest (1.50 sq. km.) in 2012. However, bare land in 2012 was changed to be grass land (0.31 sq. km.), urban (0.18 sq. km.) and water body (0.16 sq. km.) in 2017.

7.3 Accuracy assessment

The extracted LULC change map between 2012 and 2027 was further assessed accuracy based on 144 stratified random sampling points with reference image from Google Earth in 2017. Error matrix and accuracy assessment is presented in Table 7.12.

As a result it reveals that overall accuracy and Kappa hat coefficient is 97.92% and 95.98%, respectively. Meanwhile producer's accuracy of LULC change class varies between 88.46% for bare land and 100.00% for grass land, urban and water body while user's accuracy of LULC change class varies between 62.5% for urban and 100.00% for bare land, grass land and water body. Based on Fitzpatrick-Lins (1981), Kappa hat coefficient more than 80% represents strong agreement or accuracy between the predicted map and the reference map

Table 7.12 Error matrix and accuracy assessment of LULC change between 2012 and 2017.

Class Name	Reference Data				Row Total	PA	UA
	Bare land	Grass land	Urban	Water body			
Bare land	23				23	88.46	100.00
Grass land		95			95	100.00	100.00
Urban	3		5		8	100.00	62.5
Water body				18	18	100.00	100.00
Column Total	26	95	5	18	144		
Overall accuracy	97.92						
Kappa hat coefficient	95.98						

In addition, it can be observed that omission error of bare land is about 11.54%. The main cause of omission error of bare land from urban because the brightness value of bare land and urban, in general, is similar.

Likewise, it can be observed that commission error of urban area is quite high about 37.50%. The main cause of commission error of urban came from bare land because its brightness value is similar with bare land.

CHAPTER VIII

LULC UPDATING IN MIXED DECIDUOUS FOREST

The main results of land use map updating in mixed deciduous forest include (1) the development of rule set for LULC classification in mixed deciduous forest, (2) the LULC in 2017 updating and (3) the accuracy assessment.

8.1 Development of rule set for land use/land cover classification

Major results of rule set for LULC classification development of mixed deciduous forest area includes (1) image segmentation by Multiresolution segmentation, (2) feature extraction by SEaTH analysis, and (3) semantic modelling and classification.

8.1.1 Image segmentation by Multiresolution segmentation

Two steps of image segmentation were here implemented for hierarchical object structure creation as parent and child relationship (object and its super object) for OBCD. Firstly, an optimum pan-sharpened image are segmented with thematic map of LULC data in 2012 as result shown in Figure 8.1. Secondly, the derived image objects at Level 2 are segmented again at Level 1 with thematic layer as child level as a result shown in Figure 8.2. The configuration of Multiresolution segmentation at Level 2 and Level 1 is summarized in Table 8.1.

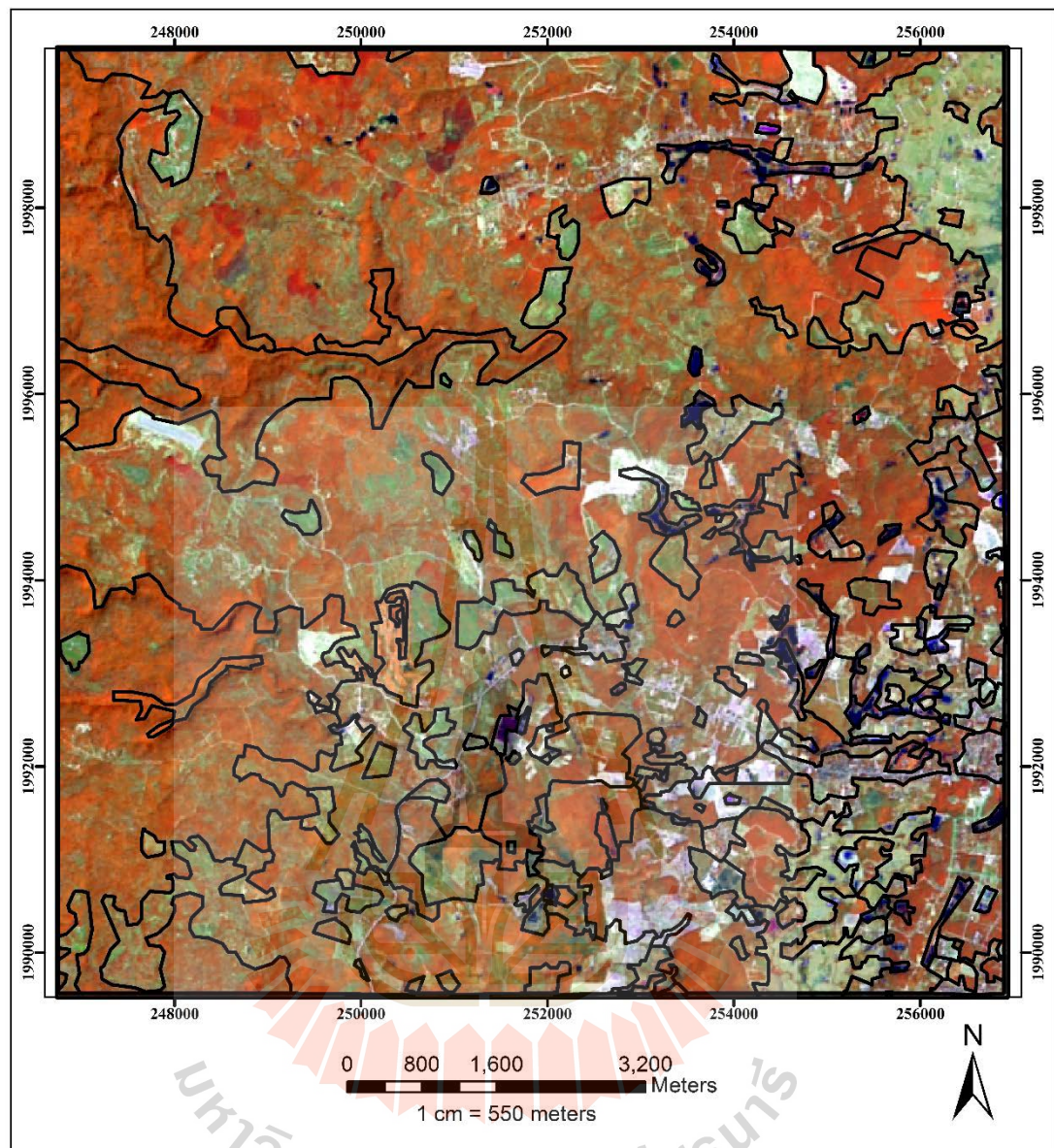


Figure 8.1 Image object of optimum pan-sharpened Landsat 8 data of 2012 by Multiresolution segmentation at level 2.

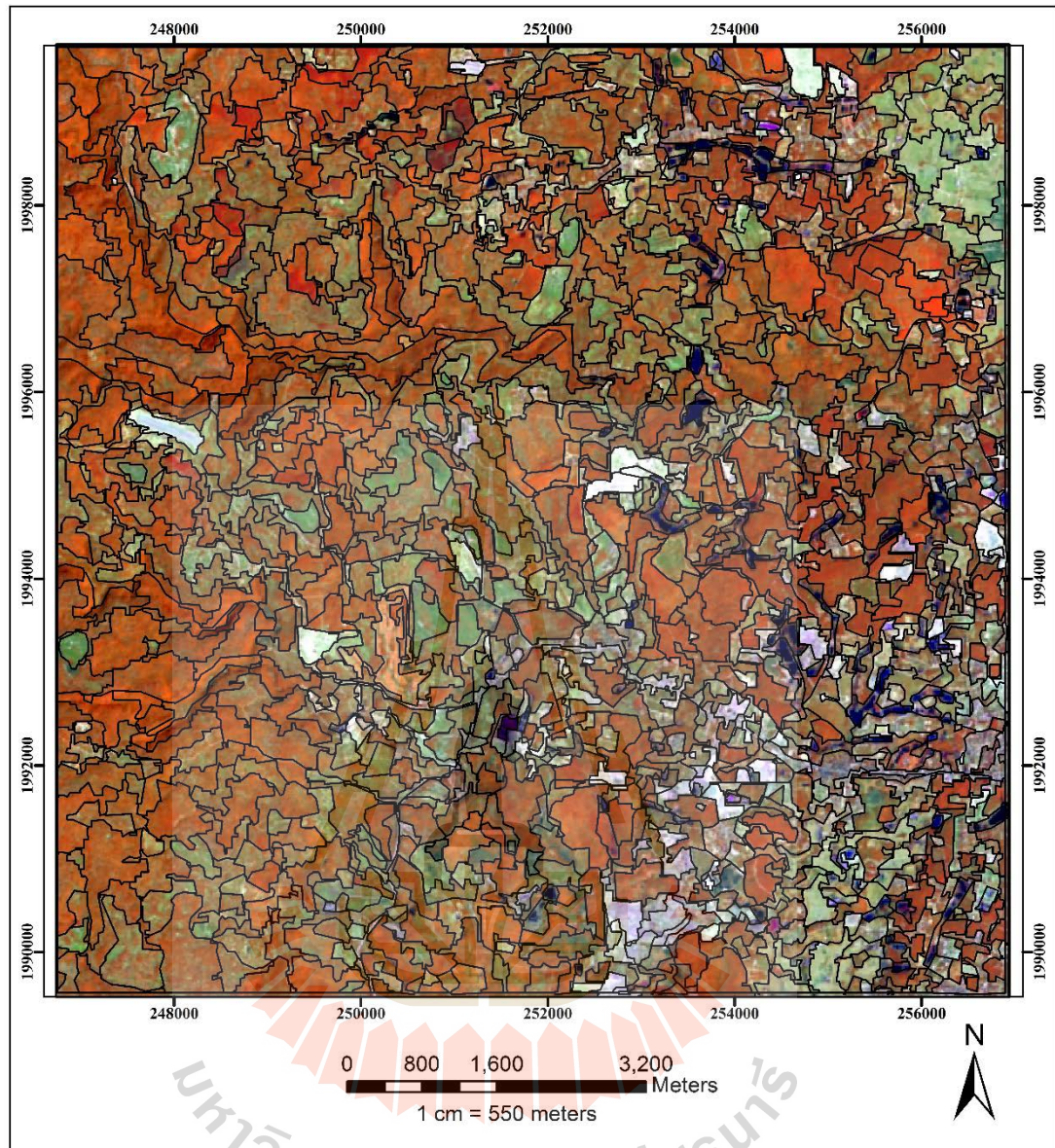


Figure 8.2 Image object of optimum pan-sharpened Landsat 8 data of 2017 by Multiresolution segmentation at level 1.

Table 8.1 Configuration of multiresolution segmentation at Level 2 and Level 1 with thematic layer.

Image object domain	Pixel level	Image object level
Level setting		
Level name	Level 2	Level 1
Segmentation setting		
Image layer weight	0, 0, 0, 0, 0, 0, 0, 0, 0	1, 1, 1, 1, 1, 1, 1, 1, 1
Thematic layer usage	Yes	YES
Scale parameters	20	20
Composition of homogeneity criterion		
Shape	0	0.1
Compactness	0	0.5

As results, it was found number of image object at Level 2 as parent level is 213 while number of image object at Level 1 as child level is 1,290. In fact, child objects that have similar spectral characteristics as parent objects are unchanged objects while any deviation is an indicator of changed objects.

8.1.2 Feature extraction by SEaTH analysis

Parent-child relationship between image objects at Level 2 and Level 1 is applied to extract changed and unchanged objects between 2012 and 2017. In this study, two main steps are required for feature extraction by SEaTH analysis.

At the first step, existence of LULC class from 2012 at Level 2 as parent level is created under class-related feature property as shown in Figure 8.3. Herein, the created existence LULC classes in mixed deciduous forest area include urban, bare land, grass land, mixed deciduous forest, paddy field, unstock forest, water body are applied as super-object (parent) of Level 1 as child level. This image property is applied to create super-object class hierarchy under Level 2 including

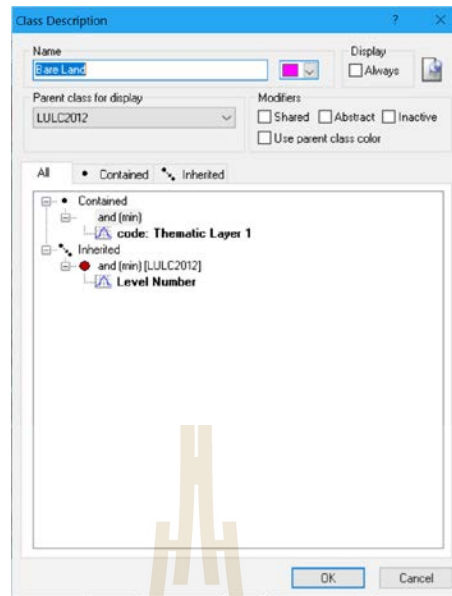


Figure 8.5 Class description of Super-object at Level 2.

At the second step, mean diff to super-object under To super-object property of layers values are applied to identify changed objects of Level 1 as child level as shown in Figure 8.6. In practice, mean value of each layer from 5 training areas are extracted and exported to MS-Excel spreadsheet software for SEaTH analysis. Examples of training areas for LULC changed object in 2017 are displayed in Figure 8.7. Meanwhile results of SEaTH analysis for separability test and threshold value extraction for rule-based development of mixed deciduous forest among other classes using Equation 2.1, 2.2 and 2.6 as results displayed in Tables 8.2 to 8.5.

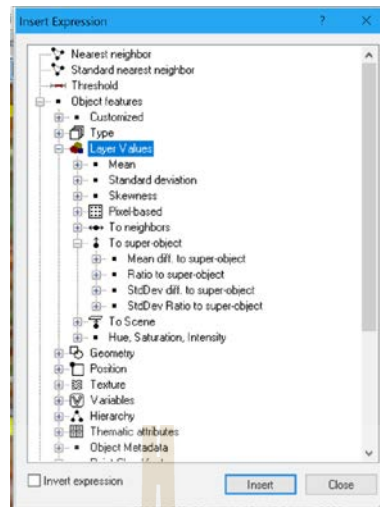


Figure 8.6 Structure of Mean diff to super-object parameter for changed object identification.

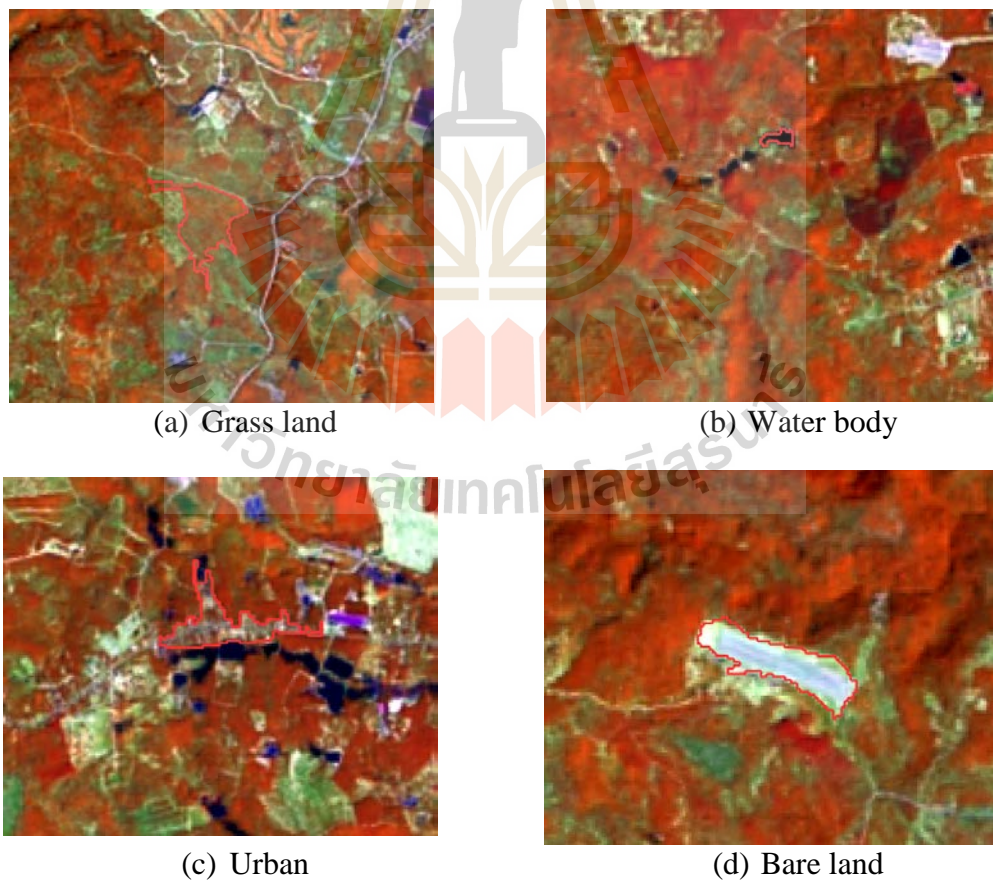


Figure 8.7 Training areas of changed objects in 2017 for SEaTH analysis.

Table 8.2 Pairwise of mean and variance between water body and urban for threshold value calculation.

Feature	Mean		Variance		J Value	Membership	LEFT	RIGHT
	water body	water body	urban	urban				
Layer 6 (1)	-8.70	0.93	10.63	17.80	1.99	Descending	-11.60	-4.97
Layer 5 (1)	-15.34	12.22	10.06	18.92	1.99	Descending	-25.83	-3.97
MNDWI (1)	26.82	126.48	-7.23	15.02	1.80	Descending	2.08	60.56
Layer 4 (1)	-20.63	75.74	0.39	5.05	1.65	Descending	-46.74	-4.45
Layer 3 (1)	-2.20	35.11	12.36	17.83	1.29	Descending	-19.97	6.05
NDBI (1)	-0.19	29.83	13.82	21.12	1.24	Descending	-16.57	7.29
Layer 1 (1)	-1.24	12.53	6.77	8.16	1.09	Descending	-11.86	3.07
NDVI (1)	-25.03	313.09	-14.13	16.31	0.80	Descending	-78.11	-18.91
Layer 2 (1)	-0.81	43.75	8.54	12.59	0.76	Descending	-20.65	4.63

Table 8.3 Pairwise of mean and variance between bare land and water body for threshold value calculation.

Feature	Mean		Variance		J Value	Membership	LEFT	RIGHT
	bare land	bare land	water body	water body				
Layer 5 (1)	35.27	20.53	-15.34	12.22	2.00	Ascending	6.74	48.87
Layer 6 (1)	34.44	31.48	-8.70	0.93	2.00	Ascending	-2.27	51.27
Layer 3 (1)	39.48	34.75	-2.20	35.11	2.00	Ascending	18.69	57.17
NDBI (1)	26.30	4.44	-0.19	29.83	1.99	Ascending	18.75	32.62
MNDWI (1)	-20.62	5.25	26.82	126.48	1.98	Descending	-27.49	-12.22
Layer 4 (1)	15.88	26.83	-20.63	75.74	1.93	Ascending	1.98	31.42
Layer 1 (1)	19.27	23.44	-1.24	12.53	1.90	Ascending	7.54	33.79
Layer 2 (1)	28.44	38.84	-0.81	43.75	1.85	Ascending	14.21	47.13
NDVI (1)	-23.47	3.53	-25.03	313.09	1.08	Descending	-29.11	-20.81

Table 8.4 Pairwise of mean and variance between grass land and urban for threshold value calculation.

Feature	Mean	Variance	Mean	Variance	J Value	Membership	LEFT	RIGHT
	grass land	grass land	urban	urban				
Layer 2 (1)	-0.38	1.77	8.54	12.59	1.59	Descending	-4.37	2.27
Layer 3 (1)	1.00	4.58	12.36	17.83	1.57	Descending	-5.43	5.05
Layer 1 (1)	0.16	1.70	6.77	8.16	1.43	Descending	-3.76	2.42
NDVI (1)	-4.76	26.41	-14.13	16.31	0.82	Ascending	-9.78	10.65
Layer 6 (1)	3.31	12.29	10.63	17.80	0.73	Descending	-7.20	6.80
Layer 4 (1)	-2.83	5.18	0.39	5.05	0.45	Descending	-9.66	-1.22
Layer 5 (1)	4.68	12.61	10.06	18.92	0.43	Descending	-5.98	7.35
NDBI (1)	10.50	51.06	13.82	21.12	0.16	Descending	-10.93	10.96
MNDWI (1)	-8.35	17.27	-7.23	15.02	0.02	Descending	-20.82	-8.19

Table 8.5 Pairwise of mean and variance between urban and water body for threshold value calculation.

Feature	Mean	Variance	Mean	Variance	J Value	Membership	LEFT	RIGHT
	urban	urban	water body	water body				
Layer 6 (1)	10.63	17.80	-8.70	0.93	1.99	Ascending	-4.97	23.29
Layer 5 (1)	10.06	18.92	-15.34	12.22	1.99	Ascending	-3.97	23.11
MNDWI (1)	-7.23	15.02	26.82	126.48	1.80	Descending	-18.85	2.08
Layer 4 (1)	0.39	5.05	-20.63	75.74	1.65	Ascending	-4.45	7.13
Layer 3 (1)	12.36	17.83	-2.20	35.11	1.29	Ascending	6.05	25.03
NDBI (1)	13.82	21.12	-0.19	29.83	1.24	Ascending	7.29	27.61
Layer 1 (1)	6.77	8.16	-1.24	12.53	1.09	Ascending	3.07	15.34
NDVI (1)	-14.13	16.31	-25.03	313.09	0.80	Ascending	-18.91	-2.01
Layer 2 (1)	8.54	12.59	-0.81	43.75	0.76	Ascending	4.63	19.19

The derived optimum threshold value of changed object are added to class description for rule set of LULC change class as an example of urban change in Figure 8.8. Herein, an optimum threshold value and the membership function (ascending or descending) is assigned for each feature under rule set as an example shown in Figure 8.9 for mean diff to super-object of layer 1 (Band 2) with ascending membership.

Class hierarchy of LULC2012 and object change (LULC change between 2012 and 2017) of urban area is displayed in Figure 8.10. All rule set of object change are then applied to create semantic model for classification in the next section.

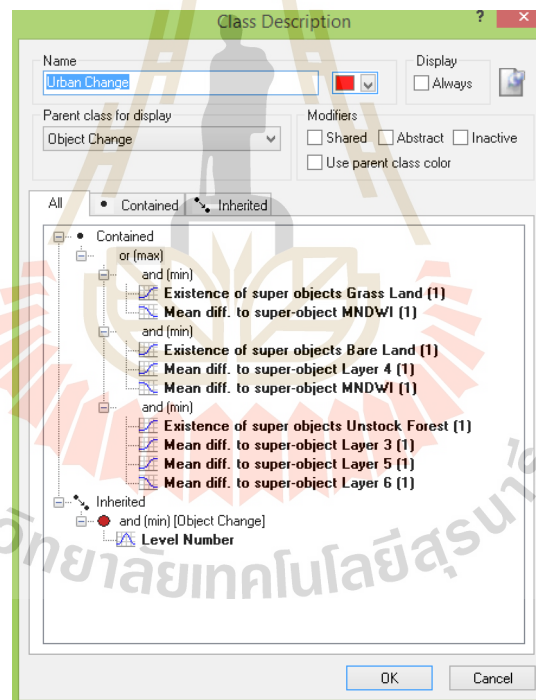


Figure 8.8 Rule set of urban change under class description.

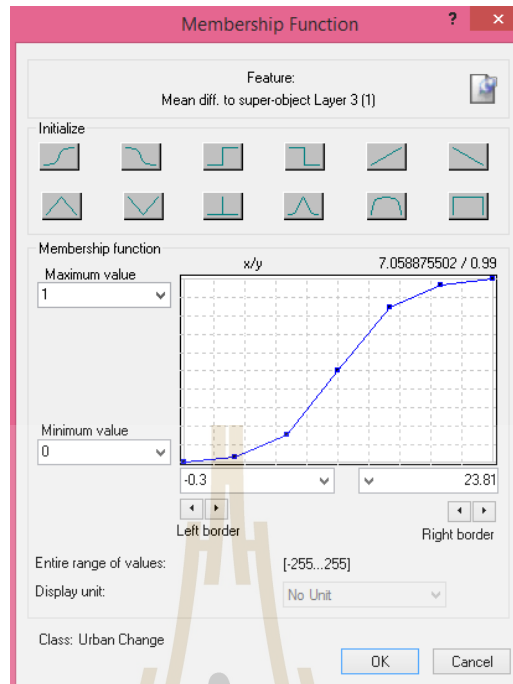


Figure 8.9 Membership function and assigned value of mean diff to-super object of layer 1.

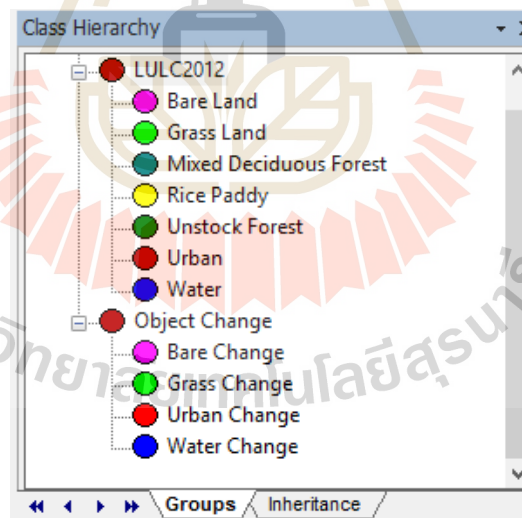


Figure 8.10 Class hierarchy of LULC2012 and Object Change.

8.1.3 Semantic modelling and classification

The developed semantic models for OBCD in mixed deciduous forest with pan-sharpened Landsat 8 data of 2017 for Layer 1 (Band 2), Layer 2 (Band 3), Layer 4 (Band 5), Layer 5 (Band 6), Layer 6 (Band 7), MNDWI, NDBI, and NDVI is presented in Tables 8.6 to 8.9. All rule set is directly applied to classify LULC change between 2012 and 2017 as result shown in Figure 8.11.

Table 8.6 Semantic model for bare land change between 2012 and 2017 in mixed deciduous forest area.

LULC classes	Membership function and threshold value		
	Membership function	Left border	Right border
Bare land and Water body			
Existence of super-object unstock forest (1)	Ascending	0	1
Mean Diff to super-object layer 1 (1)	Ascending	7.54	33.79
Mean Diff to super-object layer 2 (1)	Ascending	14.21	47.13
Mean Diff to super-object layer 3 (1)	Ascending	18.69	57.17
Mean Diff to super-object layer 4 (1)	Ascending	1.98	31.42
Mean Diff to super-object layer 5 (1)	Ascending	6.74	48.87
Mean Diff to super-object layer 6 (1)	Ascending	-2.27	51.27
Mean Diff to super-object MNDWI (1)	Descending	-27.49	-12.22
Mean Diff to super-object NDBI (1)	Ascending	18.75	32.62
Bare land and Urban			
Existence of super-object unstock forest (1)	Ascending	0	1
Mean Diff to super-object layer 1 (1)	Ascending	11.66	33.79
Mean Diff to super-object layer 2 (1)	Ascending	16.03	47.13
Mean Diff to super-object layer 3 (1)	Ascending	23.81	57.17
Mean Diff to super-object layer 4 (1)	Ascending	5.34	31.42
Mean Diff to super-object layer 5 (1)	Ascending	22.43	48.87
Mean Diff to super-object layer 6 (1)	Ascending	20.97	51.27
Mean Diff to super-object MNDWI (1)	Descending	-27.49	-15.49
Mean Diff to super-object NDBI (1)	Ascending	22.12	32.62
Mean Diff to super-object NDVI (1)	Descending	-29.11	-20.24

Table 8.6 (Continued).

LULC classes	Membership function and threshold value		
	Membership function	Left border	Right border
Bare land and Grass land			
Existence of super-object unstock forest (1)	Ascending	0	1
Mean Diff to super-object layer 1 (1)	Ascending	4.4	33.79
Mean Diff to super-object layer 2 (1)	Ascending	4.88	47.13
Mean Diff to super-object layer 3 (1)	Ascending	11.39	57.17
Mean Diff to super-object layer 4 (1)	Ascending	3.1	31.42
Mean Diff to super-object layer 5 (1)	Ascending	18.18	48.87
Mean Diff to super-object layer 6 (1)	Ascending	15.41	51.27
Mean Diff to super-object NDVI (1)	Descending	-29.11	-18.24
Existence of super-object mixed deciduous forest (1)	Ascending	0	1
Mean Diff to super-object layer 2 (1)	Ascending	3.81	39.04
Mean Diff to super-object layer 3 (1)	Ascending	6.79	51.5
Mean Diff to super-object layer 4 (1)	Ascending	-0.59	26.22

Table 8.7 Semantic model for grass land change between 2012 and 2017 in mixed deciduous forest area.

LULC classes	Membership function and threshold value		
	Membership function	Left border	Right border
Grass land and Water body			
Existence of super-object unstock forest (1)	Ascending	0	1
Mean Diff to super-object layer 1 (1)	Ascending	-1.06	4.07
Mean Diff to super-object layer 2 (1)	Descending	-4.37	1.25
Mean Diff to super-object layer 3 (1)	Ascending	-1.06	7.24
Mean Diff to super-object layer 4 (1)	Ascending	-7.13	4
Mean Diff to super-object layer 5 (1)	Ascending	-5.41	15.33
Mean Diff to super-object layer 6 (1)	Ascending	-5.95	13.83
Mean Diff to super-object MNDWI (1)	Descending	-20.82	1.7
Mean Diff to super-object NDBI (1)	Ascending	4.87	31.94
Mean Diff to super-object NDVI (1)	Ascending	-11.4	10.65

Table 8.7 (Continued).

LULC classes	Membership function and threshold value		
	Membership function	Left border	Right border
Grass land and Bare land			
Existence of super-object unstock forest (1)	Ascending	0	1
Mean Diff to super-object layer 1 (1)	Descending	-3.67	4.4
Mean Diff to super-object layer 2 (1)	Descending	-4.37	4.88
Mean Diff to super-object layer 3 (1)	Descending	-5.43	11.39
Mean Diff to super-object layer 4 (1)	Descending	-9.66	3.1
Mean Diff to super-object layer 5 (1)	Descending	-5.98	18.18
Mean Diff to super-object layer 6 (1)	Descending	-7.2	15.41
Mean Diff to super-object NDVI (1)	Ascending	-18.24	10.65
Grass land and Urban			
Existence of super-object unstock forest (1)	Ascending	0	1
Mean Diff to super-object layer 1 (1)	Descending	-3.76	2.42
Mean Diff to super-object layer 2 (1)	Descending	-4.37	2.77
Mean Diff to super-object layer 3 (1)	Descending	-5.43	5.05
Mean Diff to super-object layer 4 (1)	Descending	-9.66	-1.22
Mean Diff to super-object layer 5 (1)	Descending	-5.98	7.35
Mean Diff to super-object layer 6 (1)	Descending	-7.2	6.8
Mean Diff to super-object MNDWI (1)	Descending	-20.82	-8.19
Mean Diff to super-object NDBI (1)	Descending	-10.93	10.96
Mean Diff to super-object NDVI (1)	Ascending	-9.78	10.65
Grass land and Bare land			
Existence of super-object mixed deciduous forest (1)	Ascending	0	1
Mean Diff to super-object layer 1 (1)	Descending	-3.66	3.51
Mean Diff to super-object layer 2 (1)	Descending	-4.43	3.81
Mean Diff to super-object layer 3 (1)	Descending	-6.57	6.79
Mean Diff to super-object layer 4 (1)	Descending	-4.38	-0.59
Mean Diff to super-object layer 5 (1)	Descending	-4.27	6.67
Mean Diff to super-object layer 6 (1)	Descending	-5.82	6.44
Mean Diff to super-object MNDWI (1)	Ascending	-7.21	1.84
Mean Diff to super-object NDBI (1)	Descending	-4.83	10.86
Mean Diff to super-object NDVI (1)	Ascending	-10.09	6.93

Table 8.8 Semantic model for urban change between 2012 and 2017 in mixed deciduous forest area.

LULC classes	Membership function and threshold value		
	Membership function	Left border	Right border
Urban and Bare land			
Existence of super-object unstock forest (1)	Ascending	0	1
Mean Diff to super-object layer 3 (1)	Ascending	-0.3	23.81
Mean Diff to super-object layer 5 (1)	Ascending	-2.98	22.43
Mean Diff to super-object layer 6 (1)	Descending	-2.03	20.97
Urban and Water body			
Existence of super-object bare land (1)	Ascending	0	1
Mean Diff to super-object layer 4 (1)	Ascending	-3.85	22.13
Mean Diff to super-object MNDWI (1)	Descending	-40.81	6.27
Urban and Water body			
Existence of super-object grass land (1)	Ascending	0	1
Mean Diff to super-object MNDWI (1)	Descending	-15.65	5.53

Table 8.9 Semantic model for water body change between 2012 and 2017 in mixed deciduous forest area.

LULC classes	Membership function and threshold value		
	Membership function	Left border	Right border
Water body and Bare land			
Existence of super-object unstock forest (1)	Ascending	0	1
Mean Diff to super-object layer 1 (1)	Descending	-11.86	7.54
Mean Diff to super-object layer 2 (1)	Descending	-20.65	14.21
Mean Diff to super-object layer 3 (1)	Descending	-19.97	18.69
Mean Diff to super-object layer 4 (1)	Descending	-46.74	1.98
Mean Diff to super-object layer 5 (1)	Descending	-25.83	6.74
Mean Diff to super-object layer 6 (1)	Descending	-11.6	-2.27
Mean Diff to super-object MNDWI (1)	Ascending	-12.22	60.56
Mean Diff to super-object NDBI (1)	Descending	-16.57	18.75
Water body and Urban			
Existence of super-object paddy field (1)	Ascending	0	1
Mean Diff to super-object layer 3 (1)	Descending	-24.42	8.04
Mean Diff to super-object layer 4 (1)	Descending	-36.3	0.62
Mean Diff to super-object layer 5 (1)	Descending	-43.21	-0.83
Mean Diff to super-object layer 6 (1)	Descending	-29.31	0.57
Mean Diff to super-object MNDWI (1)	Ascending	22.13	64.43
Water body and Urban			
Existence of super-object bare land (1)	Ascending	0	1
Mean Diff to super-object layer 4 (1)	Descending	-30.15	-3.85
Mean Diff to super-object layer 5 (1)	Descending	-42.78	-4.41
Mean Diff to super-object MNDWI (1)	Ascending	6.27	59.29
Mean Diff to super-object NDVI (1)	Descending	-26.04	-4.45
Water body and Urban			
Existence of super-object grass land (1)	Ascending	0	1
Mean Diff to super-object MNDWI (1)	Ascending	5.53	46.56

Table 8.9 (Continued).

LULC classes	Membership function and threshold value		
	Membership function	Left border	Right border
Water body and Urban			
Existence of super-object unstock forest (1)	Ascending	0	1
Mean Diff to super-object layer 1 (1)	Descending	-11.86	3.07
Mean Diff to super-object layer 2 (1)	Descending	-20.65	4.63
Mean Diff to super-object layer 3 (1)	Descending	-19.97	6.05
Mean Diff to super-object layer 4 (1)	Descending	-46.74	-4.45
Mean Diff to super-object layer 5 (1)	Descending	-25.83	-3.97
Mean Diff to super-object layer 6 (1)	Descending	-11.6	-4.97
Mean Diff to super-object MNDWI (1)	Ascending	2.06	60.56
Mean Diff to super-object NDBI (1)	Descending	-16.57	7.29
Mean Diff to super-object NDVI (1)	Descending	-78.11	-18.91
Water body and Grass land			
Existence of super-object unstock forest (1)	Ascending	0	1
Mean Diff to super-object layer 1 (1)	Descending	-11.86	-1.06
Mean Diff to super-object layer 2 (1)	Descending	-20.65	-1.97
Mean Diff to super-object layer 3 (1)	Descending	-19.97	-1.06
Mean Diff to super-object layer 4 (1)	Descending	-46.74	-7.13
Mean Diff to super-object layer 5 (1)	Descending	-25.83	-5.41
Mean Diff to super-object layer 6 (1)	Descending	-11.6	-5.95
Mean Diff to super-object MNDWI (1)	Ascending	1.7	60.56
Mean Diff to super-object NDBI (1)	Descending	-16.57	4.87
Mean Diff to super-object NDVI (1)	Descending	-78.11	-11.4

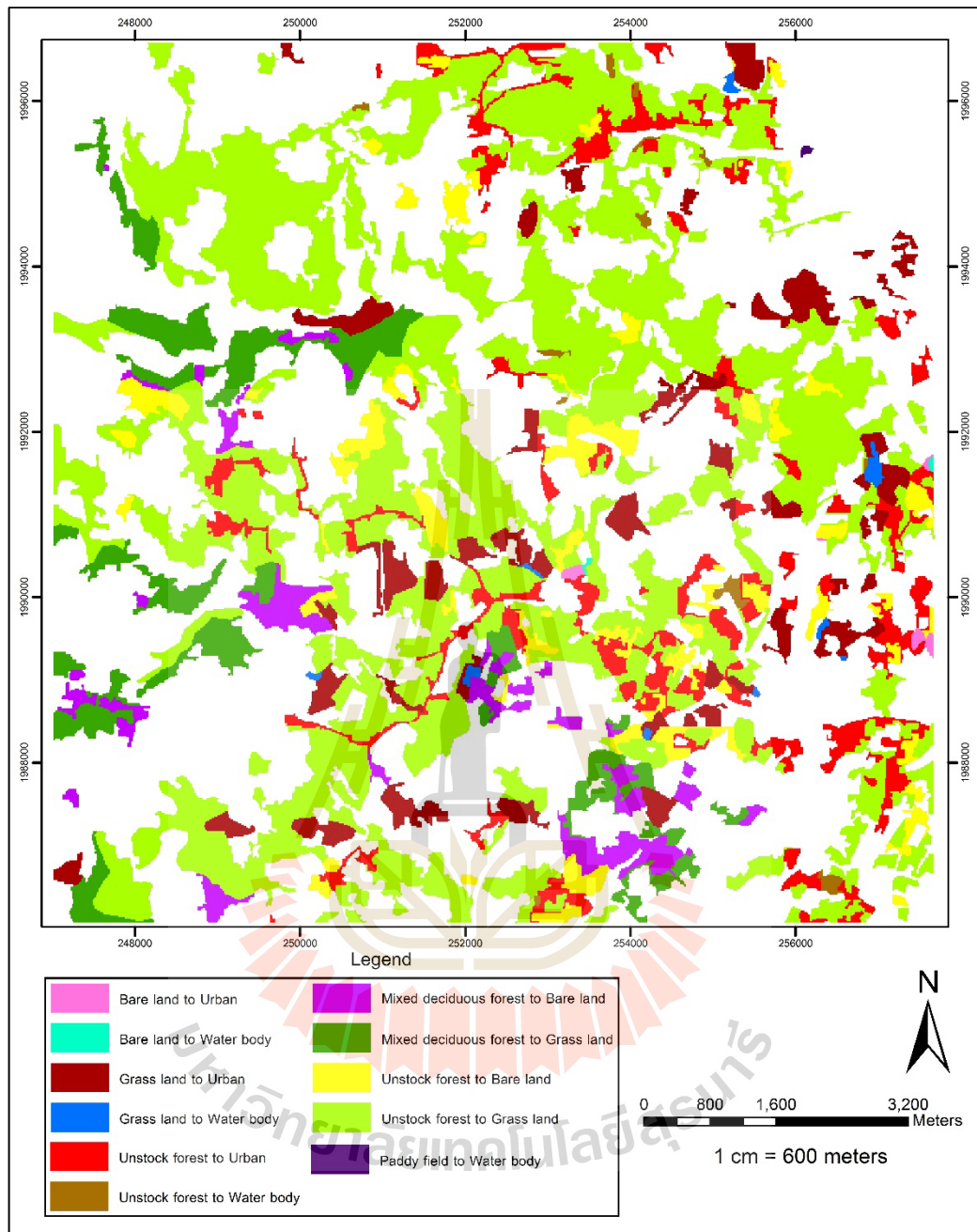


Figure 8.11 LULC change between 2012 and 2017 in mixed deciduous forest area.

8.2 Land use and land cover in 2017 updating

In addition, the LULC change data is applied to update LULC map in 2012 for final LULC map in 2017 as a result shown in Figure 8.12. Comparison of area and percentage of LULC data in 2012 and 2017 is presented in Table 8.10 and the change matrix of LULC classes between 2012 and 2017 is reported in Table 8.11.

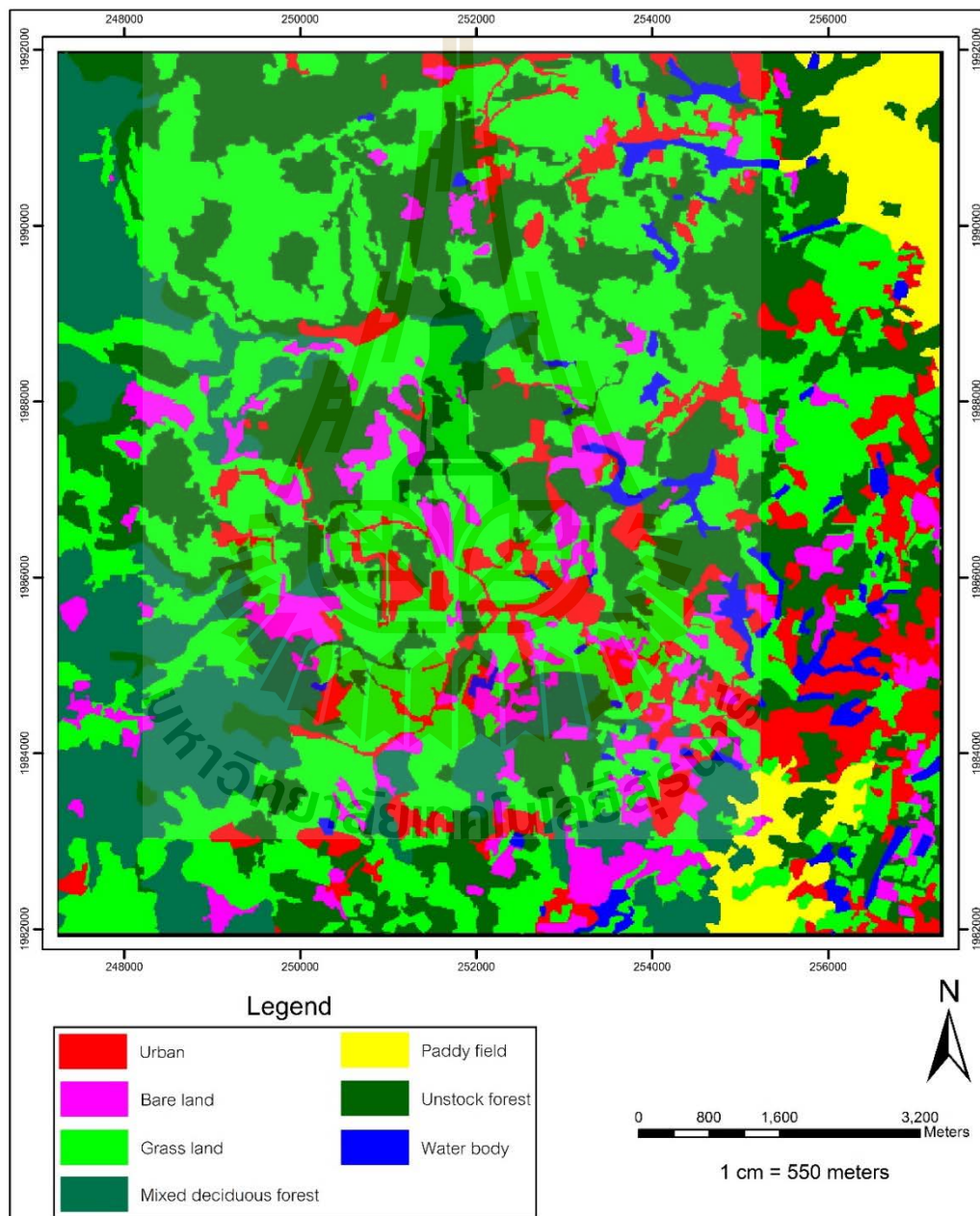


Figure 8.12 Final LULC map in 2017 in mixed deciduous forest area.

Table 8.10 Comparison of area and percentage of LULC in 2012 and 2017 in mixed deciduous forest area.

LULC class	LULC in 2012		LULC in 2017	
	Area (Sq. Km.)	%	Area (Sq. Km.)	%
Bare land	1.40	1.40	6.53	6.53
Grass land	9.50	9.51	36.04	36.05
Mixed deciduous forest	19.02	19.03	13.21	13.21
Paddy field	4.24	4.24	4.22	4.23
Unstock forest	61.97	61.99	27.31	27.32
Urban	1.69	1.69	10.05	10.06
Water body	2.14	2.14	2.60	2.60
Total	99.96	100.00	99.96	100.00

Table 8.11 Change matrix of LULC classes between 2012 and 2017 in mixed deciduous forest area.

LULC classes in 2012	LULC classes in 2017 (Unit: sq. km.)							Total
	Bare land	Grass land	Mixed deciduous forest	Paddy field	Unstock forest	Urban	Water body	
Bare land	1.29					0.09	0.02	1.40
Grass land		5.50				3.81	0.19	9.50
Mixed deciduous forest	1.96	3.86	13.21					19.02
Paddy field				4.22			0.01	4.24
Unstock forest	3.28	26.68			27.31	4.46	0.24	61.97
Urban						1.69		1.69
Water body							2.14	2.14
Total	6.53	36.04	13.21	4.22	27.31	10.05	2.60	

As result, it was found that mixed deciduous forest area between 2012 and 2017 was decreased about 5.81 sq. km. The mixed deciduous forest in 2012 was changed to be grass land (3.86 sq. km.) and bare land (1.96 sq. km.) in 2017. On contrary, grass land between 2012 and 2017 was increased about 26.54 sq. km. Most

of the increased grass land in 2017 came from unstock forest (26.68 sq. km.) in 2012. Likewise, urban between 2012 and 2017 was increased about 8.36 sq. km. Most of the increased urban in 2017 came from unstock forest (4.46 sq. km.) in 2012. Similarly, bare land between 2012 and 2017 was increased about 5.13 sq. km. Most of the increased bare land in 2017 came from unstock forest (3.28 sq. km.) in 2012.

8.3 Accuracy assessment

The extracted LULC change map between 2012 and 2017 was further assess accuracy based on 144 stratified random sampling points with reference image from Google Earth in 2017. Error matrix and accuracy assessment is presented in Table 8.12.

As a result it reveals that overall accuracy and Kappa hat coefficient is 93.06% and 85.14%, respectively. Meanwhile producer's accuracy of LULC change class varies between 73.91% for bare land and 100.00% for urban and water body while user's accuracy of LULC change class varies between 62.96% for urban and 100.00% for bare land, grass land and water body. Based on Fitzpatrick-Lins (1981), Kappa hat coefficient more than 80% represents strong agreement or accuracy between the predicted map and the reference map

Table 8.12 Error matrix and accuracy assessment of LULC change between 2012 and 2017.

Class Name	Reference Data				Row Total	PA	UA
	Bare land	Grass land	Urban	Water body			
Bare land	17				17	73.91	100.00
Grass land		99			99	96.12	100.00
Urban	6	4	17		27	100.00	62.96
Water body				1	1	100.00	100.00
Column Total	23	103	17	1	144		
Overall accuracy	93.06						
Kappa hat coefficient	85.14						

In addition, it can be observed that omission error of bare land and grass land is about 26.09% and 3.88%, respectively. The main cause of omission error of bare land from urban because the brightness value of bare land and urban is similar. Meanwhile, the main cause of omission error of grass land from urban because the brightness value of dry grass land and urban is similar.

Likewise, it can be observed that commission error of urban area is quite high about 37.04%. The main cause of commission error of urban came from bare land and dry grass land because its brightness value is similar with bare land and dry grass land.

CHAPTER IX

CONCLUSION AND RECOMMENDATION

Under this chapter, the major results according to objectives of the study, which were reported in Chapter V to VIII, are here separately concluded about LULC updating in four prototypes areas, namely, urban, paddy field, unstock forest, and mixed deciduous forest and recommendations for future research and development are suggested.

9.1 Conclusion

9.1.1 LULC updating in urban area

According to rule set development for LULC change detection between 2012 and 2017 and updating in urban area in 2017, it was found that urban area between 2012 and 2017 was increased about 2.12 sq. km. The increased urban area in 2017 came from unstock forest, paddy field, grass land, bare land, and water body in 2012. On contrary, paddy field between 2012 and 2017 was dramatic decreased about 12.99 sq. km. Paddy field in 2012 was changed to be grass land, bare land, water body and urban in 2017. In addition, overall accuracy and Kappa hat coefficient for thematic accuracy assessment of OBCD map were 93.75% and 90.45%, respectively. Herewith, producer's accuracy of LULC change class varied between 78.95% for urban and 100.00% for bare land and user's accuracy of LULC change class varied between 82.86% for bare land and 100.00% for water body.

9.1.2 LULC updating in paddy field

According to rule set development for LULC change detection between 2012 and 2017 and updating in paddy field in 2017, it was found that paddy field area between 2012 and 2017 was decreased about 8.40 sq. km. The paddy field in 2012 was changed to be urban, grass land, bare land, and water body in 2017. On contrary, grass land between 2012 and 2017 was increased about 9.35 sq. km. The increased grass land in 2017 came from unstock forest and paddy field in 2012. Likewise, urban between 2012 and 2017 was increased about 8.56 sq. km. The increased urban in 2017 came from paddy field, unstock forest, mixed deciduous forest, grass land and bare land in 2012. In addition, overall accuracy and Kappa hat coefficient for thematic accuracy assessment of OBCD map were 95.14% and 92.36%, respectively. Herewith, producer's accuracy of LULC change class varied between 88.89% for bare land and 100.00% for urban and user's accuracy of LULC change class varied between 87.04% for urban and 100.00% for bare land.

9.1.3 LULC updating in unstock forest

According to rule set development for LULC change detection between 2012 and 2017 and updating in unstock forest in 2017, it was found that unstock forest area between 2012 and 2017 was decreased about 8.22 sq. km. The unstock forest in 2012 was changed to be grass land, bare land, urban, and water body in 2017. On contrary, grass land between 2012 and 2017 was increased about 6.53 sq. km. Most of the increased grass land in 2017 came from unstock forest in 2012. Likewise, bare land between 2012 and 2017 was increased about 0.96 sq. km. Most of the increased bare land in 2017 came from unstock forest in 2012. However, bare land in 2012 was changed to be grass land, urban and water body in 2017. In addition,

overall accuracy and Kappa hat coefficient for thematic accuracy assessment of OBCD map were 97.92% and 95.98%, respectively. Herewith, producer's accuracy of LULC change class varied between 88.46% for bare land and 100.00% for grass land, urban and water body and user's accuracy of LULC change class varied between 62.5% for urban and 100.00% for bare land, grass land and water body.

9.1.4 LULC updating in mixed deciduous forest

According to rule set development for LULC change detection between 2012 and 2017 and updating in mixed deciduous forest in 2017, it was found that mixed deciduous forest area between 2012 and 2017 was decreased about 5.81 sq. km. The mixed deciduous forest in 2012 was changed to be grass land and bare land in 2017. On contrary, grass land between 2012 and 2017 was increased about 26.54 sq. km. Most of the increased grass land in 2017 came from unstock forest in 2012. Likewise, urban between 2012 and 2017 was increased about 8.36 sq. km. Most of the increased urban in 2017 came from unstock forest in 2012. Similarly, bare land between 2012 and 2017 was increased about 5.13 sq. km. Most of the increased bare land in 2017 came from unstock forest in 2012. In addition, overall accuracy and Kappa hat coefficient for thematic accuracy assessment of OBCD map were 93.06% and 85.14%, respectively. Herewith, producer's accuracy of LULC change class varied between 73.91% for bare land and 100.00% for urban and water body and user's accuracy of LULC change class varied between 62.96% for urban and 100.00% for bare land, grass land and water body.

In summary, it can be here concluded that OBCD algorithm with SEaTH analysis can be efficiently applied to develop rule set for LULC change detection and updating. Herewith, overall accuracy of OBCD map from four prototypes: urban,

paddy field, unstock forest and mixed deciduous forest varied between 93.06% and 97.92% while Kappa hat coefficient varied between 85.14% and 95.98%. Based on Fitzpatrick-Lins (1981), Kappa hat coefficient more than 80% represents strong agreement or accuracy between the classified map and the reference map. The applicable procedure for LULC map updating in all four prototype areas is displayed in Figure 9.1.



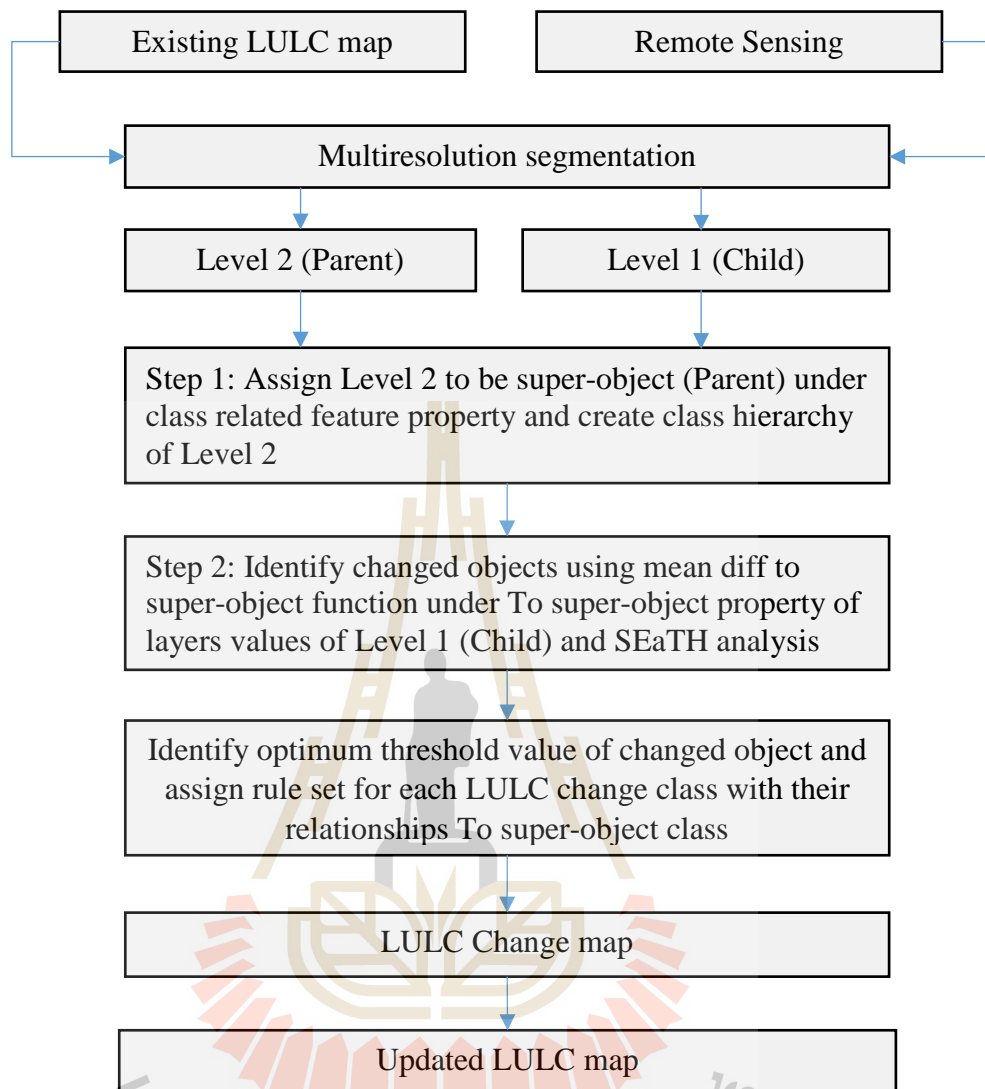


Figure 9.1 Workflow of practical procedure using class-object change detection and SEaTH analysis for LULC map updating.

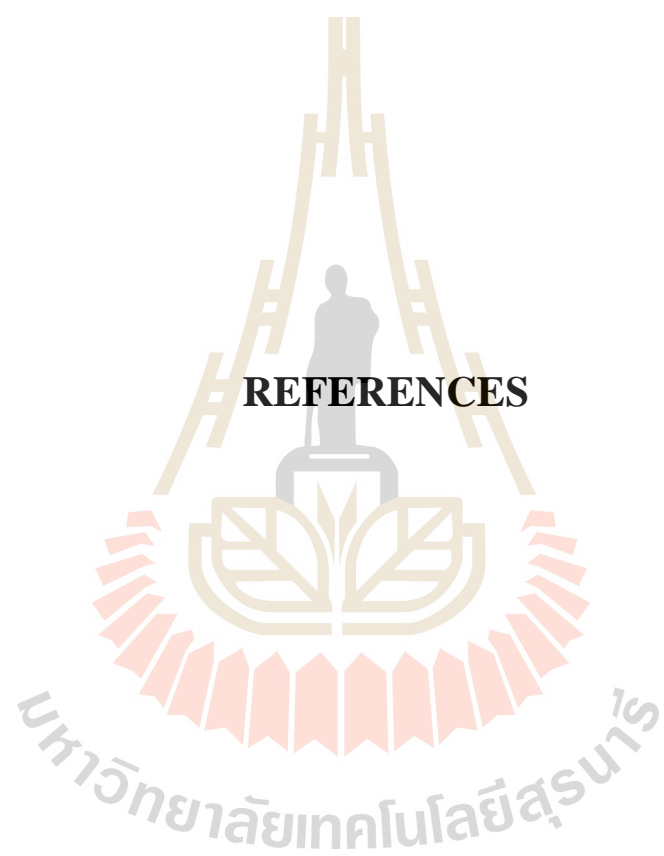
9.2 Recommendation

In this study, the rule set for LULC classification with Separability and Thresholds analysis using class-object change detection algorithm were developed to detect the change of LULC in four prototype areas. The possibly expected recommendations could be made for further studies as follows:

1. The developed rule set for LULC classification from specific prototype area should be examined in another area for validating the rule set. In practice, modification of rule set for LULC classification may be required due to spatio-temporal change of image objects.

2. The Forest Inventory and Planning Division, Department of Forest Resources, who responses for LULC classification, should develop a common rule set for LULC classification under object-based image analysis for LULC change detection and map updating at watershed or provincial levels of Lao PDR in the near future. In addition, all LULC classes according to NGD classification system should be included in rule set development.

3. Multi-temporal-object change detection algorithm for LULC classification which was implemented by many researchers such as Li et al. (2009) and Yang et al. (2015) should be examined and compared to class-object change detection algorithm from the current study.



REFERENCES

REFERENCES

- Al-Khudhairi, D.H.A., Caravaggi, I., and Glada, S. (2005). Structural damage assessments from Ikonos data using change detection, object-oriented segmentation, and classification techniques. **Photogrammetric Engineering & Remote Sensing**. 71: 825–837.
- An, K., Zhang, J., and Xiao, Y. (2007). Object-oriented urban dynamic monitoring, a case study of Haidian District of Beijing. **Chinese Geographical Science**. 17: 236–242.
- Asia Pacific Parliamentary Forum, Vientiane Capital, Lao PDR. (2009) [Online]. Available: <http://www.na.gov.la/appf17/geography.html>.
- Baatz, M., and Schäpe, A. (2000). Multiresolution segmentation: An optimization approach for high quality multi-scale image segmentation. In angewandte geographische informations-verarbeitung (12thed.). Quoted in Gao, J. (2009). **Digital analysis of remotely sensed imagery**. New York: McGraw-Hill.
- Blaschke, T. (2005). Towards a framework for change detection based on image objects. **Göttinger Geographische Abhandlungen**. 113: 1–9.
- Bontemps, S., Bogaert, P., Titeux, N., and Defourny, P. (2008). An object-based change detection method accounting for temporal dependences in time series with medium to coarse spatial resolution. **Remote Sensing of Environment**. 112: 3181–3191.

- Burnett, C., and Blaschke, T. (2003). A multi-scale segmentation/object relationship modeling methodology for landscape analysis. **Ecological Modeling**. 168(3): 233–249.
- Carvalho, L.M.T., Fonseca, L.M.G., Murtagh, F., and Clevers, J.G.P.W. (2001). Digital change detection with the aid of multi-resolution wavelet analysis. **International Journal of Remote Sensing**. 22: 3871–3876.
- Chen, G., Hay, G.J., Carvalho., and Wulder, M.A. (2012). Object-based change detection. Department of Geography, University of Calgary, AB, Canada T2N 1N4.
- Chen, G., Hay, G.J., Castilla, G., St-Onge, B., and Powers, R. (2011). A multi-scale geographic object-based image analysis (GEOBIA) to estimate Lidar-measured forest canopy height using Quickbird imagery. **International Journal of Geographic Information Science**. 25: 877–893.
- Chen, Z., and Hutchinson, T.C. (2007). Urban damage estimation using statistical processing of satellite images. **Journal of Computing in Civil Engineering**. 21:187–199.
- Conchedda, G., Durieux, L., and Mayaux, P. (2008). An object-based method for mapping and change analysis in mangrove ecosystems. **Journal of Photogrammetry and Remote Sensing (ISPRS)**. 63: 578–589.
- Congalton, R.G., and Green, K. (1999). Assessing the Accuracy of Remotely Sensed Data: Principles and Practices. Boca Raton. FL: Lewis Publishers.
- Cracknell, A. (1998). "Review article Synergy in remote sensing-what's in a pixel?". **International Journal of Remote Sensing**. 19(11): 2025-2047.

- Dai, X., and Khorram, S. (1998). "The effects of image misregistration on the accuracy of remotely sensed change detection", **Geoscience and Remote Sensing**, IEEE Transactions on. 36(5): 1566-1577.
- Dale, Pat., Chandica, A.L., and Evans, M. (1996). Using image subtraction and classification to evaluate change in sub-tropical inter-tidal wetland. *Int. J. Remote sensing*. 17: 703–719.
- De Chant, T., and Kelly, M. (2009). Individual object change detection for monitoring the impact of a forest pathogen on a Hardwood forest. **Photogrammetric Engineering and Remote Sensing**. 75: 1005–1013.
- Desclée, B., Bogaert, P., and Defourny, P. (2006). Forest change detection by statistical object-based method. **Remote Sensing of Environment**. 102: 1–11.
- Dupuy, S., Herbreteau, V., Feyfant, T., Morand, S., and Tran, A. (2012). Land cover dynamics in Southeast Asia: Contribution of object-oriented techniques for change detection. CIRAD, UMR TETIS, F-34398 Montpellier, France.
- Durieux, L., Lagabrielle, E., and Nelson, A. (2008). A method for monitoring building construction in urban sprawl areas using object-based analysis of Spot 5 images and existing GIS data. **ISPRS Journal of Photogrammetry and Remote Sensing**. 63: 399–408.
- Duveiller, G., Defourny, P., Desclée, B., and Mayaux, P. (2008). Deforestation in central Africa: estimates at regional, national and landscape levels by advanced processing of systematically-distributed Landsat extracts. **Remote Sensing of Environment**. 112: 1969–1981.

- FAO. (2016). State of the world's forests. Forests and agriculture: **Land use challenges and opportunities**. Food and Agriculture Organization of the United Nations.
- Fitzpatrick-Lins, K. (1981). Comparison of Sampling Procedures and Data Analysis for a Land-use and Land-cover Map. **Photogrammetric Engineering & Remote Sensing**. **55** (4): 475–478.
- Foody, G.M. (2002). Status of land cover classification accuracy assessment. **Remote Sensing of Environment**. **80**: 185–201.
- Franklin, S.E., Lavigne, M.B., Moskal, L.M., Wulder, M.A., and McCaffrey, T.M. (2001). Interpretation of forest harvest conditions in New Brunswick using Landsat TM enhanced wetness difference imagery (EWDI). **Canadian Journal of Remote Sensing**. **27**: 118–128.
- Fujita, Yayoi. (2006). “Understanding the History of Change in Laos: An Important Premise for Development Effects”. **Mountain Research and Development**. **26**: 197–199.
- Fuller, R.M., Smith, G.M., and Devereux, B.J. (2003). The characterization and measurement of land cover change through remote sensing: problems in operational applications? **International Journal of Applied Earth Observation**. **4**: 243–253.
- Gamanya, R., De Maeyer, P., and De Dapper, M. (2009). Object-oriented change detection for the city of Harare, Zimbabwe. **Expert Systems with Applications**. **36**: 571–588.
- Gangkofner, U.G., Pradhan, P.S., and Holcomb, D.W. (2008). Optimizing the high-pass filter addition technique for image fusion.

- Gladstone, C.S., Gardiner, A., and Holland, D. (2012). A semi-automatic method for detecting changes to ordnance survey topography data in rural environments. **Ordnance survey, research**, Adanac drive, SOUTHAMPTON, United Kingdom, SO16 0AS.
- Gong, J., Sui, H., Sun, K., Ma, G., and Liu, J. (2008). Object-level change detection based on full-scale image segmentation and its application to Wenchuan Earthquake. *Science in China Series E: Technological Sciences*. 51: 110–122.
- Grenzdörffer, G.J. (2005). Land use change in Rostock, Germany since the reunification a combined approach with satellite data and high resolution aerial images. **In Proceedings of the ISPRS WG VII/1 ‘Human Settlements and Impact Analysis’ 3rd International Symposium Remote Sensing and Data Fusion Over Urban Areas (URBAN 2005) and 5th International Symposium Remote Sensing of Urban Areas**. 2005.
- Guizhou Wang, Guojin He, and Jianbo Liu. (2012). A new classification method for high spatial resolution remote sensing image based on mapping mechanism. **Center for Earth Observation and Digital Earth Chinese Academy of Sciences**. Beijing, China.
- Hall, O., and Hay, G.J. (2003). A multi-scale object-specific approach to digital change detection. **International Journal of Applied Earth Observation and Geo-information**. 4: 311–327.
- Hazel, G.G. (2001). Object-level change detection in spectral imagery. **IEEE Transactions on Geoscience and Remote Sensing**. 39: 553–561.
- He, C., Li, J., Zhang, J., Pan, Y., and Chen, Y. (2005). Dynamic monitor on urban expansion based on an object-oriented approach. **In Proceedings of the**

International Geoscience and Remote Sensing Symposium (IGARSS'05).

2005. Seoul, South Korea. (4).

<https://www.internationalrivers.org/resources/map-of-key-existing-and-proposed-dams-in-laos-4019>.

Im, J., Jensen, J.R., and Tullis, J.A. (2008). Object-based change detection using correlation image analysis and image segmentation. **International Journal of Remote Sensing**. 29: 399–423.

International River. (2007). Map of key existing and proposed dams in Laos [Online]. Available: <https://www.internationalrivers.org/resources/map-of-key-existing-and-proposed-dams-in-laos-4019>.

IPP (Independent power producer) Hydropower Project. (2016). 20 Concession Agreement (CA). Ministry of Energy and Mines. Department of Energy Business [Online]. Available: <http://www.poweringprogress.org/new/power-projects/construction>.

Jensen, J.R. (2005). Introductory Digital Image Processing. **A Remote Sensing Perspective** (3rd ed). Prentice-Hall, Upper Saddle River, NJ.

Johnson, R.D. and Kasischke, E. (1998). "Change vector analysis: a technique for the multispectral monitoring of land cover and condition". **International Journal of Remote Sensing**. 19(3): 411–426.

King, R.L., and Wang, J. (2001). A wavelet based algorithm for pan sharpening Landsat 7 imagery. **In Geoscience and Remote Sensing Symposium. IGARSS 2001. IEEE 2001 International**. (pp. 849–851).

- Klonus, S., and Ehlers, M. (2009). Performance of evaluation methods in image fusion. **In International Conference on Information Fusion. FUSION '09:** 1409–1416.
- Laben, C.A., and Brower, B.V. (2000). Process for enhancing the spatial resolution of multispectral imagery using Pan-sharpening. United States Patent No. 6011875.
- Laliberte, A.S., Rango, A., Havstad, K.M., Paris, J.F., Beck, R.F., and Mcneely, R. (2004). Object-oriented image analysis for mapping shrub encroachment from 1937 to 2003 in southern New Mexico. **Remote Sensing of Environment.** 93: 198–210.
- Lefebvre, A., Corpetti, T., and Hubert-Moy, L. (2008). Object-oriented approach and texture analysis for change detection in very high resolution images. **In Proceedings of the IEEE International Geoscience and Remote Sensing Symposium (IGARSS'08)**, 6–11 July 2008, Boston, MA, USA.(pp 663–666).
- Li, J., and Narayanan, R.M. (2003). A shape-based approach to change detection of lakes using time series remote sensing images. **IEEE Transactions on Geoscience and Remote Sensing** 41: 2466–2477.
- Li, X., Yeh, A.G., Qian, J., Ai, B., and Qi, Z. (2009). A matching algorithm for detecting land use changes using case-based reasoning. **Photogrammetric Engineering and Remote Sensing.** 75: 1319–1332.
- Lillesand, T.M., and Keifer, R.W. (1994). Remote Sensing and Image Interpretation. (3rd ed).
- Linke, J., Mcdermid, G.J., Laskin, D.N., Mclane, A.J., Pape, A., Cranston, J., Hallbeyer, M., and Franklin, S.E. (2009). A disturbance-inventory framework

- for flexible and reliable landscape monitoring. **Photogrammetric Engineering and Remote Sensing**. 75: 981–995.
- Lu, D; Mausel, P; Brondizio, E., and Moran, E. (2002) "Assessment of atmospheric correction methods for Landsat TM data applicable to Amazon basin LBA research", **International Journal of Remote Sensing**. 23(13): 2651–2671.
- Lu; Mausel; Brondizio., and Moran. (2004). Change detection techniques. **International Journal of Remote Sensing**. (ISSN 0143-1161) print/ISSN 1366-5901 online (2004) Taylor and Francis Ltd.
- Macleod, R.D., and Congalton, R.G. (1998). "A quantitative comparison of change-detection algorithms for monitoring eelgrass from remotely sensed data". **Photogrammetric Engineering and Remote Sensing**. 64(3): 207–216.
- Mcdermid, G.J., Linke, J., Pape, A., Laskin, D.N., Mclane, A.J., and Franklin, S.E. (2008). Object-based approaches to change analysis and thematic amp update: challenges and limitation. **Canadian Journal of Remote Sensing**. 34: 462–466.
- Miller, O., Pikaz, A., and Averbuch, A. (2005). **Objects based change detection in a pair of gray-level images**. **Pattern Recognition**. 38: 1976–1992.
- Mouflis, G.D., Gitasa, I.Z., Iliadoua, S., and Mitria, G.H. (2008). Assessment of the visual impact of marble quarry expansion (1984–2000) on the landscape of Thasos island, NE Greece. **Landscape and Urban Planning**. 86: 92–102.
- Nielsen, A.A., Conradsen, K., and Simpson, J.J. (1998). "Multivariate alteration detection (MAD) and MAF postprocessing in multispectral, bitemporal image data: New approaches to change detection studies". **Remote Sensing of Environment**. 64: 1–19.

- Niemeyer, I. (2003). Pixel-based and object-oriented change detection analysis using high-resolution imagery. **Institute for Mine-Surveying and Geodesy**, TU Bergakademie Freiberg, D-09599 Freiberg, Germany.
- Niemeyer, I., Nussbaum, S., and Canty, M.J. (2005). Automation of change detection procedures for nuclear safeguards-related monitoring purposes. In **Proceedings of the IEEE International Geoscience and Remote Sensing Symposium (IGARSS'05)**. (2005). Seoul, South Korea. (4 pp).
- Nikolakopoulos, K.G. (2008). Comparison of Nine Fusion Techniques for Very High Resolution Data. **Photogrammetric Engineering and Remote Sensing**, 74(5): 647-659.
- Nolintha Vanthana. (2011). Cities, SEZs and Connectivity in Major Provinces of Laos. In **Intra- and Inter- Connectivity in the Mekong Region**, edited by Masami Ishida, BRC Research Report No.6, Bangkok Research Center, IDE-JETRO, Bangkok, Thailand. [Online]. Available: http://www.ide.go.jp/English/Publish/Download/Brc/pdf/06_chapter4.pdf.
- Nussbaum, S., and Menz, G. (2008). Object-Based Image Analysis and Treaty Verification. Berlin: Springer.
- Otsu, N. (1979). A threshold selection method from gray-level histograms. **IEEE Transactions on Systems, Man and Cybernetics**. 9: 62–66.
- Owojori, A., and Xie, H. (2005). Landsat image-based LULC changes of San Antonio, Texas using advanced atmospheric correction and object-oriented image analysis approaches. In **Proceedings of the 5th International Symposium on Remote Sensing of Urban Areas**. 2005. USA. (4 pp).

- Pal, N.R., and Pal, S.K. (1993). A review on image segmentation techniques. **Pattern Recognition**. 26: 1277–1294.
- Park, N.-W., and Chi, K.-H. (2008) Quantitative assessment of landslide susceptibility using high-resolution remote sensing data and a generalized additive model. **International Journal of Remote Sensing**. 29: 247–264.
- Pholsena, Phonekeo. (2004). United Nations Symposium on hydropower and sustainable development. Beijing International Convention Centre 27-29 October, Beijing, China.
- Rogan. J., Franklin, J., and Roberts, D.A. (2002). "A comparison of methods for monitoring multitemporal vegetation change using Thematic Mapper imagery". **Remote Sensing of Environment**. 80(1): 143–156.
- Schöpfer, E., Lang, S., and Albrecht, F. (2008). Object-fate analysis – spatial relationships for the assessment of object transition and correspondence. Quoted in T. Blaschke, S. Lang and G.J. Hay (Eds.) **In Object-Based Image Analysis – Spatial Concepts for Knowledge-Driven Remote Sensing Applications**. (pp785–801). Berlin: Springer.
- Siddiqui, Y. (2003). The Modified IHS Method for Fusing Satellite Imagery. **In ASPRS Annual Conference Proceedings**. USA.
- Singh, A. (1989). "Digital change detection techniques using remotely-sensed data". **International Journal of Remote Sensing**. 10(6): 989–1003.
- Somchay. (2015). Country Report, Lao People’s Democratic Republic. Department of Forest and Forest Inventory and Planning Division and FAO.

- Stow, D., Hamada, Y., Coulter, L., and Anguelova, Z. (2008). Monitoring shrubland habitat changes through object-based change identification with airborne multispectral imagery. **Remote Sensing of Environment**. 112: 1051–1061.
- Sun, K., Chen, Y., and Li, D. (2006). Multiscale image segmentation and its application in image information extraction. **Proceedings of SPIE The International Society for Optical Engineering**. 6419:64191I. Quoted in Gao, J. (2009). **Digital analysis of remotely sensed imagery**. New York: McGraw-Hill.
- Timble Germany GmbH. (2011). **eCognition developer 8.7 reference book**. München: Wikipublisher.
- U.S. Geological Service. (2017). Landsat 8. [On-line]. Available: <http://landsat.usgs.gov/landsat8.php>.
- United Nation. (2004). Geospatial Information Section. Department of Field Support [Online]. Available: <http://www.un.org/Depts/Cartographic/map/profile/laos.pdf>.
- Vongdeuane Vongsiharath. (2005). Forest cover and land use changes in Lao PDR according to the National Forest Reconnaissance Survey .Department of Land Planning and Development, National Land Management Authority, Lao PDR.
- Walter, W. (2004). Object-based classification of remote sensing data for change detection. **ISPRS Journal of Photogrammetry and Remote Sensing**. 58: 225–238.
- Wang, Z., and Bovik, A.C. (2002). A Universal Image Quality Index. **IEEE Signal Processing Letters**. 9(3): 81–84.

- Willhauck, G. (2000). Comparison of object oriented classification techniques and standard image analysis for the use of change detection between SPOT multispectral satellite images and aerial photos. In Proceedings of XIX ISPRS Congress, 16–23 July 2000. (pp214–221). Amsterdam. The Netherlands.
- World Bank Group. (2015). East Asia's Changing Urban Landscape. Measuring a Decade of Spatial Growth.
- World Bank Group. (2015). Urban development series. East Asia's changing urban landscape. Measuring a decade of spatial growth. International Bank for Reconstruction and Development / The World Bank 1818 H Street NW, Washington DC 20433.
- Wulder, M.A., Ortleypp, S.M., White, J.C., and Coops, N.C. (2008). Impact of sun-surface-sensor geometry upon multi-temporal high spatial resolution satellite imagery. **Canadian Journal of Remote Sensing**. 34: 455–461.
- Xiao tong Yang, Huiping Liu, and Xiaofeng Gao. (2015). Land cover changed object detection in remote sensing data with medium spatial resolution. **International Journal of Applied Earth Observation and Geo-information**.
- Yu, Q.P., Gong, N., Clinton, G., Biging, M.K., and Shirokauer, D. (2006). Object-based detailed vegetation classification with airborne high spatial resolution remote sensing imagery. *Photogrammetry Engineering and Remote Sensing*. 72(7): 799–811.
- Yu, X., Hyypä, J., Kaartinena, H., and Maltamo, M. (2004). Automatic detection of harvested trees and determination of forest growth using airborne laser scanning. **Remote Sensing of Environment**. 90: 451–462.

CURRICULUM VITAE

Name Mr. Sithnalong SITTHIDETH

Date of Birth February 04, 1989

Place of Birth Vientiane capital, Laos.

Education

2007 - 2012 Bachelor of Environment Science, Faculty of Environment
Science, National University of Lao, Vientiane capital, Laos.

Grant and Fellowships

Teaching assistants and ASEA-UNINET scholarship, Suranaree
University of Technology.



มหาวิทยาลัยเทคโนโลยีสุรนารี